Development of methodologies for tyre characterization and performance evaluation from on-board sensors data

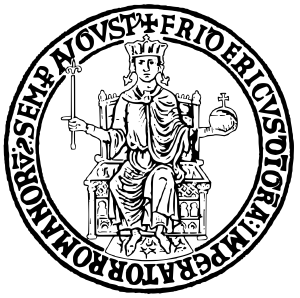

Lorenzo Mosconi

Supervisor: Prof. Flavio Farroni

Department of Industrial Engineering
University of Naples "Federico II"

This dissertation is submitted for the degree of
Doctor of Philosophy in Mechanical Engineering

March 2022

"All models are wrong, but some are useful."

George Box

Declaration

I hereby declare that except where specific reference is made to the work of others, the contents of this dissertation are original and have not been submitted in whole or in part for consideration for any other degree or qualification in this, or any other university. This dissertation is my own work and contains nothing which is the out come of work done in collaboration with others, except as specified in the text.

Lorenzo Mosconi
March 2022

Acknowledgements

In the first place i would like to acknowledge the professor Flavio Farroni that strongly believed in me and, together with Luca Dusini from Maserati, created the opportunity of and industrial PhD.

Thanks to Fabio Gerbino, Giuseppe Raimondi and all the Maserati vehicle dynamics team to sharing with me their immense expertise.

Thanks to all the colleagues in the department, who have created a place of freedom of thought, where innovative ideas are welcomed with enthusiasm.

Finally, thanks to all the Neapolitan people that welcomed me and made my staying in their city unforgettable.

Lorenzo Mosconi

Abstract

In recent years, aiming to reduce costs and time to market, the automotive world has experienced a drastic increase in the demand to reproduce vehicle dynamics through simulation models.

Autonomous vehicles are increasingly widespread and more advanced, often electric, they are strictly dependent on control algorithms that need to know the dynamic state of the vehicle and the tyre, which vary continuously both for road conditions, for wear, for the change in temperature and pressure.

This manuscript illustrates procedures that allow the estimation of tyre modeling parameters from the data collected by the vehicle in its real operating conditions, obtaining the results from post-processing procedures, and employed on the vehicle design process, or in real-time, for vehicle control.

The first methodology presented can estimate the instantaneous grip in real-time using the vehicle standard sensors with the addition of a chassis velocity sensor. The second methodology can perform the tyre transient parameters characterization with the same measurements. The last is an algorithm based on an Extended Kalman filter able to estimate the vehicle velocity, inclination angle, tyre grip and cornering stiffness.

Table of contents

List of figures

List of tables

Introduction

Nowadays, industries in the automotive field face several challenges, fastest time-to-market, tight budgets and increase in demands. Driving simulators are an exceptional way to help car manufacturers to solve costs and get feedback from test drivers before the design process. Virtual development allows to optimize the vehicle design and to get mature solutions without doing costly tests on prototype vehicles.

The vehicle interface with the ground is constituted by the sum of small surfaces, wide about as one of our palms where tyre/road interaction forces are exchanged. So, the optimization of tyre behaviour could represent a key factor in the definition of the whole vehicle best setup. The most powerful engine, the most sophisticated aerodynamics devices, the most complex control system would not ever be able to improve vehicle performances if the forces exchanged with the road are not maximized.

The target of the research activity described in this manuscript is the development of a procedure able to estimate tyre interaction characteristics and vehicle behaviour, it has been defined in the context of a collaboration between the vehicle dynamics research group of the University of Naples Federico II and Maserati S.p.a, that financed the scholarship.

Three methodologies for the estimation and measurement of hidden physical quantities of the vehicle/tyre system are presented.

In detail, the work is structured as follows:

- Chapter 1 - The Tyre: in this chapter, information about tyre structure and tyre models are provided. A special mention is made to the Pacejka model, through which an analytical method for tyre-road force estimation is possible.

- Chapter 2 - TRICK tool for the grip loss evaluation, Tyre/Road Interaction Characterization Knowledge: in this chapter, it is described a vehicle model able to process experimental signals acquired from vehicle CAN bus and from side-slip angle measurement additional instrumentation, providing a real time estimation of the tyre exerted forces and sliding. This robust estimation, strongly related with the real friction conditions, is compared to the results of a pre-identified tyre model in order to evaluate the friction loss.

- Chapter 3 - Identification of Tyre Transient Parameters from Vehicle On board Sensors Data: in this chapter, the procedure to estimate the tyre relaxation length and tyre lateral stiffness is explained. To perform this task, a specific vehicle model, a track testing maneuver and a data post-processing methodology were designed.

- Chapter 4 - Kalman filter for the vehicle state estimation: in this chapter, the Kalman filter algorithm, that is a strong tool for the real time estimation of physical quantities that cannot be directly measured, is illustrated. Furthermore, the tuning methodology of the algorithm parameters, that make it suitable on complex models like the presented in this work, are explained.

- Chapter 5 - Adaptive vehicle dynamics state estimator: in this chapter is presented a novel algorithm based on an Extended Kalman filter applied on a complex vehicle model, that using a sensor set that is available on commercial vehicles, is able to perform the simultaneous estimation of hidden states of the vehicle/tyre system like side-slip angle, road slope and banking, tyre grip and cornering stiffness.

Chapter 1

The Tyre

1.1 Description and General Considerations

The tyre is an under pressure, inextensible and deformable casing, made of composite material of polymeric matrix (vulcanized rubber and additives such as carbon black and silica) with reinforcement plies of steel or synthetic fibres [1–3].

It has the shape of a solid of revolution (toroidal ring) with the function to bear statically and dynamically a given load, to transmit to the ground the longitudinal and lateral forces necessary to motion, to ensure the directionality of the vehicle enabling the steering and the insertion of it in the driver's desired trajectory, to perform both traction and braking force by means of adherence with the road surface, improve passenger comfort contributing to the vehicle suspension.

Currently, the most common tyre in automotive industry is the tubeless type, lacking of inner tube. The inner side of the tyre is constituted by a special rubber coating, highly airtight, called liner. The parts constituting a tubeless tyre are the followings (Figure 1.1) [4]:

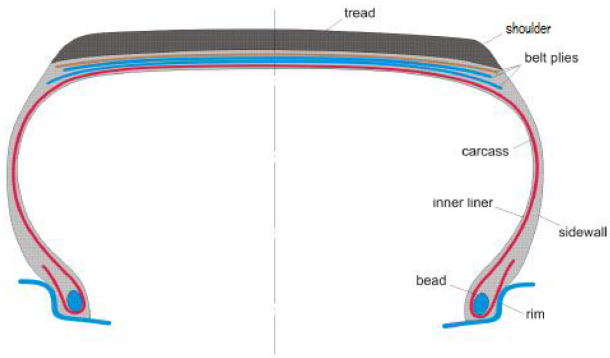

Fig. 1.1 Tyre structure

- Tread: consists of a rubber compound, commonly styrene-butadiene (SBR) copolymers [5], whose surface is crossed by a "pattern" able to ensure a good grip in both wet and dry conditions, as well as good characteristics of silent running. The pattern is composed by a particular arrangement of full (ribs) and void (grooves) volumes; the latter are designed to channel the water out and away ensuring a "dry" contact between rubber and soil.

- Shoulder: is the area including the tread lateral extreme edge and the beginning of the sidewall. A tyre needs to offer good heat dispersal and for this the shoulder section plays a crucial role.

- Sidewall: is the area between the shoulder and the bead bundle. It consists of a thin rubber layer, intended to protect the carcass plies against side impacts, such as the sidewalks edges. The sidewall helps to make tyre rigid and improves the ride quality; generally speaking, a high sidewall tyre is more comfortable than a low one as it is more flexible and hence able to better absorb the road unevennesses.

- Bead: tyre / rim coupling element; the core of a tyre's bead is made up of several individually rubber-coated steel wires formed into a hoop,

that is then provided with a rubber apex. Bead function is to ensure that the tyre sits firmly on the rim, in order to prevent relative rotations. This coupling is particularly critical, considering that all the actions exchanged between tyre and road are transmitted to the vehicle via the bear / rim contact surface that has a very limited extension and therefore is subjected to high stress levels.

- Inner liner: is a thin, specially formulated compound placed on the inner surface of tubeless tyres to improve air retention by lowering permeation outwards through the tyre.

- Belt plies: restrict expansion of carcass plies, stabilizing the tread area and providing impact resistance. Varying the belt width and angles affects vehicle ride and handling characteristics. Alternate belt constructions with materials other than steel is also often utilized.

- Carcass (or body plies): constitutes the resistant structure, mainly acting in normal interaction, composed of one or more layers of plies placed under the tread (or under belt plies in radial tyres). Every single ply is composed by a series of mutually parallel cords of very durable and at the same time flexible material, surrounded by the vulcanized rubber compound.

Each carcass ply extends from bead to bead, wrapping and transferring on them the stresses generated by inflation pressure and interaction forces. Body plies arrangement (Figure 1.2) gives the name to the structure of the tyre: nowadays the most commonly employed structure is the radial one, in which the carcass is composed of one or more plies disposed through the meridian planes of the toroid. The radial carcass is made more stable by the belt annular reinforcing structure which runs below the tread. The belt plies have very small inclination angles, between 5° and 10° and absorb the shear stresses which arise in working conditions.

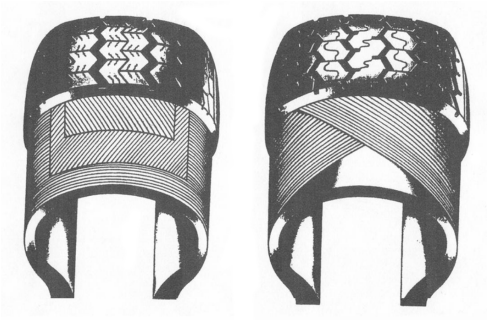

Fig. 1.2 Radial (left) and diagonal or bias (right) tyre structure

The other type of structure, still used in some applications for trucks, trailers and farm implements, is called diagonal or bias because the plies cross on the carcass being disposed according to proper inclinations respect to equatorial plane called "crown angles". Note that in these tyres there are not belt plies; therefore it is quite simple to recognize a radial tyre, being the sidewall plies fewer than the tread ones, for the presence in the latter of the belt reinforcements.

The advantages of radial are mainly due to the fact that the tread is independent from the carcass; consequently, the tangential stresses (absorbed by the belt plies) are decoupled from normal ones (absorbed by radial carcass plies), while in bias tyres all stresses decompose according to the crown angles. Furthermore the radial arrangement reduces fatigue and wear: being the sidewall thinner, the material is less subjected to hysteresis, occurring for shear between plies and generating heat to be dissipated.

Radial tyres are characterized by better grip, more stability and a higher braking efficiency, acting as safer than conventional ones; they also allow greater energetic saving (increased durability and fuel economy) and a greater level of comfort (more shock absorption) [1, 6].

1.2 Historical Notes

In 1844 Goodyear invented the vulcanization process of natural rubber which consisted in manufacturing it in an environment saturated with sulphur under certain conditions of temperature and pressure. This technological step was essential for the subsequent evolution of the tyre, considering that natural rubber exhibits low yield strength and strongly varies its resistance with temperature. The vulcanization, through the sulphur bonds in the polymer chains, allows to natural rubber to increase its strength and its attitude to resist to deformation.

In 1846, Thomson patented an "air wheel": the first prototype of tyre. He had the idea to employ an air chamber in the wheels in order to both reduce the effort of the horses (the work was reduced by 40%) and to cushion noise and harshness. Despite the innovation, Thomson was not understood and his idea had no developments.

Only in 1888, Dunlop, in an attempt to build a tricycle for his son, began to study the wheels. He verified experimentally that between a solid rubber wheel and an hollow one filled with air, the latter bounced more; it was a proof of the excellent elastic behaviour of what would have become the first industrial manufactured tyre. Solid rubber is significantly visco-elastic, retrieving original shape after deformations with strong delay; moreover, being more insulating, cannot easily dissipate the heat generated by hysteresis, degrading consequently very quickly. On the contrary, the air contained in the hollow rubber accelerates the recovery after the deformation and the degradation is lower because the amount of rubber is reduced.

The huge commercial success of the Dunlop tyres was due to a cyclist who first used them and repeatedly won against his rivals who yet adopted solid rubber wheels.

The tyres were originally nailed to the rim; only after time the bead / rim coupling system was developed. Over the years the constructive structure has changed, bringing to the disappear of the inner tubes (which can still

be found today for bicycles) and to the progressive diffusion of the radial plies arrangement. Even the colour has changed; initially the tyres were white because natural rubber is white, then the carbon black was added to composition to enhance performance under wear and fatigue and to prevent the action of ultraviolet rays. Finally, to further improve the mechanical properties, the silica and many other materials have been recently added, leading to very complex tyres, constituted by dozens of different compounds.

In the last few years, tyremakers have given a new shape to tyres, developing airless prototypes. Michelin announced the Tweel in 2005 and presented it recently, while Bridgestone has shown his "Air Free Concept Tyre" at Tokyo Motor Show 2013. The prototypes don't use a traditional wheel hub assembly: a solid inner hub surrounded by polyurethane spokes arrayed in a pattern of wedges mounts to the axle. A shear band is stretched across the spokes, forming the outer edge of the tyre (the part that comes in contact with the road). The tension of the shear band on the spokes and the strength of the spokes themselves replace the air pressure of a traditional tyre. The tread is then attached to the shear band [7]. It must still be understood if airless tyres will be able to substitute common pneumatic tyres, but they could represent an interesting solution for the advantages that they can offer as concerns punctures and damage resistance.

1.3 Sidewall Markings

Automobile tyres are described by an alphanumeric tyre code, which is generally moulded into the sidewall (Figure 1.3). This code specifies the dimensions of the tyre and some of its key limitations, such as load-bearing ability and maximum speed. Sometimes the inner sidewall contains information not included on the outer sidewall, and vice versa.

The code has grown in complexity over the years, as is evident from the mix of metric and imperial units, and ad-hoc extensions to lettering

and numbering schemes. New automotive tyres frequently have ratings for traction, tread wear and temperature resistance (collectively known as The Uniform Tyre Quality Grade (UTQG) ratings). Most tyres sizes are given using the ISO Metric sizing system. However, some pickup trucks and SUVs use the Light Truck Numeric or Light Truck High Flotation system.

The ISO Metric tyre code consists of a string of letters and numbers, as follows:

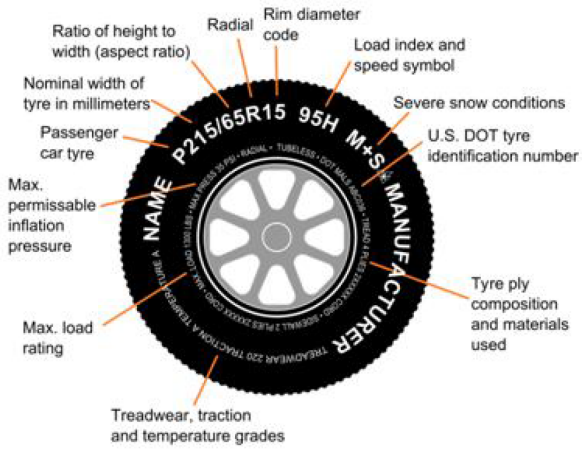

Fig. 1.3 Tyre sidewall markings

- An optional letter (or letters) indicating the intended use or vehicle class:

  - P: Passenger Car

  - LT: Light Truck

  - ST: Special Trailer

  - T: Temporary (restricted usage for "Space-Saver" spare wheels)

  Use of the letter P indicates that the tyre is engineered to TRA standards and absence of a letter indicates that the tyre is engineered to ETRTO standards. In practice, the standards of the two organizations have

evolved together and are fairly interchangeable, but not fully since the Load Index will be different for the same size tyre.

- 3 digit number: the "nominal section width" of the tyre in millimetres; the widest point from both outer edges (sidewall to sidewall). The tyre surface in contact with the road usually has smaller width.
- /: slash character for numbers separation.
- 2 or 3 digit number: the "aspect ratio" of the sidewall height as a percentage of the total width of the tyre. If the information is omitted, it is assumed to be 82written, it should be like xxx/82). If the number is larger than 200, then this is the diameter of the entire tyre in millimetres.
- An optional letter indicating construction of the tyre carcass:

  - B: bias belt

  - D: diagonal

  - R: radial

  if omitted, then it is a cross ply tyre.
- 1 or 2 digit number: diameter in inches of the rim that the tyres are designed to fit.
- 2 or 3 digit number: load index [8]; some light truck tyres are approved for "dual use", that is they can be run in pairs next to each other. If so, separate load indices will be specified for single and dual usage. Tyres without this designation for dual usage are unsafe to use as such.
- 1 or 2 digit/letter combo: speed rating [8].
- Additional marks: the most common are the followings:

  - M+S or M&S: mud and snow; a tyre that meets the Rubber Manufacturers Association (RMA) and Rubber Association of Canada

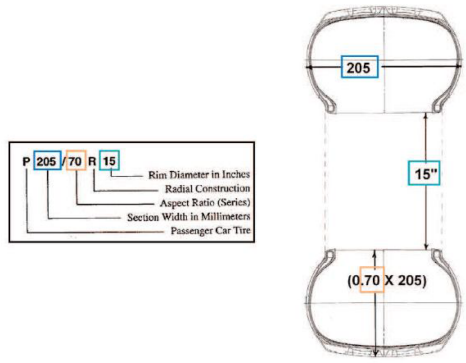

Fig. 1.4 Tyre size graphic explanation

(RAC) all-season tyre definition. These are all-weather tyres, with self-cleaning tread and aboveaverage traction in muddy or very light snowy conditions, and at low ambient temperatures. Spike tyres have an additional letter, "E" (M+SE).

- M+T or M&T: mud and terrain; designed to perform in mud or on other terrain that requires additional traction such as on rocks, in deeper snow, and in loose gravel.

- SFI or Inner: Side Facing Inwards; inside of asymmetric tyres.

- SFO or Outer: Side Facing Outwards; outside of asymmetric tyres.

- TWI: Tread Wear Indicator; a device, such as a triangle, located where the tread meets the sidewall. It indicates the location of the raised wear bars in between the tyre tread channels.- LL: Light Load; tyres for light usage and loads.

- SL: Standard Load; tyre for normal usage and loads.

- XL: eXtra Load; a tyre that allows a higher inflation pressure than a Standard Load tyre, which increases the tyre's maximum load.

- RF: Reinforced - for Euro metric tyres - the term means the same thing as 'Extra Load'.

- Arrows: some tread designs are "directional", and designed to perform better when driven in a specific direction (clockwise or counter-clockwise). Such tyres have an arrow showing which way the tyre should rotate when the vehicle is moving forwards. It is important not to put a "clockwise" tyre on the left hand side of the car or a "counter-clockwise" tyre on the right side.

- DOT code: all tyres for use in the USA have the DOT code, as required by the Department of Transportation (DOT). It specifies the company, factory, mould, batch, and date of production (two digits for week of the year plus two digits for year). JATMA, the Japanese Automotive Tyre Manufacturers Association recommends that all tyres be inspected at five years and that all the ones manufactured more than ten years before be replaced.

1.4 Mechanics of Tyres

1.4.1 Topology Notes

Tyres are generally required to fulfil the following functions:

- to support the weight of the vehicle;
- to cushion the vehicle over surface irregularities;
- to provide sufficient traction for driving and braking;
- to provide adequate steering control and direction stability.

The study of the mechanics of tyres therefore is of fundamental importance to the understanding of the performance and characteristics of ground vehicles. To describe the behaviour of a tyre and the forces and moments acting on it, it is necessary to define an axis system that serves as a reference for the

definition of various parameters. One of the commonly used axis systems recommended by the ISO8855 standard and shown in Figure 1.5 [9]. The origin of the axis system is the centre of tyre contact (CTC), x axis is the intersection of the wheel plane and the ground plane with a positive direction forward, z axis is perpendicular to the ground plane with a positive direction upward and y axis is in the ground plane, and its direction is chosen to make the axis system orthogonal and right hand. There are three forces and three moments acting on the tyre from the ground: tractive force (or longitudinal force) F_x is the component in the x direction of the resultant force exerted on the tyre by the road, lateral force F_y is the component in the y direction, and normal force F_z is the component in the z direction. "Overturning moment" M_x is the moment about the x axis exerted on the tyre by the road, "rolling resistance" moment M_y is the moment about the y axis, and "aligning torque" M_z is the moment about the z axis.

With this axis system, many performance parameters of the tyre can be conveniently defined; for instance, the longitudinal shift of the centre of normal pressure is determined by the ratio of the rolling resistance moment to the normal load, the lateral shift of the centre of normal pressure is defined by the ratio of the overturning moment to the normal load and the integration of longitudinal shear stresses over the entire contact patch represents the tractive or braking force.

There are two important angles associated with a rolling tyre: "slip angle" and "camber angle": slip angle α is the angle from the x axis to the velocity vector of the centre of tyre contact, about the z axis; camber angle γ is the angle formed between the xz plane and the wheel plane. Lateral interaction forces at the tyre/ground interface are a function of both the slip angle and the camber angle.

In the following, brief notes about lateral and longitudinal tyre dynamics will be provided; for more detailed analyses the consultation of the wide available bibliography is suggested [10–13].

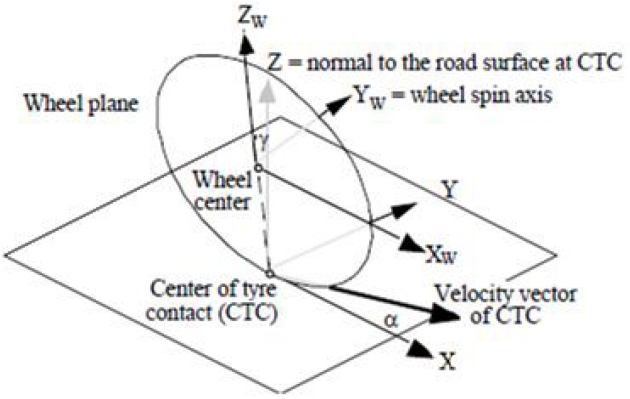

Fig. 1.5 ISO wheel reference system

1.4.2 Lateral Interaction

When a tyre is not subject to any force perpendicular to the wheel plane, it will move along this last; if a side force F_s is applied to a wheel, a lateral force will be developed at the contact patch, and the tyre will move along a path at an angle equal to the slip angle α with the wheel plane, mainly due to the lateral elasticity of the tyre, as shown in Figure 1.6.

The lateral force developed at the tyre/ground contact patch is usually called cornering force F_{y_α} when the camber angle of the wheel is zero; the relationship between the cornering force and the slip angle is of fundamental importance to the directional control and stability of road vehicles. When the tyre is moving at a uniform speed, the side force F_x applied at the wheel centre and the cornering force F_{y_α} developed in the ground plane are usually not collinear: at small slip angles, the cornering force in the ground plane is normally behind the applied side force, giving rise to a torque which tends to align the wheel plane with the direction of motion. This torque is called the "aligning" or "self-aligning torque", and it is one of the restoring moments which help the steered tyre return to the original position after performing a curving manoeuvre. The distance t between the side force and the cornering

force is called the "pneumatic trail", and the product of the cornering force and the pneumatic trail determines the self-aligning torque.

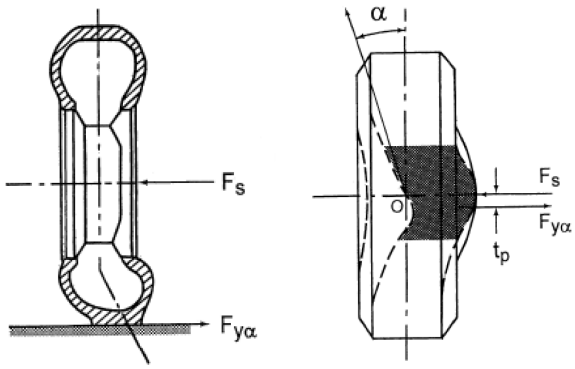

Fig. 1.6 Tyre cornering behaviour and definition of slip angle α

The relationships between the slip angle and the cornering force of various types of tyre under a variety of working conditions have been investigated extensively. Typical plots of the cornering force as a function of the slip angle show that for slip angles below a certain value the cornering force is approximately proportional to the slip angle. Beyond that, the cornering force increases at a lower rate with an increase of the slip angle, and it reaches a maximum value where the tyre begins sliding laterally. For passenger car tyres, the maximum cornering force may occur at a slip angle about three times higher than for racing car tyres (characterized by definitely higher values of lateral stiffness).

A number of factors affect the cornering behaviour of tyres, as for example the normal load: it can be seen that for a given slip angle, the cornering force generally increases with an increase of the normal load. However, the relationship between the cornering force and the normal load is nonlinear (Figure 1.7); it means that the transfer of load from the inside to the outside tyre during a turning manoeuvre will reduce the total cornering force that a pair of tyres can perform, making so possible to act on the under/oversteering

behaviour of the whole vehicle modifying the value of the roll stiffness, able to manage the load transfers [10].

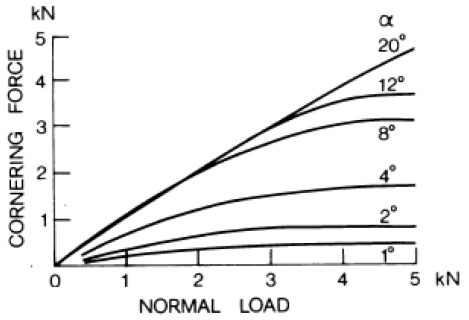

Fig. 1.7 Effect of normal load on the cornering characteristics of a tyre

To provide a measure for comparing the cornering behaviour of different tyres, a parameter called "cornering stiffness" C_{y_α} is used. It is a very important parameter in determining the linear range behaviour of vehicles, the area in which most driving is done and is defined as the derivative of the cornering force F_{y_α} with respect to slip angle α evaluated at zero slip angle:

$$C_{y_\alpha} = \frac{\partial F_{y_\alpha}}{\partial \alpha}\bigg|_{\alpha=0} \tag{1.1}$$

The cornering stiffness generally increases with load, but the rate of increase declines as load increases. The peak of the lateral force curve occurs at higher and higher slip angles as the normal force increases. However, if a pseudo coefficient of friction is computed by dividing the peak value of F_y at each load by the load itself, one discovers that the frictional capability of the tyre declines with increasing load. Thus, high performance vehicles on a dry road will exhibit their maximum cornering ability using large tyres operating at relatively light loads. Inflation pressure usually has a moderate effect on the cornering properties of a tyre, but in general, cornering stiffness increases with an increase of the inflation pressure.

1.4.3 Camber Thrust

Camber causes a lateral force usually referred to as "camber thrust" $F_{y\gamma}$, and the development of this thrust may be explained in the following way: a free-rolling tyre with a camber angle would revolve about point O, as shown in figure 1.8; however, the cambered tyre in a vehicle is constrained to move in a straight line, developing therefore a lateral force in the direction of the camber in the ground plane. It has been shown that the camber thrust is approximately one fifth the value of the cornering force obtained from an equivalent slip angle for a bias-ply tyre and somewhat less for a radial-ply tyre.

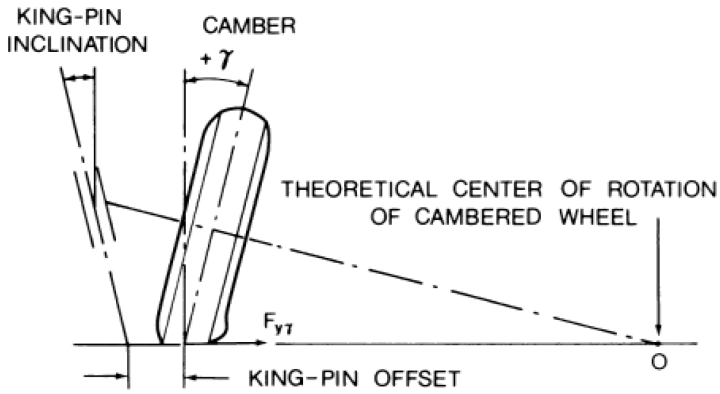

Fig. 1.8 Behaviour of a cambered tyre

To provide a measure for comparing the camber characteristics of different tyres, a parameter called "camber stiffness" is often used; it is defined as the derivative of the camber thrust with respect to the camber angle evaluated at zero camber angle:

$$C_\gamma = \left.\frac{\partial F_{y\gamma}}{\partial \gamma}\right|_{\gamma=0} \tag{1.2}$$

Similarly to the cornering stiffness, normal load and inflation pressure have an influence on the camber stiffness. It has been calculated that for truck

tyres, the value of the camber stiffness is approximately one tenth to one fifth of that of the cornering stiffness under similar operating conditions.

The total lateral force of a cambered tyre operating at a certain slip angle is the sum of the cornering force F_{y_α} and the camber thrust F_{y_γ}:

$$F_y = F_{y_\alpha} \pm F_{y_\gamma} \tag{1.3}$$

If the cornering force and the camber thrust are in the same direction, the positive sign should be used in the above equation. For small slip and camber angles, the relationship between the cornering force and the slip angle and the one between the camber thrust and the camber angle are essentially linear; the total lateral force of a cambered tyre at a slip angle can, therefore, be determined by:

$$F_y = C_{y_\alpha}\alpha \pm C_{y_\gamma}\gamma \tag{1.4}$$

As discussed previously, the lateral forces due to slip angle and camber angle produce a torque, but the component due to slip angle, however, is usually much greater and mainly responsible of the aligning torque acting on tyres in ordinary driving conditions.

1.4.4 Longitudinal Interaction

When a driving torque is applied to a tyre, a tractive force is developed at the tyre/ground contact patch, as shown in Figure 1.9. At the same time, the tyre tread zone in front of and within the contact patch is subjected to compression and a shear deformation of the sidewall is also developed. As tread elements are compressed before entering the contact region, the distance that the tyre travels when subject to a driving torque will be less than that in free rolling. This phenomenon is usually referred to as longitudinal slip.

Tyre longitudinal slip, when a driving torque is applied, is usually defined by:

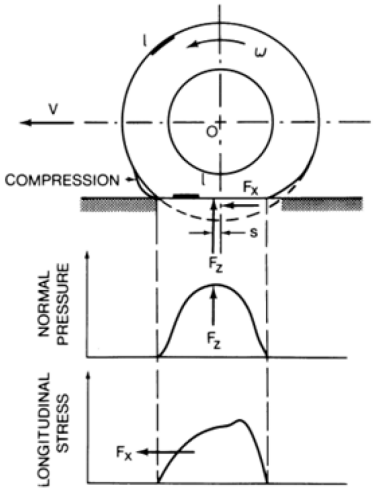

Fig. 1.9 Behaviour of a tyre under the action of a driving torque

$$\kappa_T = \frac{\omega R_r - V_x}{\omega R_r} \tag{1.5}$$

where V_x is the longitudinal linear speed of the tyre centre, ω is the tyre angular speed and R_r is the rolling radius of the free-rolling tyre. When a driving torque is applied, ωR_r is greater than V_x and a positive value for κ_T results; if a tyre is rotating at a certain angular speed but the linear speed of its centre is zero, then in accordance with equation 1.5, the longitudinal slip will be 100%. This is often observed on an icy surface, where the driven tyres are spinning at high angular speeds, while the vehicle does not move forward.

As the tractive force developed by a tyre is proportional to the applied wheel torque under steady-state conditions, slip is a function of tractive effort. Generally speaking, at first the wheel torque and tractive force increase linearly with slip because, initially, slip is mainly due to elastic deformation of the tread. A further increase of wheel torque and tractive force results in part of the tread sliding on the ground, that explains why the relationship between the tractive force and the slip is notoriously nonlinear.

Based on available experimental data, the maximum tractive force of a tyre on hard surfaces is usually reached somewhere between 15 and 20% slip. Any further increase of slip beyond that results in an unstable condition, with the tractive effort falling rapidly from the peak value to the pure sliding value.

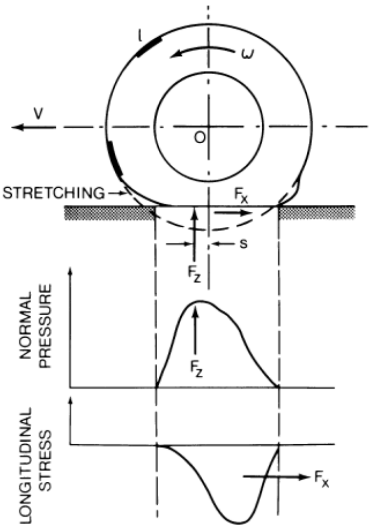

Fig. 1.10 Behaviour of a tyre under the action of a braking torque

When a braking torque is applied to the tyre, a stretching of the tread elements occurs prior to entering the contact area, as shown in figure 1.10, in contrast with the compression effect described for a driven tyre. The distance that the tyre travels when a braking torque is applied, therefore, will be greater than that in free rolling and κ_B is the index usually employed to quantify the skid of the tyre:

$$\kappa_B = \frac{V_x - \omega R_r}{V_x} \tag{1.6}$$

For a locked wheel, the angular speed is zero, whereas the linear speed of the tyre centre is not zero; under this condition, the skid is denoted 100%.

Both in traction and in braking manoeuvres the contact patch can be split in two different parts: a first one, considered in adherence, in which tangential

force is proportional to tread deformation along x direction; a second one, where sliding between tread and ground takes place, linked to normal pressure distribution and dynamic friction coefficient. If no sliding takes place on the contact patch, the relationship between the longitudinal force and the slip can be considered as linear:

$$F_x = C_{x_\kappa} \kappa \tag{1.7}$$

in which κ is equal to κ_T in traction phases and to κ_B in braking ones and C_{x_κ} is tyre longitudinal stiffness, often called "braking stiffness", even in traction phases:

$$C_{x_\kappa} = \left. \frac{\partial F_x}{\partial \kappa} \right|_{\kappa=0} \tag{1.8}$$

1.4.5 Interaction between Tangential Forces

In the discussion about the cornering behaviour of tyres, the effect of the longitudinal force has not been considered. However, quite often both the side force and the longitudinal force are present, such as braking in a turn. In general, tractive (or braking) effort will reduce the cornering force that can be generated for a given slip angle; the cornering force decreases gradually with an increase of the tractive or braking effort. At low values of tractive (or braking) effort, the decrease in the cornering force is mainly caused by the reduction of the cornering stiffness of the tyre. A further increase of the tractive (or braking) force results in a pronounced decrease of the cornering force for a given slip angle. This is due to the mobilization of the available local adhesion by the tractive (or braking) effort, which reduces the amount of adhesion available in the lateral direction.

It is interesting to point out that if an envelope around each family of curves of figure 1.11 is drawn, a curve approximately semi-elliptical in shape

may be obtained. This enveloping curve is often referred to as the friction ellipse.

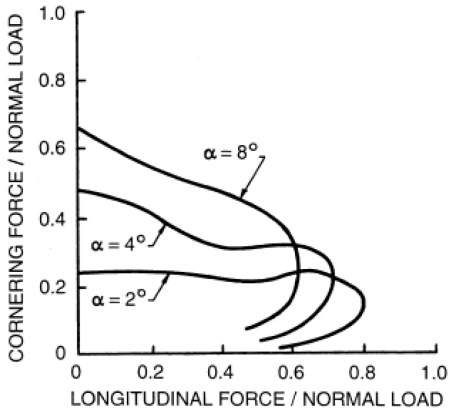

Fig. 1.11 Effect of longitudinal force on the cornering characteristics of tyres

The friction ellipse concept is based on the assumption that the tyre may slide on the ground in any direction if the resultant of the longitudinal force (either tractive or braking) and lateral (cornering) force reaches the maximum value defined by the coefficient of friction and by the normal load on the tyre. However, the longitudinal and lateral force components may not exceed their respective maximum values $F_{x_{max}}$ and $F_{y_{max}}$, as shown in Figure 1.12. $F_{x_{max}}$ and $F_{y_{max}}$ can be identified from measured tyre data and constitute respectively the major and minor axis of the friction ellipse.

1.5 Tyre Models

Experimental evidence shows that the tyre-road interaction is mainly a function of vertical load, camber angle, slip ratio and slip angle.

$$F = f(F_z, \gamma, \kappa, \alpha) \tag{1.9}$$

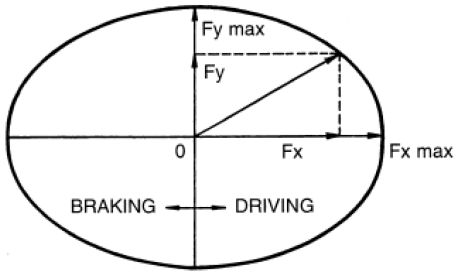

Fig. 1.12 The friction ellipse concept relating the maximum available cornering force to a given longitudinal force

An interaction model is a mathematical structure that explicates this function and makes it possible to predict the magnitude of the exchanged forces, known as the kinematic conditions and the attitude of the tyre.

Since the 1930s, many mathematical models have been developed, each with its own target and a different approach.

A distinction is between empirical and physical models:

- Empirical models: These models are built on empirical evidence. It is a way of describing physical phenomena by means of direct and indirect observation or experience. Empirical evidence can be analysed quantitatively or qualitatively. Referring to tyre models systems and formulas are derived from experimental tests and characterized by parameters lacking physical meaning.

- Physical models: They describe a system using mathematical equations. A model may help to explain a system and to study the effects of different components, and to make predictions about behaviour. In this case, a physical model is based on the theoretical description of the tyre physics and the mechanics of the contact.

The distinction of these two categories is not clear, in recent years physical-experimental models (or semi-empires) have been proliferated, they are characterized by different levels of accuracy and complexity.

In Figure 1.13, from left to right, the model is based less on experimental tests and more on theoretical analysis of the physics of the tyre. In the central region, the model is simpler but less accurate, in the far right most complex and appropriate to performance analysis and virtual prototyping.

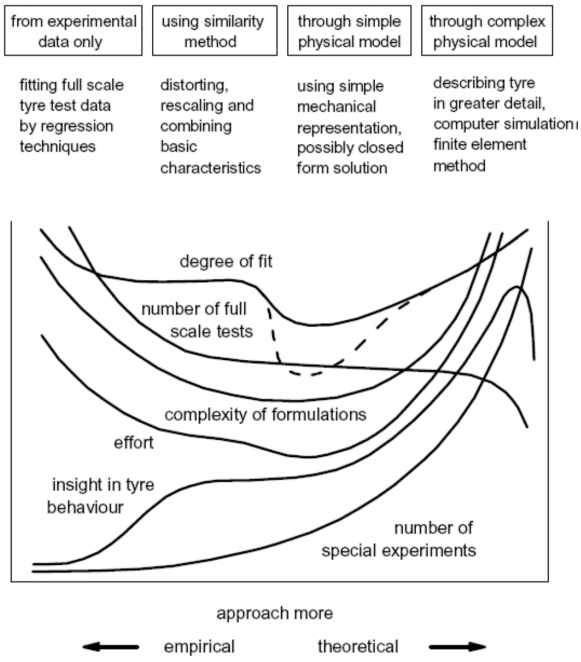

Fig. 1.13 Interaction model classification

The models on the far left (empirical sayings) are obtained starting from experimentation campaigns aimed at compiling maps and printouts containing a vast series of behaviours of the tyre-road system. Once the data are collected, a functional analysis is carried out to establish the schema, the analytical structure that best fits the maps.

The result is usually a combination of polynomial, exponential, trigonometric functions containing parameters to be determined using regression techniques (parametric identification). It must be emphasized that the param-

eters thus obtained have no physical meaning, but they are the result of a mathematical procedure.

The second category (centre-left of the graph) is represented by the similarity methods. They are based on the calculation of the interaction characteristics under nominal or reference conditions from measured data. The characteristics obtained in this way are scaled, modulated and distorted according to physical inputs such as camber, vertical load and sliding.

The main difference compared to the previous case is that the parameters ascribable to these models have a physical meaning, so they are "semi-empirical" methods. This is the category that best lends itself to vehicle dynamics simulations as it offers quick times calculation and a good reproduction of the physics of the problem.

The third category (centre-right of the graph) consists of simple physical-analytical methods. They are based on the theoretical analysis of contact mechanics, often offering solution in closed form. These methods are excellent for understanding the phenomena under consideration, but they lack in terms of accuracy, especially when they are based on strong simplification hypotheses introduced to lighten the formulation.

On the extreme right there are the complex physical models (also called physical-numerical). They are based on the use of the finite element method (FEM), a very efficient and accurate technique, but also very costly from a computational point of view, for which it is suitable for predicting the properties and performance of the tyre, but it lacks simulation applications.

1.5.1 Pacejka Magic Formula

This is a semi-empirical method that requires a campaign of experimental tests in order to characterize the tyre-road system. The model was developed during the 80s in the context of a cooperation between TU Delft and Volvo. It was later reworked by Michelin which went from a predominantly physical to an empirical approach. The result was a rather difficult mathematical expression

to interpret, yet able to interpolate very well a vast range of experimental data, hence the curious name [13, 14].

This model is very useful to simulate the steady-state behaviour by providing a set of mathematical formulae, which are partly based on a physical background. It calculates the forces F_x, F_y and moments M_x, M_y, M_z acting on the tyre under pure and combined slip conditions, using longitudinal and lateral slip κ,α, wheel camber γ and the vertical force F_z as input quantities.

In addition to the Magic Formula description, a set of differential equations is defined, representing the transient behaviour of the tyre with respect to handling at frequencies up to 8 Hz [14, 15].

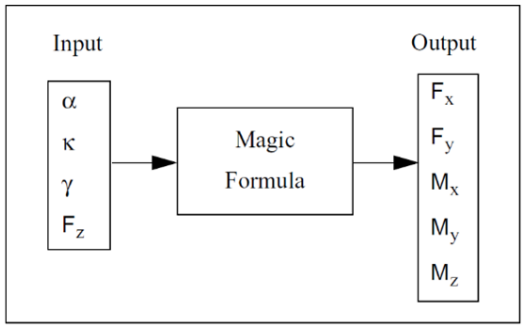

Fig. 1.14 Input and Output variables of the Magic Formula Tyre Model

The general expression of the MF is:

$$y(x) = D\sin[C\arctan\{Bx - E(Bx - \arctan(Bx)\} \tag{1.10}$$

with:

$$Y(x) = y(x) + S_v \tag{1.11}$$

$$x = X + S_h \tag{1.12}$$

where:

- $Y(x)$ is the output F_x , F_y or M_z
- X is the input (slip ratio or slip angle)
- B is the rigidity factor
- C is the shape factor
- D is the peak value
- E is the bending factor
- S_v is the vertical shift
- S_h is the horizontal shift

The result, shown in figure 1.15, is a curve that passes through the origin (unless the imposed translations), reaches a peak value and then assumes a horizontal asymptotic pattern. The 6 coefficients listed above are called Pacejka's macro parameters and govern the trend of the curve.

The BCD product corresponds to the slope of the curve in the origin. C controls the shape of the curve and governs the abscissa of the maximum and the curvature in its surroundings. The shifts allow to translate the curve and to contemplate the contribution of camber, hysteresis, asymmetry and taper of the tyre.

It is important to note that for $C \leq 1$ the maximum value of the curve coincides with the asymptote and that for $E > 1$ the curve degenerates (the model is infeasible).

The expression just described allows to represent the characteristics of pure interaction. In combined interaction, at the same load, total sliding condition occur for smaller value of slip (ratio or angle), since part of the available adherence is engaged by the complementary interaction. This

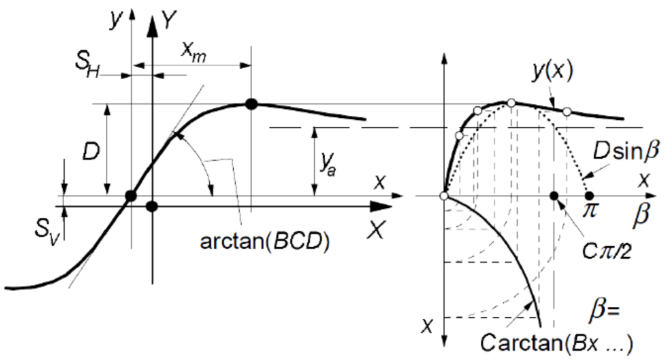

Fig. 1.15 Curve produced by the original sine version of the Magic Formula

observation led to the development and implementation of the "cosine version" of the Pacejka formula.

The first expression elaborated was:

$$G = D\cos[C\arctan(Bx)] \tag{1.13}$$

$$x = X + S_h \tag{1.14}$$

With B, C, D and S_h distinct from the previously defined macro parameters. As shown in Figure 1.15, parameter D represents the maximum value (slightly less than 1 in the presence of offset), C determines the position of the horizontal asymptote placed at the base of the curve, B governs the shape and intercepts with the axis of the abscissas.

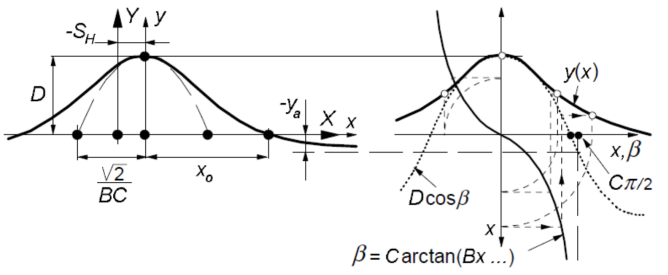

Fig. 1.16 Curve produced by the cosine version of the Magic Formula

This expression is also known as the "hill function" due to the bell-like performance that characterizes it. Parameter G, multiplied by pure interaction, returns the combined interaction. This is evidently a weight function, a reduction factor that has a physical sense only if it is within the range $[0,1]$.

The most recent expressions of the formula, particularized for longitudinal and lateral interaction, are:

$$G_{x\alpha} = \frac{\cos[C_{x\alpha}\arctan\{B_{x\alpha}\alpha_s - E_{x\alpha}(B_{x\alpha}\alpha_s - \arctan(B_{x\alpha}\alpha_s))\}]}{\cos[C_{x\alpha}\arctan\{B_{x\alpha}S_{Hx\alpha} - E_{x\alpha}(B_{x\alpha}S_{Hx\alpha} - \arctan(B_{x\alpha}S_{Hx\alpha}))\}]} \tag{1.15}$$

$$G_{y\kappa} = \frac{\cos[C_{y\kappa}\arctan\{B_{y\kappa}\kappa_s - E_{y\kappa}(B_{y\kappa}\kappa_s - \arctan(B_{y\kappa}\kappa_s))\}]}{\cos[C_{y\kappa}\arctan\{B_{y\kappa}S_{Hy\kappa} - E_{y\kappa}(B_{y\kappa}S_{Hy\kappa} - \arctan(B_{y\kappa}S_{Hy\kappa}))\}]} \tag{1.16}$$

In general, the interaction characteristic, i.e. the law that binds the force (longitudinal or lateral) to the slip (ratio or angle), varies according to the vertical load, the camber angle, the inflation pressure, the spin. It also depends on the construction characteristics, the thermo-mechanical and tribological properties of the tyre, as well as on the road surface conditions. The subject is further complicated by the non-linear behaviour of the system under examination.

To introduce dependence on all these factors into the economy of the equation, the macro parameters have been expressed as a combination of micro-parameters. Over the last few years, the modelling work has been focused on the development and optimization of the expressions that link macro and micro-parameters, without prejudice the general formulation.

Before proceeding it should be noted that Magic Formula is defined in the privileged reference system according to the ISO convention.

MF-Tyre conforms to the TYDEX STI conventions described in the TYDEX-Format and the Standard Tyre Interface (STI). Two TYDEX coordi-

nate systems with ISO orientation are particularly important, the C- axis and W-axis systems as detailed in Figure 1.17:

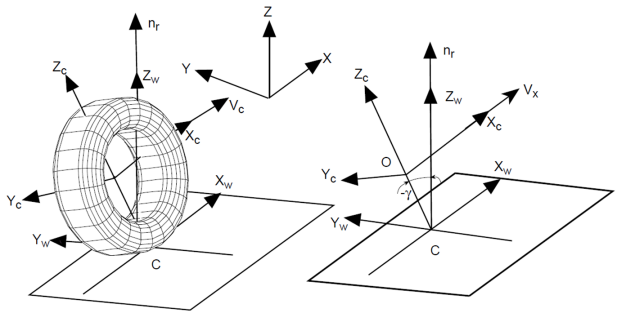

Fig. 1.17 TYDEX C – and W- Axis Systems used in MF-Tyre, according to TYDEX

The C-axis system is fixed to the wheel carrier with the longitudinal x_c – axis parallel to the road and in the wheel plane (x_c - z_c – plane). The origin O of the C-axis system is the wheel centre.

The origin of the W-axis system is the road contact-point (or point of intersection) C defined by the intersection of the wheel plane, the plane through the wheel spindle and the road tangent plane. The orientation of the W-axis system agrees to ISO.

The forces and torques calculated by MF-MC Tyre, which depend on the vertical wheel load F_z along the z_w- axis and the slip quantities are projected in the W-axis system. The x_w - y_w- plane is the tangent plane of the road in the contact point C.

The geometrical and kinematical quantities involved are so defined:

- V, wheel centre speed;
- V_x and V_y, respectively longitudinal and lateral speed of the wheel centre;
- ω, the peripheral speed of the wheel around its own kinematic axis;

- R_e, pure rolling radius;
- $V_{sx} = V_x - \omega R_e$, longitudinal sliding speed, that is the speed difference between centre and periphery of the wheel that occurs during the braking or the acceleration phases;
- $V_{sy} = V_y$, lateral sliding speed, it occurs when the velocity vector does not lie on the equatorial plane of the wheel, i.e. when the vehicle is engaged in a curve;
- $\kappa = -\frac{V_{sx}}{V_x}$, slip ratio, it constitutes the abscissa of the longitudinal interaction characteristic (the "-" sign is introduced to have concord force and slip);
- $\alpha = \arctan\left(\frac{V_{sy}}{|V_y|}\right)$), slip angle, it constitutes the abscissa of the lateral interaction characteristic;
- γ, camber angle;
- F_z, vertical thrust exerted by the road on the wheel in correspondence of the contact patch, it coincides with the vertical load on the wheel centre;
- F_{z0}, nominal load used in the parametric identification by the manufacturer;
- $\lambda_{F_{z0}}$, scale factor of nominal (rated) load.
- $F'_{z0} = F_{z0}\lambda_{F_{z0}}$, vertical load scaled;
- $dF_z = \frac{F_z - F'_{z0}}{F'_{z0}}$, load increase with respect to the nominal condition (possibly scaled).

Sometimes the interaction characteristics dictated by the MF are significantly far from the experimental points detected by the telemetry. This is due

to the impossibility of faithfully reproducing in the laboratory the conditions of humidity, temperature, inflation pressure, adhesion, wear, taper which the tyre is subjected once mounted on a real vehicle.

To buffer this problem, scaling factors have been introduced that allow modulating macro parameters and modifying the shape of the curve due to experimental data. They are indicated with the letter λ and are listed in the table below 1.1 1.2.

Table 1.1 Scaling coefficient, pure slip

Name	Name used in tyre property file	Explanation
$\lambda_{F_{z0}}$	LFZO	Scale factor of nominal (rated) load
λ_{Cx}	LCX	Scale factor of F_x shape factor
$\lambda_{\mu x}$	LMUX	Scale factor of F_x peak friction coefficient
λ_{Ex}	LEX	Scale factor of F_x curvature factor
λ_{Kx}	LKX	Scale factor of F_x slip stiffness
λ_{Hx}	LHX	Scale factor of F_x horizontal shift
λ_{Vx}	LVX	Scale factor of F_x vertical shift
$\lambda_{\gamma x}$	LGAX	Scale factor of camber for F_x
λ_{Cy}	LCY	Scale factor of F_y shape factor
$\lambda_{\mu y}$	LMUY	Scale factor of F_y peak friction coefficient
λ_{Ey}	LEY	Scale factor of F_y curvature factor
λ_{Ky}	LKY	Scale factor of F_y slip stiffness
λ_{Hy}	LHY	Scale factor of F_y horizontal shift
λ_{Vy}	LVY	Scale factor of F_y vertical shift
$\lambda_{\gamma y}$	LGAY	Scale factor of camber for F_y
λ_t	LTR	Scale factor of peak of pneumtic trail
λ_{Mr}	LRES	Scale factor of offset of residual torque
$\lambda_{\gamma z}$	LGAZ	Scale factor of camber for Mz
λ_{Mx}	LMX	Scale factor of overturning couple
λ_{vMx}	LVMX	Scale factor of M_x vertical shift
λ_{My}	LMY	Scale factor of rolling resistance torque

Table 1.2 Scaling coefficient, combined slip

Name	Name used in tyre property file	Explanation
$\lambda_{x\alpha}$	LXAL	Scale factor of alpha influence on F_x
$\lambda_{y\kappa}$	LYKA	Scale factor of kappa influence on F_y
$\lambda_{Vy\kappa}$	LVYKA	Scale factor of kappa induced F_y
λ_S	LS	Scale factor of moment arm of F_x
$\lambda_{\sigma\kappa}$	LSGKP	Scale factor of relaxation length of F_x
$\lambda_{\sigma\alpha}$	LSGAL	Scale factor of relaxation length of F_y
λ_{gyr}	LGYR	Scale factor of gyroscopic torque

Chapter 2

TRICK tool for the grip loss evaluation

2.1 Introduction

The first grip estimation methodology described in this thesis is based on the Farroni's TRICK (Tyre/Road Interaction Characterization and Knowledge) tool [16], that is an "inverse" application of a vehicle model with the purpose of estimating the tyre behaviour. The "inverse" term is referred to the fact that the conventional vehicle models purpose is estimating the vehicle velocity and acceleration when the vehicle and tyre model is known, this tool instead, use the vehicle dynamics data as input, that must be previously acquired by sensor on experimental tests, in order to estimate the tyre behaviour in term of exerted tangential forces, slip ratio and slip angles.

The main aims for the original TRICK tool are:

- tyre characterization without test bench availability: complete and detailed studies of tyres in a wide range of working conditions are commonly carried out by means of complex, bulky and expensive test

benches; the proposed procedure allows to employ the vehicle as a moving lab, easily applying experimental and processing techniques.

- real thermal and frictional tyre characterization: tyre test rigs bring unavoidably to adoption of expedients useful to analyse tyres under controlled conditions, but that sometimes result to be quite far from reality; an example can be the employment of sliding flat belts, able to keep the tyre in rolling, but very different from real road as concerns roughness characteristics, stiffness and thermal conductivity. The possibility to test tyres under real working conditions allows to take into account the real effect of frictional and thermal phenomena, usually neglected or misestimated.

- tyre testing session results analysis: testing departments often employ the opinion of specialized drivers as unique tyre performance evaluation instrument; this essential subjective phase could be supported by a pure objective tool, able to provide an immediate comparison among the different tested tyres.

- race and test performances analysis: tyres directly influence the vehicle performances; consequently, a detailed analysis of the tangential interaction characteristics and of the effects that tyres generate on the whole vehicle behaviour can provide useful suggestions about the direction in which the performance improvement strategies should move.

- tyre models parameters identification: with the availability of a wide data set, eventually acquired by means of dedicated track sessions, it is possible to predict the behaviour of tyres in all its possible working configurations; it allows to identify physical [17–19] and empirical [13, 20] tire tyre models parameters, tuning their output in order to fit the experimental ones.

In this section is showed a methodology [21] that extends the capability of the TRICK model, increasing its estimation accuracy and using the data obtained to perform a road grip estimation able to be used in real time, that is a fundamental prerequisite for using electronic controls in vehicle dynamics, which are rapidly increasing their complexity and, consequently, the required accuracy from the measurement systems [22, 23].

The system uses dynamic equilibrium for the calculation of forces and kinematic relations for the calculation of slips. Due to the simplicity of the methodology, the TRICK is robust and requires a low computational burden. Moreover, during the last few years, it has been validated in real world using dynamometric hubs in situations of use of various surfaces, ranging from track to track in the motorsport field to the use in the snow applications with transport vehicles. To the validations in the real world can be also added those in the simulation field with diverse commercial software

The capabilities of the upgraded methodology are:

- Improve driving performance in motorsport, translating results into performance indicators that can be shown to the driver in real time within an intuitive interface.
- Inform the control systems of the actual tyre grip level at each corner to permit the optimization of the control strategies.
- Perform an offline characterization of the tyre in the same way as performed by the TRICK tool.

As mentioned before, the accuracy of the estimation process of the forces, both longitudinal and lateral, has been increased. Regarding the longitudinal forces, the force component induced by the steering was modeled separately, improving the distribution of the total longitudinal force measured by the accelerometer. Regarding the lateral forces, a procedure mixing up the forces estimated by the TRICK (based on the accelerometer signals) with those

estimated by the Pacejka model [13], has been specifically designed. Note that, although a tyre model is used into the process, this plays a marginal role, unlike what is performed by Kalman filter-based force estimators [24].

Finally, the estimated lateral forces are compared with those generated by a Pacejka of reference identified at full adherence. If the vehicle is in poor conditions, a difference between the two estimates can be observed.

2.2 The Algorithm

2.2.1 Algorithm summary

The algorithm is composed by the subsequent stages:

- Reading data from the CAN bus.
- Correction of the sensors offsets.
- Application of the low pass filter to the acquired data.
- Calculation of vertical tyre forces.
- Calculation of the lateral tyre forces in vehicle reference system.
- Calculation of the tyre steering angles.
- Calculation of the longitudinal tyre forces in vehicle reference system.
- Calculation of the tyre slip angles.
- Rotation of the tangential forces from vehicle reference system to wheel reference system.
- Calculation of the tyre slip ratio.
- Calculation of the tyre inclination angles.

- Calculation of the opposing component of lateral force.
- Comparison with the results of the known Pacejka model.

Each data sample acquired by sensors is processed with the operations, in the order indicated in the above list.

2.2.2 Input parameters

The system requires the following parameters:

- Vehicle mass and geometry: mass, centre of gravity height, inertia moment about vertical axis, front and rear wheelbase, front and rear track, wheels inertia moment about rotation axis, tyre effective rolling radius.
- Elasto-kinematic parameters of vehicle suspensions: static values of toe and camber, toe and camber compliances about the lateral force, steering ratio, Ackermann steering contribution, toe and camber variation respect to the suspension travel maps, camber variation due to the steering wheel angle.
- Aerodynamic characterization parameters: Vehicle front section area, C_x, C_z front, C_z rear.
- Correction values of the sensors obtained with appropriate procedures. [16]
- Pacejka parameters of the equipped tyre.

2.2.3 Input signals

The TRICK requires data acquired in the vehicle from the vehicle CAN (Control Area Network) [25]. In addition, measurements of the chassis

velocity are required, which must be provided by an optical sensor or an Inertial Measurement Unit (IMU) [26, 27].

The necessary signals are the following:

- Steering wheel angle δ_{sw}
- Chassis longitudinal and lateral velocity V_x and V_y
- Vehicle longitudinal and lateral acceleration a_x and a_y
- Vehicle yaw rate r
- Wheel angular speeds Ω_{ij}

2.2.4 Signal filtering

All input signals, before being used, are subjected to a low-pass filter. If the algorithm is employed in real-time, the calibration constant of the filter must be chosen by carrying out a trade-off between the eliminated noise and the delay of the filtered signal, which will determine the delay of the entire system. A recomended value of the cutoff frequency is 5 Hz.

2.2.5 Vehicle model

Vertical and lateral forces are calculated using dynamic equilibrium. Briefly exposing the formulas reported in the Guiggiani's book [10]:

$$F_{z_{ij}} = F_{zstat_{ij}} + \Delta F_{zlong_{ij}} + \Delta F_{zlat_{ij}} + F_{zaero_{ij}} \tag{2.1}$$

where:

- $F_{zstat_{ij}}$: Wheel static load.
- $F_{zstat_{ij}}$: Longitudinal load transfer.

- $\Delta F_{zlat_{ij}}$: Lateral load transfer.
- $F_{zaero_{ij}}$:aerodynamic force calculated from longitudinal velocity and aerodynamic parameters.

Lateral forces for each axle are calculated from the single-track model:

$$F_{y_1} = \frac{ma_y a_2 - J_z \dot{r}}{a_1 + a_2} \tag{2.2}$$

$$F_{y_2} = \frac{ma_y a_1 - J_z \dot{r}}{a_1 + a_2} \tag{2.3}$$

where:

- m: vehicle mass
- F_{y_1}: front axle lateral force
- F_{y_2}: rear axle lateral force
- J_z: vehicle moment of Inertia about z-axis
- $\dot{r}$: yaw acceleration
- a_1 and a_2 are the distances of front and rear axle to the COG

Assuming that wheel grip and slip stiffness are proportional to the vertical force applied on the tyre, the axle lateral force distribution between the two wheels can be calculated:

$$\overline{F}_{y_{ij}} = F_{y_i} \frac{F_{z_{ij}}}{F_{z_i}} \tag{2.4}$$

Where $\overline{F}_{y_{ij}}$ are the lateral forces exerted by the tyre on the axle i (1 front, 2 rear) and side j (1 left, 2 right) in the vehicle reference system, $F_{z_{ij}}$ is the tyre load, F_{y_i} and F_{z_i} are the lateral and vertical force on the i axle. Longitudinal forces calculation is carried out through two steps. First, the longitudinal forces that are not attributable to traction or braking are calculated:

- Rolling resistance
- Wheel inertia
- Longitudinal force from wheel steering

The steering component is calculated from another physical assumption: if the wheel is in free rolling, it can only exert a force perpendicular to its steering direction. If it is not in free rolling, the forces derived from the steering will simply be added to the others.

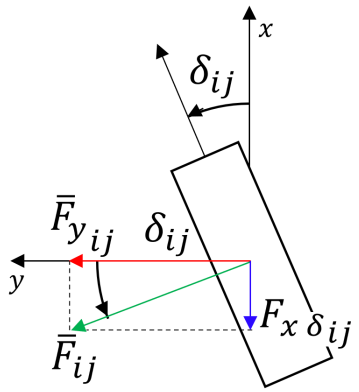

Fig. 2.1 Longitudinal forces from steering

From the figure is easy to find that:

$$F_{x\delta_{ij}} = -\overline{F}_{y_{ij}} \tan(\delta_{ij}) \tag{2.5}$$

Longitudinal force is not obtained by the rotation of lateral forces. The lateral force (in vehicle reference system) is previously calculated from the dynamic equilibrium, the longitudinal component must exist because the resultant force from the pure lateral interaction must be perpendicular to the wheel. Then, all known forces are summed (including aerodynamic), if this sum is not equal to mass times acceleration, the difference must be given by traction or braking.

$$F_{x_{mdl}} = \sum_{ij}(F_{xI_{ij}} + F_{xRR_{ij}} + F_{x\delta_{ij}}) - \frac{1}{2}d_a C_d A V_x^2 \tag{2.6}$$

Where $F_{x_{mdl}}$ is the total longitudinal force exerted from components that can be obtained from the modeling of a specific phenomena: $F_{xI_{ij}}$ is the component that balances the wheel rotational acceleration, $F_{xRR_{ij}}$ balances the rolling resistance, $F_{x\delta_{ij}}$ is the already discussed force from steering and the last term is the aerodynamic drag. d_a is the air density, C_d is the drag coefficient, A is the frontal section area.

$$F_{xI_{ij}} = -\frac{\dot{\Omega}_{ij} J_{y_w}}{R_e} \tag{2.7}$$

Where J_{y_w} is the wheel inertia moment around the hub axis and R_e is the effective rolling radius.

$$F_{xRR_{ij}} = -C_{RR_{ij}} F_{z_{ij}} \tag{2.8}$$

Where $C_{RR_{ij}}$ is the rolling resistance coefficient of the tyre.

Once $F_{x_{mdl}}$ is defined, it can be used to calculate the longitudinal force on a single wheel.

$$\overline{F}_{x_{ij}} = F_{xI_{ij}} + F_{xRR_{ij}} + F_{x\delta_{ij}} + (ma_x - F_{x_{mdl}})TBD_{ij} \tag{2.9}$$

The tyre longitudinal force $\overline{F}_{x_{ij}}$ in the vehicle reference system can be found from the sum of all the mentioned components, $F_{xI_{ij}}$, $F_{xRR_{ij}}$ and $F_{x\delta_{ij}}$, plus the component provided by the engine or the brakes, that is equal to $ma_x - F_{x_{mdl}}$, splitted on the four tyres though the ratio TBD.

It must be higlighted that, following those rules, the vehicle longitudinal equilibrium is always respected, the following can be obtained by substituting 2.6 in 2.9, taking in account that the sum of TBD_{ij} is always 1:

$$X = \sum_{ij}(\overline{F}_{x_{ij}}) = ma_x + \frac{1}{2}d_a C_d A V_x^2 \tag{2.10}$$

TBD (traction or braking distribution) is a matrix that represents how the total traction, or braking force is distributed through the four wheels. *TBD* can assume three values:

For braking manoeuvres: $ma_x - F_{x_{mdl}} < 0$

$$TBD = \frac{1}{2}\begin{bmatrix} \frac{F_{z_1}}{F_{z_1}+F_{z_2}} & \frac{F_{z_1}}{F_{z_1}+F_{z_2}} \\ \frac{F_{z_2}}{F_{z_1}+F_{z_2}} & \frac{F_{z_2}}{F_{z_1}+F_{z_2}} \end{bmatrix} \tag{2.11}$$

where F_{z_1} and F_{z_2} are the vertical forces on the vehicle axles. The braking force is assumed proportional to the total vertical force on each axle and split in equal parts in each side.

For braking manoeuvres: $ma_x - F_{x_{mdl}} > 0$

- For vehicles with rear traction, equipped with open differential:

$$TBD = \begin{bmatrix} 0 & 0 \\ \frac{1}{2} & \frac{1}{2} \end{bmatrix} \tag{2.12}$$

  The traction force is assumed split in equal parts in each side of the rear axle.

- For vehicles with rear traction, with no differential (or limited slip differential, which is modelled as locked):

$$TBD = \begin{bmatrix} 0 & 0 \\ \frac{F_{z_{12}}}{F_{z_2}} & \frac{F_{z_{22}}}{F_{z_2}} \end{bmatrix} \tag{2.13}$$

  The traction force is assumed proportional to the distribution of the vertical force on the rear axle.

Note that, when TBD is switched, $ma_x - F_{x_{mdl}} = 0$. This grants that the function $\overline{F}_{x_{ij}}$ vs time is always continuous, despite TBD vs time is not.

Once all forces on vehicle reference system are calculated, those can be rotated on wheel reference system:

$$\begin{bmatrix} F_{x_{ij}} \\ F_{y_{ij}} \end{bmatrix} = \begin{bmatrix} \cos(\delta_{ij}) & \sin(\delta_{ij}) \\ -\sin(\delta_{ij}) & \cos(\delta_{ij}) \end{bmatrix} \begin{bmatrix} \overline{F}_{x_{ij}} \\ \overline{F}_{y_{ij}} \end{bmatrix} \tag{2.14}$$

where $F_{x_{ij}}$ and $F_{y_{ij}}$ are the forces in vehicle reference system, $\overline{F}_{x_{ij}}$ and $\overline{F}_{y_{ij}}$ are the forces in vehicle reference system.

The described procedure calculates the axle forces from the single-track model, these are then split between the sides, proportionally to the vertical load. This equation set has proven to be robust and accurate in most of cases [10], but specific situations where the estimated forces are less accurate (according to the reference model in Vi-CarRealTime) has been identified.

The TRICK equation set is not able to detect the opposing side forces generated by the thrust of the static toe and the camber, this component is extremely reduced in the condition of high slip angles, but more consistent at low slip, particularly when the vehicle travels straight. In these situations, the comparison with the reference Pacejka model can be difficult, both because the estimation error is higher, and because the forces are overall low.

The correction of the force generated by the wheel toe starts from the assumption that, in the case of axles with parallel wheels, the lateral forces estimated by the TRICK are correct. If the wheels are not parallel, to these must be added a force component Fto_{ij} derived from the contribution of the static toe.

$$F_{y_{ij}} = F_{y_i} \frac{F_{z_{ij}}}{F_{z_i}} + Fto_{ij} \tag{2.15}$$

Fto_{ij} is calculated starting from the force Ft_{ij} which is equal to the slip stiffness K_{ij} of the wheel at a given instant, multiplied by the static toe.

$$Ft_{ij} = \delta_{stat_{ij}} K_{ij} \tag{2.16}$$

The slip stiffness is obtained from the partial derivative of the Pacejka formula respect to the slip angle at the given time.

$$K_{ij} = \frac{\partial Pacejka(\alpha_{ij}, F_{z_{ij}}, \gamma_{ij})}{\partial \alpha_{ij}} \tag{2.17}$$

The force contribution due to the static toe Ft_{ij} is separated into two components: Ftc_{ij} the concordant component, which contributes to the axle force, and Fto_{ij} the opposite component which does not contribute to the axle force.

$$Ft_{i1} = Ft_{i1} - \frac{Ft_{i1} + Ft_{i2}}{2} + \frac{Ft_{i1} + Ft_{i2}}{2} = Fto_{i1} + Ftc_{i1} \tag{2.18}$$

$$Fto_{i1} = Ft_{i1} - \frac{Ft_{i1} + Ft_{i2}}{2} \tag{2.19}$$

$$Ftc_{i1} = \frac{Ft_{i1} + Ft_{i2}}{2} \tag{2.20}$$

Similarly, Fto_{i2} and Ftc_{i2} can be derived. It can be verified that Fto_{ij} does not contribute to the axle force since:

$$Fto_{i1} + Fto_{i2} = Ft_{i1} - \frac{Ft_{i1} + Ft_{i2}}{2} + Ft_{i2} - \frac{Ft_{i1} + Ft_{i2}}{2} = 0 \tag{2.21}$$

Therefore, only Ftc_{ij} provides a contribution to the axle force, but since this is already correctly estimated from the single-track model, this component must not be considered. Fto_{ij}, instead, not contributing to the axle force, has influence only in the distribution of forces between the two sides.

The opposing forces of camber can be estimated from the simple model:

$$Ftc_{ij} = F_{z_{ij}} \sin(\gamma_{ij}) K_{\gamma} \tag{2.22}$$

where K_γ must be known from the reference Pacejka model. Also, in this case, it must be considered that the camber forces have a non-zero result, but this result is already included since it is calculated by the single-track model. For this reason, the same procedure must be carried out as was done for the forces generated by the static toe to separate the component that contributes to the axle thrust Fcc_{ij} from the opposite component Fco_{ij}.

$$Fco_{i1} = Fc_{i1} - \frac{Fc_{i1} + Fc_{i2}}{2} + Ft_{i2} \tag{2.23}$$

$$Fco_{i2} = Fc_{i2} - \frac{Fc_{i1} + Fc_{i2}}{2} + Ft_{i2} \tag{2.24}$$

Finally, Fcc_{ij} will be added to the already calculated lateral force which will result:

$$F_{y_{ij}} = F_{y_i} \frac{F_{z_{ij}}}{F_{z_i}} + Fto_{ij} + Fco_{ij} \tag{2.25}$$

Please note that, to respect industrial confidentiality agreements, plots and diagrams will be shown as normalized.

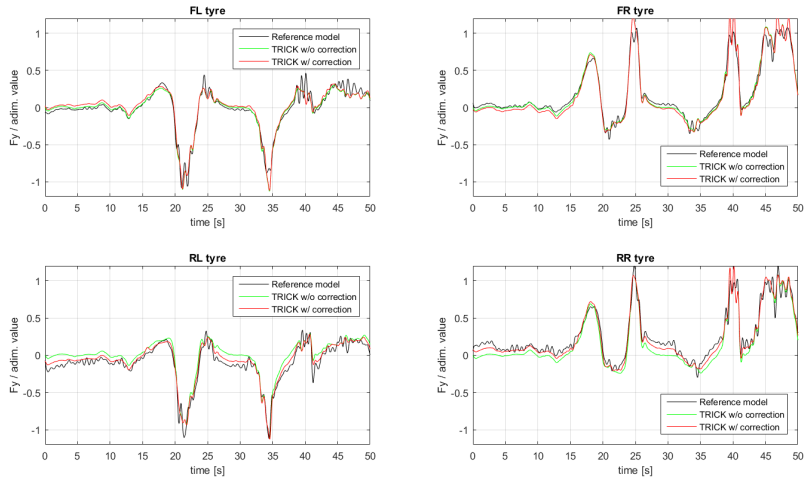

Fig. 2.2 TRICK tyre forces with static toe correction

Figure 2.2 shows the comparison between the reference model, (commercial VD simulation software) TRICK forces without correction and TRICK forces with slip angle correction. The vehicle runs with toe out on the front axle (negative), and toe in on the rear axle (positive). The camber angle is closed (negative) on both axles. On the rear axle the toe and the camber forces are directed to the same direction, so the toe force correction gives only a partial improvement. On the front axle, toe and camber forces are pushing to opposite sides and are cancelling themselves, so considering the toe correction only doesn't improve the force estimation accuracy.

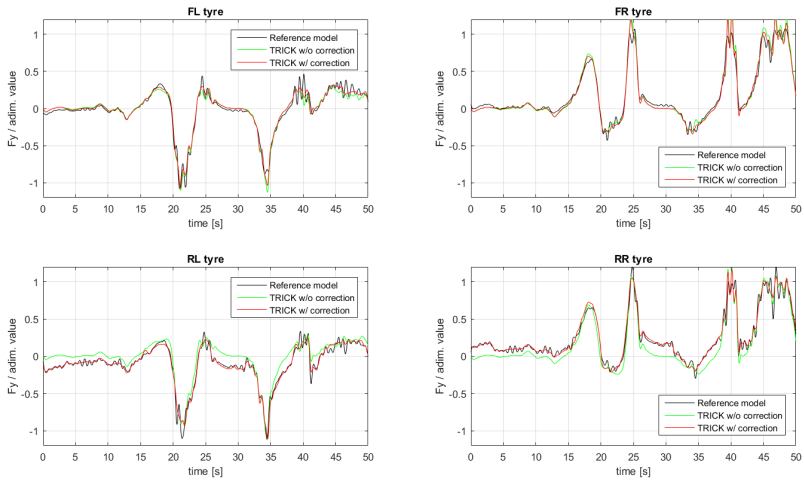

Fig. 2.3 TRICK tyre forces with static toe and camber correction

Figure 2.3 shows the comparison between the reference model, TRICK forces without correction and TRICK forces with both toe and camber correction. On the front axle the toe correction is cancelled by the camber correction. On the rear axle, the camber correction provides the additional force needed to match the reference model force. Delta angles (steering angles) are calculated through this formula:

$$\delta_{ij} = \delta_{steer} + \delta_{ak_{ij}} + \delta_{stat_{ij}} + C_{sf_{ij}} F_{y_{ij}} + C_{\delta fax_i} F_{y_i} + \delta_{Fz_{ij}}(F_{z_{i1}}, F_{z_{i2}}) \quad (2.26)$$

where:

- δ_{steer}: Steering wheel angle divided by the steering ratio.
- $\delta_{ak_{ij}}$: Ackermann steering contribution.
- $\delta_{stat_{ij}}$: Static toe angle.
- $C_{sf_{ij}}$: Toe variation due to lateral wheel force (in vehicle reference system).
- $C_{\delta fax_i}$: Toe variation due to lateral axle force (in vehicle reference system, its value is 0 for rear axle).
- $\delta_{Fz_{ij}}(F_{z_{i1}}, F_{z_{i2}})$: Nonlinear relationship, which models the toe variation due to suspension travel.

Inclination angles γ_{ij} are obtained with:

$$\gamma_{ij} = \gamma_{stat_{ij}} + C_{\gamma f_{ij}} F_{y_{ij}} + \gamma_{Fz_{ij}} F_{z_{ij}} + \gamma_{\delta_{ij}} + \phi \tag{2.27}$$

where:

- $\gamma_{stat_{ij}}$: Static inclination angle
- $C_{\gamma f_{ij}}$: Inclination angle variation due to lateral wheel force (in wheel reference system)
- $\gamma_{Fz_{ij}}$: Inclination angle variation due to suspension travel
- $\gamma_{\delta_{ij}}$: Inclination angle variation due to steering wheel angle
- ϕ: Vehicle roll angle

All listed coefficients must be found fitting the data from kinematics & compliance apparatus or provided directly from car manufacturer.

2.3 Comparison of TRICK forces with Pacejka model

Once the TRICK forces are calculated and corrected, these can be compared to the forces generated by the Pacejka model which uses reference coefficients (pre-identified). The model calculates the F_x and F_y tangential forces starting from inputs calculated by the trick model: Vertical forces, Slip Ratios, Slip Angles and Inclination Angles.

The coefficients of the Pacejka model are identified in conditions of full adherence, so if the vehicle is in the same identification conditions, the forces estimated by the TRICK must overlap with Pacejka forces. In poor grip conditions, instead, a deviation between the two signals will be observed. This difference is the lack of adherence to be measured.

The estimation of the available grip is carried out through the analysis of the lateral interaction, differently from that performed in other works that prefer longitudinal interaction [28, 29]. This due to the simplicity of the slip angles estimate compared to the slip ratio.

Please note that, to respect industrial confidentiality agreements, plots and diagrams will be shown as normalized.

Figure 2.4 shows the vehicle forces in a Slow Ramp Steer with open loop performed in a commercial Vehicle Dynamics simulation software. The vehicle runs in the same conditions as the Pacejka coefficients have been identified. TRICK forces (red) are overlapped with the Pacejka forces. Note that, in the first moments, when the manoeuvre has not yet begun, the forces on the rear axle are not null, despite the acceleration it is. Without the correction, the TRICK forces would be as null as the acceleration. In this case the correction relative to the toe and camber forces is necessary to make the TRICK forces congruent with the Pacejka.

Figure 2.5 shows the vehicle forces in the same Slow Ramp Steer with open loop showed in figure 2.4, but in this case, the coefficient of road friction

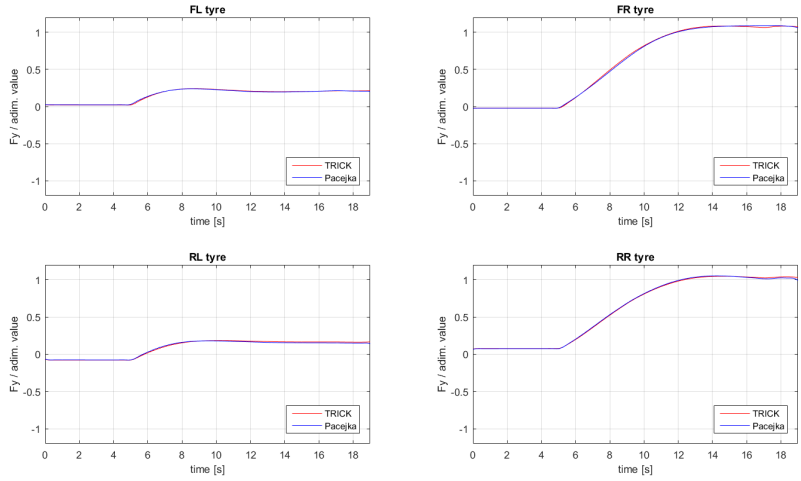

Fig. 2.4 Comparison between Pacejka reference model and TRICK forces with normal grip coefficient

has been specifically reduced. The test is an "open loop", i.e. without the feedback that a virtual pilot would have applied, which would keep the tyre within the grip area. As expected, the discrepancy between the two signals is caused by the grip difference between the identification conditions of the Pacejka model and the operating conditions. Therefore, the system is able to detect the lack of grip and can give a feedback to the driver or control systems.

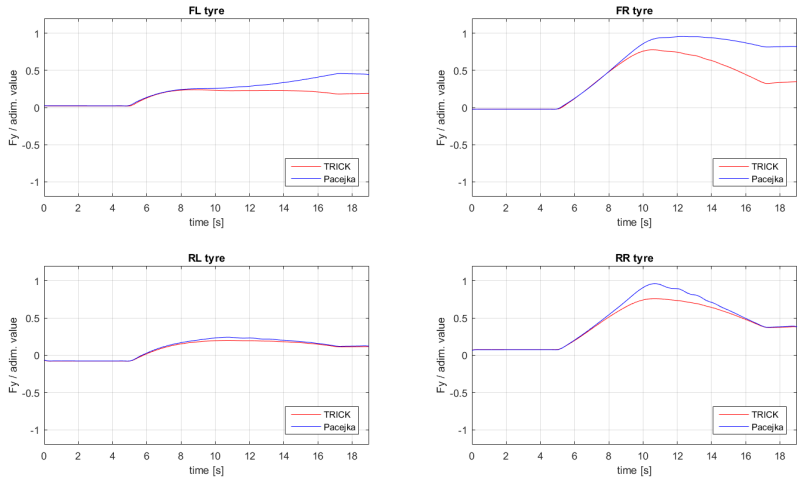

Fig. 2.5 Comparison between Pacejka reference model and TRICK forces with low grip coefficient

Chapter 3

Identification of Tyre Transient Parameters from Vehicle Onboard Sensors Data

3.1 Introduction

Correctly simulating the behavior of the vehicle is now becoming fundamental for manufacturers in its prototyping phase, when, even in the early stages of design, there is the need to correctly predict and reproduce all aspects of vehicle motion, including the driver's feedback, which is heavily affected by delays between inputs and the system dynamics [30].

The transient behavior of the car is mainly governed by the tyres, but also the construction characteristics of the vehicle itself play a fundamental role. This methodology based on the use of a vehicle model conceived to be as simple as possible, but which includes all the effects necessary to accurately reproduce the vehicle lateral transient dynamics, excluding those that have negligible influence on it [31].

The model receives as inputs the vehicle's acquisitions of longitudinal speed and steering, giving as an output lateral speed, lateral acceleration,

yaw speed and yaw acceleration. These quantities are compared with the experimental acquisitions coming from outdoor test sessions. The delay between the tyre slip angle and the exterted force, known as the relaxation length, which is directly related to the tyre carcass lateral stiffness, is identified within the described methodology, then, the parameters are tuned to minimize the difference between experimental and model output. During the process, also the instantaneous tyre carcass lateral deflection is estimated.

Those quantities can be directly measured on a rolling tyre with traditional methods like a test bench [32] or on a vehicle, using a rim mounted camera and markers on the tyre inner liner [33].

The approach followed here, based on running a vehicle simulation to validate results through transfer function analysis, has been followed also by [34–36] using single-track model without roll motion but, during this study, has emerged that roll is necessary to get correlation with experimental data at frequencies higher than 2 Hz. The simulative approach is also used to analyze the steer response [37], where a single-track model with roll is used. A single-track with roll can follow experimental results at frequency higher than 2 Hz, but the purpose of this work is the identification of a single tyre parameters, so, a double-track model will be necessary.

The tyre characteristics estimated by this procedure can be used also to parametrize physical tyre models like [38–40] without using bench tests.

The double-track model, developed specifically for this purpose, was validated for the proposed maneuver both on experimental data and simulation data from a digital twin of the vehicle, developed by the manufacturer in the Vi-CarRealTime software environment.

3.2 Proposed Methodology

The target parameter of the identification procedure is the tyre carcass lateral stiffness, C_{F_y}, from which the relaxation length σ_α is obtained:

$$\sigma_\alpha = \frac{C_{F\alpha}}{C_{F_y}} \tag{3.1}$$

Where $C_{F\alpha}$ is the cornering stiffness. The lateral relaxation length σ_α is the spatial shift between the slip angle calculated on the rim, α, and contact patch's slip angle α', that feeds the Magic Formula from which the lateral force F_y is calculated [13].

$$\frac{\sigma_\alpha}{V_x}\frac{\partial \alpha'}{\partial t} + \alpha' = \alpha \tag{3.2}$$

The identification of the unknown parameters, $C_{F_{y_1}}$ and $C_{F_{y_2}}$ (subscripts indicate axle). Right and left wheel are assumed identical, so there is only one parameter per axle. The identification procedure takes place according to the procedure shown in Fig 3.1:

From the vehicle acquisitions of longitudinal velocity V_x, lateral velocity V_y, lateral acceleration a_y, yaw rate r and steering wheel angle δ_{sw}, six transfer functions are calculated. The transfer functions show the behavior of the single-track model corresponding to the real vehicle [11].

The transfer functions are (s is the Laplace transform domain variable):

- $\frac{a_y(s)}{\delta(s)}$: lateral acceleration / steering angle at ground
- $\frac{r(s)}{\delta(s)}$: yaw rate / steering angle at ground
- $\frac{\beta(s)}{a_y(s)}$: side-slip angle / lateral acceleration
- $\frac{\beta(s)}{r(s)}$: side-slip angle / yaw rate

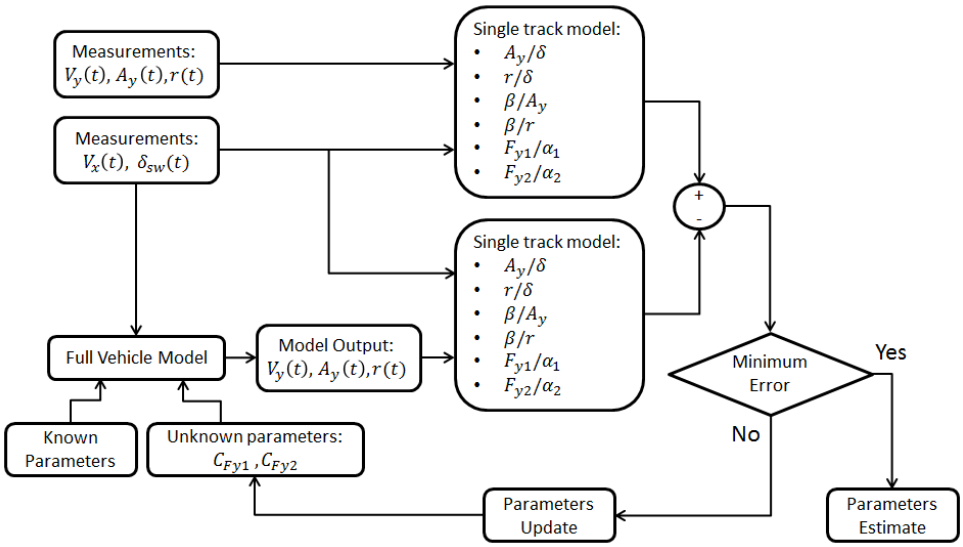

Fig. 3.1 Identification procedure scheme

- $\frac{F_{y_1}(s)}{\alpha_1(s)}$: front axle lateral force / front axle slip angle
- $\frac{F_{y_2}(s)}{\alpha_2(s)}$: rear axle lateral force / rear axle slip angle

All the transfer functions of the single-track model are dependent on the axle characteristics $C_{\alpha_1}(s) = \frac{F_{y_1}(s)}{\alpha_1(s)}$ and $C_{\alpha_2}(s) = \frac{F_{y_2}(s)}{\alpha_2(s)}$. F_{y_i} are the axle lateral forces, and α_i are the axle slip angles.

$$F_{y_1} = \frac{ma_y a_2 + J_z \dot{r}}{a_1 + a_2} \tag{3.3}$$

$$F_{y_2} = \frac{ma_y a_1 - J_z \dot{r}}{a_1 + a_2} \tag{3.4}$$

$$\alpha_1 = \tau \delta_{sw} - \frac{V_y + r a_1}{V_x} \tag{3.5}$$

$$\alpha_2 = -\frac{V_y - r a_2}{V_x} \tag{3.6}$$

Where m is the total mass of the vehicle, J_z is the yaw inertia moment, a_1 and a_2 are the axle distances from the center of gravity, τ is the steering ratio, V_x is the longitudinal velocity of the center of gravity (CG) and V_y is the lateral velocity .

Longitudinal velocity V_x, steering wheel angle δ_{sw}, lateral velocity V_y, lateral acceleration a_y and yaw rate r are required inputs for the methodology. Those experimental acquisition are divided on two categories: model inputs and validation quantities. Longitudinal velocity V_x and steering wheel angle δ_{sw} are used as input for the double-track vehicle model, which gives as output simulation results for a_y, V_y and r, those, will be correlated to the experimental ones in the frequency domain, though the transfer functions. Fig. 3.2 shows the comparison between the single-track model transfer functions coming from reference model outputs (black) and from the double-track model developed in the presented work (red). The reference model is at the state of the art, and its results were provided by Maserati.

A model capable of faithfully reproduce the axle characteristics at varying frequencies will also coincide with the real on all the other transfer functions, because all the single-track model dynamics is determined from axle characteristics and other few macro-parameters that are given as known in this work: vehicle mass, rotational inertia, wheelbase, center of gravity longitudinal position and steering ratio [11]. The gain values of $C_{\alpha_1}(s)$ and $C_{\alpha_2}(s)$ are determined by the known parameters: tyre cornering stiffness pre-identified with laboratory procedures or on-board identification methodologies like [16, 41, 42], while the delay values are determined by both the known and unknown parameters: the tyre carcass lateral stiffness C_{Fy_1} and C_{Fy_2}.

By varying the tyre carcass stiffness, the delays of $C_{\alpha_1}(s)$ and $C_{\alpha_2}(s)$ vary uniformly over the entire frequency range, therefore determining the appropriate values is a simple task even without using an optimization algorithm. Once the procedure is completed, all model transfer function will coincide with experimental ones, and C_{Fy_1}, C_{Fy_2} will be assumed correct.

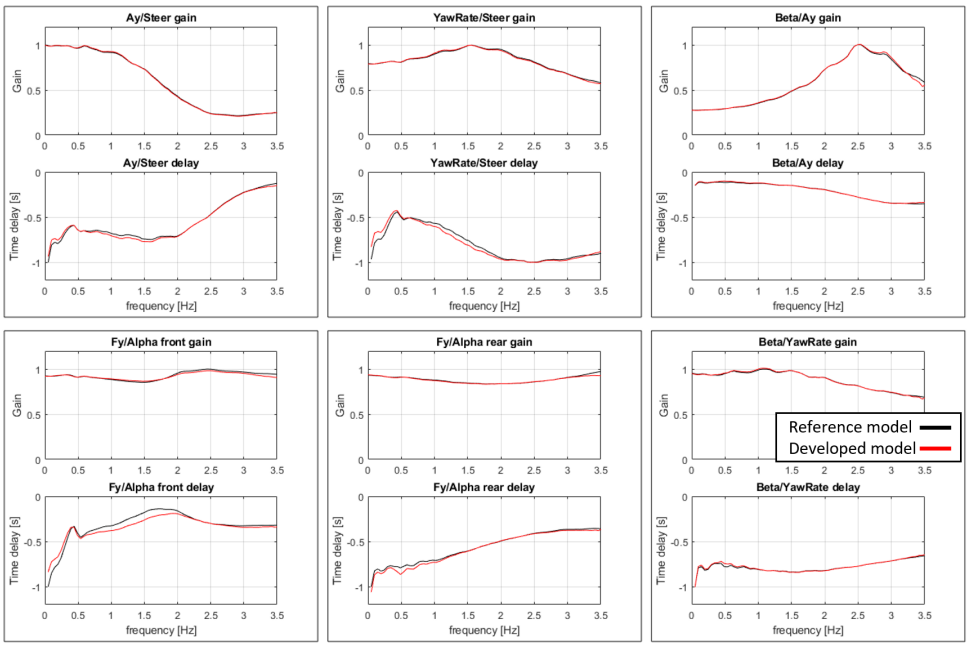

Fig. 3.2 Single-Track model transfer functions, reference model vs developed model

In order to obtain the actual transfer functions from the procedure shown, it is necessary that the tests were performed at constant longitudinal velocity and sinusoidal steering angle, at increasing frequency (chirp signal). Constant longitudinal velocity is needed because, according to equation 3.2, the phase shift between force and slip angle is inversely proportional to the vehicle speed, keeping it constant ensures that frequency is the only variable that induces a delay variation. The "chirp" shaped steering wheel angle excite the system in all the desired frequency range, that has been chosen from 0 to 3.5 Hz, as shown in figure 3.3. The amplitude of the steering sinusoids should be chosen in order to keep the tyre into their linear range, so the vehicle should reach lateral accelerations between $0.3\frac{m}{s^2}$ and $0.5\frac{m}{s^2}$.

Y-axis in figure 3.2 are hidden for industrial agreements.

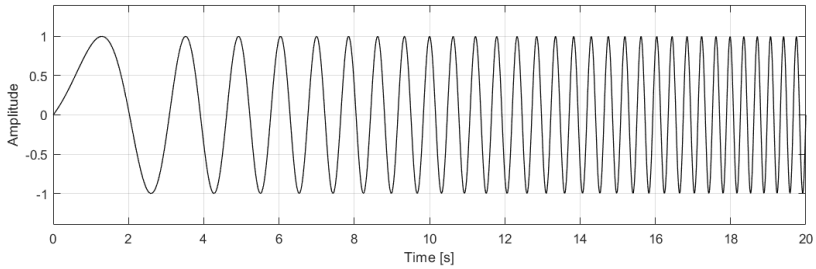

Fig. 3.3 Chirp shaped signal, amplitude 1, from 0.1 to 3.5 Hz over 20 seconds.

3.3 Double-track model

The model used to replicate the behaviour of the real vehicle in the experimental test manouvers is a double-track with seven degrees of freedom:

- Lateral translation
- Yaw
- Roll
- 4 DoF relative to the lateral translation of the tyre contact patches respect to the wheel center

The simulation inputs are the acquisitions of steering angle and longitudinal speed. With imposed longitudinal speed, only the lateral dynamics is modeled.

Figures 3.4 and 3.5 shows the degrees of freedom of the model: the lateral speed V_y, the yaw rate r, the roll angle ϕ, the lateral velocities of the contact patches $V'_{y_{ij}}$ ($i = 1$ for front axle, $i = 2$ for rear axle, $j = 1$ for left side, $j = 2$ for right side).

The angles β_{ij} and α_{ij} shown in the figure are calculated with:

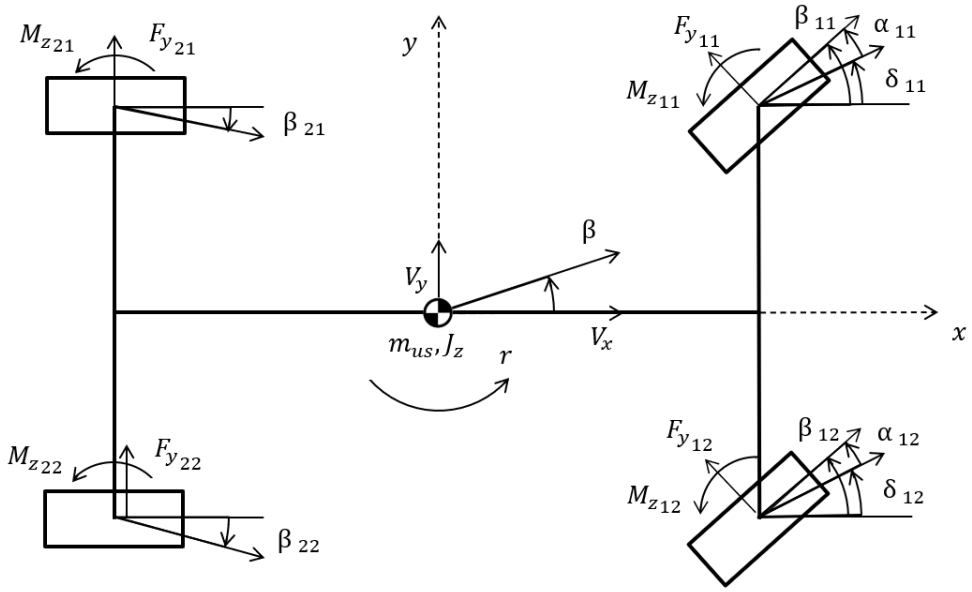

Fig. 3.4 Double-track model, top view

$$\beta_{ij} = \arctan\left(\frac{V_y + x_{ij} r}{V_x + y_{ij} r}\right) \tag{3.7}$$

$$\alpha_{ij} = \beta_{ij} - \delta_{ij} \tag{3.8}$$

Where β_{ij} are the tyre velocity vector angles in vehicle reference system α_{ij} the slip angles δ_{ij} the steering angles, determined from a formula that requires parameter obtained from kinematic and compliance data (KnC). x_{ij} and y_{ij} are the tyre coordinates in vehicle reference system, calculated from the vehicle track t_1, t_2 and the axle distance from CG a_1 and a_2. Note that, at the rear axle, the δ_{2j} angles are not shown in the figure for simplification, but are included in the model and are not null due suspension elasto-kinematic.

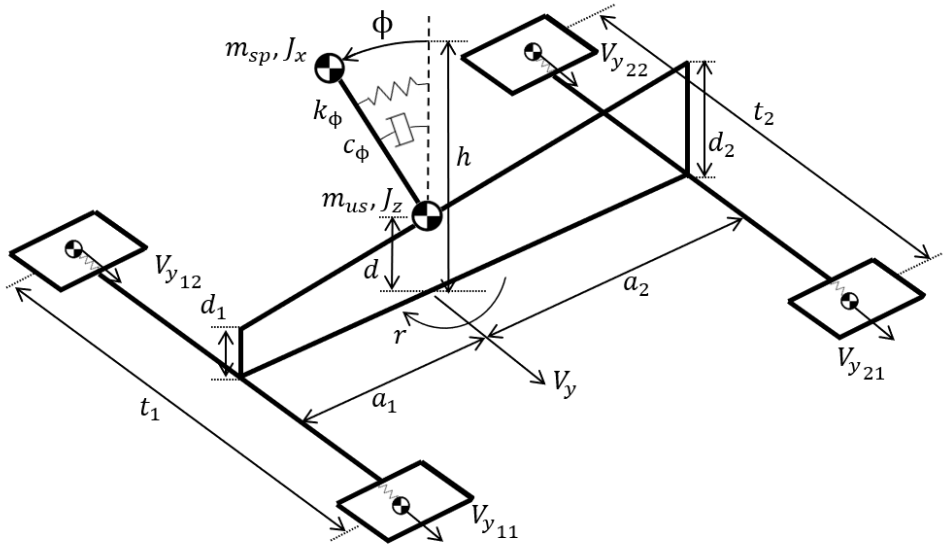

Fig. 3.5 Double-track model, lateral view

Tyre lateral forces $F_{y_{ij}}$ and aligning moment $M_{z_{ij}}$ are calculated using Pacejka's Magic Formula, that requires parameters identified from test bench data or experimental steady state maneuvers [41, 42].

$$F_{y_{ij}} = F_{y_{ij}}(F_{z_{ij}}, \alpha_{ij}, \gamma_{ij}, \rho_{ij}) \tag{3.9}$$

$$M_{z_{ij}} = M_{z_{ij}}(F_{z_{ij}}, \alpha_{ij}, \gamma_{ij}, \rho_{ij}) \tag{3.10}$$

Where $F_{z_{ij}}$ are the tyre vertical forces, γ_{ij} the inclination angles and ρ_{ij} the parameters of the Magic Formula.

The lateral force forces obtained will be in the wheel reference system, which must be projected into the vehicle reference system, using a simple rotation matrix by the angle δ_{ij}, obtaining the four tyre lateral forces in vehicle reference system Y_{ij}, that added together return the total lateral force

Y applied on the unsprung mass m_u. The Y_{ij} forces also contribute to the total yaw moment N, which accelerates the entire inertia vehicle J_z to rotation.

$$N = \sum_{ij}(Y_{ij}x_{ij} + M_{z_{ij}}) \tag{3.11}$$

3.3.1 Roll Dynamics

The sprung mass is connected to the roll center, at distance d from ground, and rotates around it in the yz plane. The roll center height is calculated from the axle roll centers d_1 and d_2.

$$d = \frac{a_2 d_1 + a_1 d_2}{a_1 + a_2} \tag{3.12}$$

In the developed model, the rotational motion was approximated to translational assuming small angles. the inertia moment appears as the sum between m_s and a translational inertance J_{res}.

$$J_{res} = \frac{J_x}{(h-d)^2} - m_s \tag{3.13}$$

Mass matrix M is structured as follows:

$$M = \begin{bmatrix} m_s + J_{res} & -J_{res} \\ -J_{res} & m_u + J_{res} \end{bmatrix} \tag{3.14}$$

The rotational stiffness k_ϕ is calculated from the roll angle value at 1 g. The effect of gravity acceleration is proportional to the roll angle, like the effect of the spring. By calculating k_ϕ as in the following formula, the effect of gravity is included.

$$k_\phi = \frac{m_s g(h-d)}{\phi_{1g}} \tag{3.15}$$

The damping value c_ϕ must be calculated starting from the characteristic of the shock absorbers.

The stiffness and damping matrices are:

$$K = \begin{bmatrix} k_\phi & -k_\phi \\ -k_\phi & k_\phi \end{bmatrix} / (h-d)^2 \tag{3.16}$$

$$C = \begin{bmatrix} c_\phi & -c_\phi \\ -c_\phi & c_\phi \end{bmatrix} / (h-d)^2 \tag{3.17}$$

Now that the single elements of the lateral dynamics are defined, the following differential equation can be written:

$$M\left(\begin{bmatrix} \ddot{y'}_s \\ \ddot{y'}_u \end{bmatrix} + ur\right) + C\begin{bmatrix} \dot{y'}_s \\ \dot{y'}_u \end{bmatrix} + K\begin{bmatrix} y'_s \\ y'_u \end{bmatrix} = \begin{bmatrix} 0 \\ Y \end{bmatrix} \tag{3.18}$$

Where y'_s and y'_u are the positions of the sprung and unsprung masses. From this point, $\dot{y'}$ will be indicated as V_y and $\ddot{y'}$ as $\dot{V}_y$. Lateral acceleration is:

$$a_y = \dot{V}_y + V_x r \tag{3.19}$$

The roll angle ϕ and the roll rate $\dot{\phi}$ are obtained from mass lateral position:

$$\phi = \frac{y'_s - y'_u}{h-d} \tag{3.20}$$

$$\dot{\phi} = \frac{V_{y_s} - V_{y_u}}{h-d} \tag{3.21}$$

Where V_{y_s} and V_{y_s} are the lateral velocities of the sprung and unsprung masses.

3.3.2 Vertical forces

The vertical forces $F_{z_{ij}}$ are obtained from the sum of static term F_{zS_i}, rigid load transfer ΔF_{zR_i}, spring and damping load transfers ΔF_{K_i} and ΔF_{D_i}. Subscripts

indicates axle and side, terms with one subscript term only are equal for both sides of the axle.

$$F_{z_{i1}} = F_{zS_i} + \Delta F_{zR_i} + \Delta F_{K_i} + \Delta F_{D_i} \tag{3.22}$$

$$F_{z_{i2}} = F_{zS_i} - \Delta F_{zR_i} - \Delta F_{K_i} - \Delta F_{D_i} \tag{3.23}$$

The static load depends on mass and CG axle distances a_i, and its constant:

$$F_{zS_i} = \frac{mg(a_1 + a_2 - a_i)}{2(a_1 + a_2)} \tag{3.24}$$

The rigid load transfer calculated from the equilibrium equation between the overturning moment on the axle roll center, induced by its lateral acceleration times its height, and the vertical load transfer times the axle track.

$$\Delta F_{zR_1} = \frac{(ma_2 a_{y_u} + J_z)d_1}{(a_1 + a_2)t_1} \tag{3.25}$$

$$\Delta F_{zR_2} = \frac{(ma_1 a_{y_u} + J_z)d_2}{(a_1 + a_2)t_2} \tag{3.26}$$

Spring and damping load transfer are induced by the variation of roll angle. This term are always delayed respect to the rigid term:

$$\Delta F_{K_i} = -\frac{k_{\phi i}\phi}{t_i} \tag{3.27}$$

$$\Delta F_{D_i} = -\frac{c_{\phi i}\dot{\phi}}{t_i} \tag{3.28}$$

3.3.3 Steering subsystem

The steering wheel is connected to the wheels through the steering system, which is made up of several mechanical components that are subjected to

severe mechanical stresses that induce deformations that alter the relative position between the steering wheel and wheels. Considering a typical design configuration where the steering axis intercepts the ground at a point ahead than the wheel center projection on the ground, the steering force generated at the wheel-road contact point will tend to decrease the steering angle of the wheels, making request a higher angle at the wheel. If the steering system is softer, the cornering stiffness of the axle decreases.

In a non-stationary maneuver such as the one described in section 3.2, the deviation between the steering angle at the steering wheel and the wheels will have an impact on the transfer function of the $\frac{F_{y_1}(s)}{\alpha_1(s)}$ front axle characteristic shown in figure 3.2, impacting both gain and in the delay of the transfer function. To achieve congruence between simulation and experimental, correct modeling and parameterization of the steering system is necessary. As part of this work, different model configurations were tested, at different complexities, trying to include only the modeling complexity necessary to make the model accurate in the domain of the analysis in question.

A configuration with only one degree of freedom was chosen, the position of the rack, where various mechanical elements appear, including the spring and torsional damper of the steering column and the clutch of the sliding of the rack. The various elements of the steering column are modeled as a single element.

The following differential equation describes the steering system dynamics:

$$m_r\ddot{x}_r + F_s(x_r - \tau_{sr}\delta_{sw}, V_x) + \frac{D_s}{\tau_{sr}^2}(\dot{x}_r - \tau_{sr}\dot{\delta}_{sw}) + F_r \tanh\left(\frac{K_r}{F_r}\dot{x}_r\right) = \frac{M_k}{\tau_{ta}} \quad (3.29)$$

Where x_r is the steering rack position, m_r is the apparent mass of the rack (includes the mass of the toe link and the rotational inertia of the front wheels multiplied by the toe link arm length), F_s is the force exterted by the steering column elasticity and the power steering together, τ_{sr} is the ratio between the

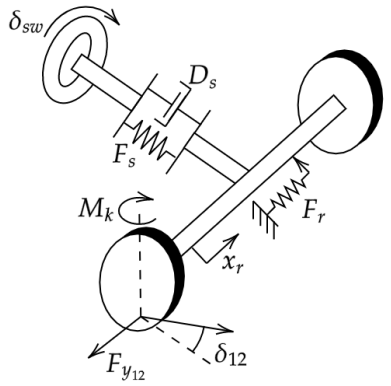

Fig. 3.6 Steering system model

steering wheel rotation and the rack translation, V_x is the vehicle longitudinal speed, D_s is the rotational damping of the steering system, F_r is the rack friction force saturation, K_r is the rack friction stiffness, M_k is the kingpin moment and τ_{ta} is the toe link arm length,

The second term of the equation, $F_s(x_r - \tau_{sr}\delta_{sw}, V_x)$, represents a nonlinear relationship between the steer column displacement and the elastic force. It is not a simple spring governed by the Hooke's law because this term includes the action of the power steering, that depends on the steering column deformation and on the vehicle speed, due to the fact that the power steering must exert a stronger force when the vehicle is at low speed. The contribution from the steering column elasticity and from the power steering were not seen separately because, since both depends mainly from the steering column deformation, it's very difficult to measure separately those two phenomena in the parametrization process.

The fourth term represents the friction force that comes from the steering rack sliding. The friction can be modeled with more complex formula, in order to keep in account the residual friction force that remains in steady state after the sliding process stops. Those formulas must have an additional internal degree of freedom that adds complexity and it's not necessary for the methodology described here, since steady-steady state manouvers are not

taken in account. F_r is the rack friction force saturation, is the magnitude of the friction force when the rack is at full sliding, K_r represents the slope of the hyperbolic tangent (tanh) function at the origin.

M_k, the kingpin moment, is the moment comes from the following equation:

$$M_k = (F_{y_{11}} + F_{y_{12}})\tau_{ct} + M_{z_{11}} + M_{z_{12}} \tag{3.30}$$

Where τ_{ct} is the caster trail length.

τ_{sr}, the ratio between the steering wheel rotation and the rack translation, can be easily get from the C factor, a well known parameter in the automotive design, that represents the rack displacement in millimeters when the steering wheel is rotated by one full turn:

$$\tau_{sr} = \frac{C_{fac}}{2000\pi} \tag{3.31}$$

The toelink arm length τ_{ta} can be easily obtained if the τ_{sr} and the steer ratio τ_{sw} are known.

$$\tau_{ta} = \tau_{sr}\tau_{sw} \tag{3.32}$$

3.3.4 Wheel steering and inclination angles

The steering angles δ_{ij} are calculated with:

$$\delta_{ij} = \delta_{T_{ij}} + \delta_{S_{ij}}(\delta_{sw}) + \delta_{C_{y_{ij}}} F_{y_{ij}} + \delta_{C_{z_{ij}}} M_{z_{ij}} + \delta_{L_{ij}}(\Delta F_{K_i}) \tag{3.33}$$

Where all coefficients shown are linear or nonlinear, obtained from KnC (kinematic and compliance) data. Those parameters are the static toe angle, $\delta_{T_{ij}}$ the steering map $\delta_{S_{ij}}(\delta_{sw})$, the elastic compliances $\delta_{C_{y_{ij}}}$ and $\delta_{C_{z_{ij}}}$, and

the steering induced by the suspension travel $\delta_{L_{ij}}(\Delta F_{K_i})$, expressed as a load dependency.

Inclination angles γ_{ij}, in the same way, are calculated with:

$$\gamma_{ij} = \gamma_{T_{ij}} + \gamma_{S_{ij}}\delta_{sw} + \gamma_{C_{y_{ij}}}F_{y_{ij}} + \gamma_{L_{ij}}(\Delta F_{K_i}) \tag{3.34}$$

This second equation is analogous to the previous (3.33) with the difference that the dependancy between the steering wheel angle and the induced inclination variation is assumed as linear and there is no inclination variation induced by the aligning moment $M_{z_{ij}}$.

3.3.5 Contact patch dynamics

The contact patch is modelled as a mass that can translate in lateral direction respect to the rim, this translation represents the tyre carcass deformation [13]. This mass is connected to the rim with a spring and a damper. The slip angle between the contact patch and the road α'_{ij}, feeds the Magic Formula that calculate the lateral force applied on the contact patch. The spring stiffness is the system unknown parameter and, as explained in paragraph 3.2, it determines the the tyre lateral relaxation length, so the delay between the steering input and the dynamic response of the entire vehicle.

$$m_{ij}\ddot{y'_{ij}} + D_{Fy_{ij}}(\dot{y'_{ij}} - \dot{y_{ij}}) + C_{Fy_{ij}}(y'_{ij} - y_{ij}) = F'_{y_{ij}}(F_{z_{ij}}, \alpha'_{ij}, \gamma_{ij}, \rho_{ij}) \tag{3.35}$$

Contact patch dynamics equation, $D_{Fy_{ij}}$ and $C_{Fy_{ij}}$ are the tyre carcass damping and stiffness coefficients, $F'_{y_{ij}}$ is the Magic Formula force. The contact mass m_{ij} and the damping coefficient have small influence on results. If those values are unknown, the model user can set them high just enough to eliminate vibrations, for example $m_{ij} = 1kg$, $D_{Fy_{ij}} = 100\frac{Ns}{m}$ are values that grant the stability of the system.

$$F_{y_{ij}} = -D_{Fy_{ij}}(\dot{y'_{ij}} - \dot{y_{ij}}) - C_{Fy_{ij}}(y'_{ij} - y_{ij}) \tag{3.36}$$

$F_{y_{ij}}$ is the force applied on rim, transmitted to the vehicle. For small contact masses $F_{y_{ij}} \approx F'_{y_{ij}}$

$$\alpha = \frac{\dot{y}_{ij}}{u_{ij}} = \frac{v_{ij}}{u_{ij}} \tag{3.37}$$

$$\alpha' = \frac{\dot{y'}_{ij}}{u_{ij}} = \frac{v'_{ij}}{u_{ij}} \tag{3.38}$$

The contact patch slip angle α' feeds the Magic Formula instead of the rim slip angle α, that is calculated with formulae 3.7 and 3.8, $\dot{y'}_{ij}$ that appears in formula 3.35 is obtained from the inversion of the equation 3.37.

3.4 Experimental results

The double-track model was validated by comparing its results with the reference model in the variable-frequency sine sweep test described in the chapter 3.2. The reference model for the validation is a digital twin of the real vehicle developed by the industrial partner, Maserati, in the Vi-CarRealTime software environment. The correlation results with the reference model were shown in figure 3.2.

After the model was validated, the methodology was applied on experimental data provided by the industrial partner. The parameters $C_{F_{\alpha_1}}$ and $C_{F_{\alpha_2}}$ were tuned until the $\frac{F_y}{\alpha}(s)$ gain on the front and real axle of the transfer functions from the model matched the experimental one, then the parameters $C_{F_{y_1}}$ and $C_{F_{y_2}}$ were tuned until the delay on the same transfer functions matched the experimental ones. The tyre model used on the developed double-track model is a MF-tyre 5.2 [43]. In this model the cornering stiffnes can be tuned

acting on the parameter $\lambda_{Ky\alpha}$ or p_{Ky1} and the lateral stiffness on the parameter C_{y0}.

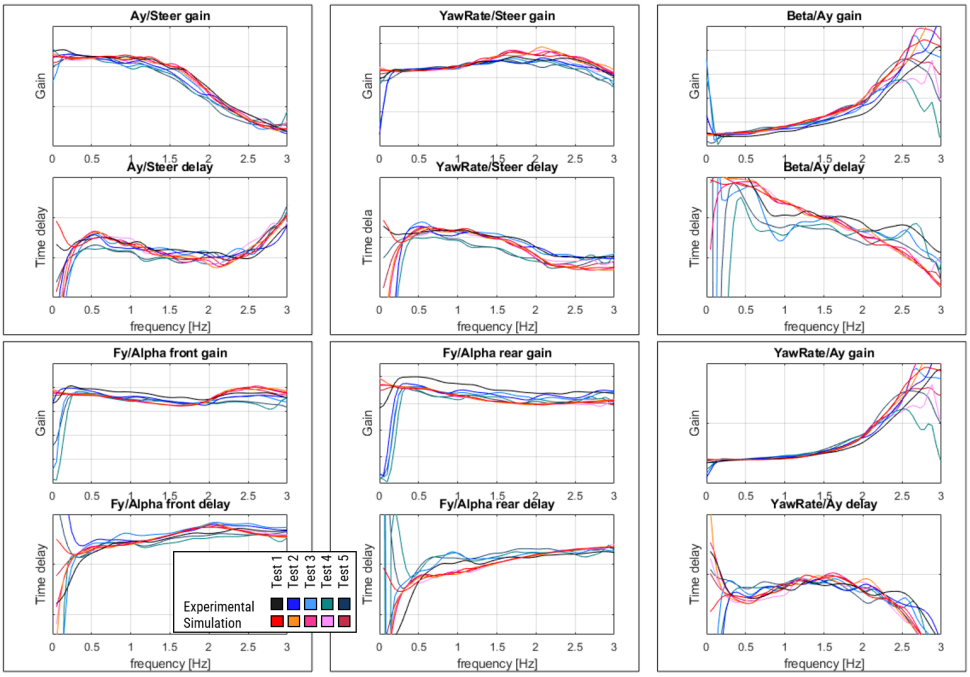

Fig. 3.7 Single-Track model transfer functions, experimental vs develped model

The experimental data consists in 5 tests where the vehicle was driven at a constant speed of $100\frac{km}{h}$ reaching a lateral acceleration of $3\frac{m}{s^2}$. The transfer functions obtained are shown in figure 3.7 with cold colors. The double-track model results, after the parameters tuning, are shown with warm colors. The tuning procedure was aiming for the best fitting of the frequencies between 0.5 and 2.5 Hz. The experimental data is not reliable from 0 to 0.5 Hz because those frequencies are too close to the steady-state conditions so this data comes from portion of time outside of the intervel when the maneuver is performed, furthermore, this frequency range data is heavily affected from small imperfections of the sensors offset tuning. The frequencies over 2.5 Hz

are higher than the typical excitation range of a vehicle and can be considered out of the range of interest.

The application of the methodology in this specific dataset gave exceptional good results, where the identified values of the parameters were inside the error of 5% with respect to the values that were previously known by the industrial partner. It must be noted that good results can be obtained only if acquisitions from all the sensors are perfectly synchronous, as even small time shift on the sensors timestamp data can lead to big vertical shifts of the transfer function delays. Since the scale of the $\frac{F_y}{\alpha}(s)$ transfer functions (hidden) is less than $0.1s$, the acceptable time shift of the sensors must be inside the hundredth of a second.

Chapter 4

Kalman filter for the vehicle state estimation

4.1 Introduction

The estimation of a state of a dynamic system that is not normally measurable or the possibility to fuse measurements to find the optimal estimate of a state is a problem to which various solutions have been given over time. This chapter will introduce the basic concepts that later led Rudolf Emil Kalman, a Hungarian-American electrical engineer and mathematician, to the development of his famous algorithm that today is widely used in signal processing, control systems, guidance, navigation, and control. For this work, U.S. President Barack Obama awarded Kalman the National Medal of Science on 2009.

It is evident from a literature [44, 45] that Kalman filters are by far the most widely used technique for estimating the state of a vehicle, and in particular its side-slip angle. The reasons why the Kalman filter finds so much space while other techniques have more niche applications are manifold: one of the main reasons for this is certainly that the presence of "outlier" measurement values (perhaps due to sensor outliers, e.g., GPS bad signal)

makes the obtained estimate of deterministic algorithms, like least squares, much worse. In other words, least-square estimates are significantly affected by outliers.

It is therefore necessary to be aware of the presence of these abnormal values before applying one of the techniques mentioned above: the Kalman filter is capable of doing this. It is called a filter in the sense that it removes the noise of the measurements to construct the estimates. In addition, the Kalman filter makes it possible to extend the discussions on parameter estimation of linear systems made so far with Least Squares Method, to continually varying states that may have more complex nonlinear models associated with them.

Kalman filter is one of the most famous algorithms in all of engineering. It's the best linear unbiased estimator, widely used in the field of robotics, automotive and aerospace for:

- Estimation of variables (better knows as states) that cannot be directly measured
- Sensor fusion: merge measurements that are available from various sensors but might be subject to noise. For example, it could combine information from vehicle IMU, odometer and GPS to get the best possible estimate of the vehicle's position.

As vehicle autonomous driving advances, more complex control algorithms are required to make the vehicle behaviour within the desired conditions. These algorithms usually provide accurate knowledge of the system states.

Vehicle in its entirety is a complex nonlinear system, with plenty of variables influencing them and it is not always possible to measure all the states through sensors. Some physical quantities like the side-slip angle or the maximum available grip parameters are not directly measurable either for technical or economic reasons.

It is essentially a set of mathematical equations [46] which recursively provides an efficient estimation exploiting the measurements. He resolves the problem of estimating the instantaneous "state" of a linear dynamic system perturbed by Gaussian white noise, by using measurements linearly related to the state, but corrupted by Gaussian white noise. The name 'filter' is due to its capability to remove the measurement and process noise component during estimation. The fact that it is recursive is a great advantage: each updated estimate of the state is computed from the previous estimate and the new measurements, thus no storage is required except for the last estimate. This gives the filter low computational weight, robustness, and simplicity.

In particular, Kalman filter is used when:

- The variables of interest can only be measured indirectly
- Measurements are available from various sensors but might be subject to noise.

The Kalman filter is not the only known state observer. In fact, before it, several other state observatories have been developed as Luenberger [47]. The main difference is that while the Luenberger observer is deterministic, the Kalman filter is concerned with stochastic processes. Luenberger works well in a deterministic environment where the feedback gain L of Luemberg Observer (LO) is constant. In a noisy environment, the Kalman filter computes the filter gain recursively; this allows it to adapt to some instances of mismodeling of the model. With the Kalman filter theory, it is possible to combine a statistical knowledge of the state (mean value and covariance), propagating it by way of the available measurements, which allow reaching the state estimation in a simpler and faster way and with a more restricted uncertainty. The Kalman filter is an 'optimal' filter in the sense that it returns the gain that minimizes the sum of the residual squares known as the 'Dumped Last Square'. This is true under certain assumptions that will be seen later and among which we also find the hypothesis of linear dynamic system. Reality

is, in general, non-linear, as well as equations governing vehicle dynamics, tyre-road contact etc. are all non-linear equations. To handle this situation, other versions of the Kalman filter have been developed over time that handles non-linearities: the Extended Kalman Filter (EKF), useful for the state estimation in non-linear system; and the Unscented Kalman Filter (UKF), which work on all kinds of system, but it is really helpful on strongly non-linear ones [48, 49].

An adequate theoretical approach when trying to estimate the state is important for obtaining a robust estimation. About, it must be remembered that Kalman Filter, in its original formulation, makes the following assumptions:

- The system must be linear and fully state observable.
- The process and measurement noise must be withe and Gaussian and uncorrelated.

The second hypothesis is related to the "Central Limit theorem". When driving a car, there are many, many sources of noise. The central limit theorem establishes that, in many situations, when independent random variables are added, their properly normalized sum tends toward a normal distribution even if the original variables themselves are not normally distributed [50, 51]. Therefore, thanks to it, is possible to state that the sum of different errors will tend to be Gaussian, making these methods applicable in a real case. Also, if the noise is Gaussian (and we can consider it as such), it can be described our model with a probabilistic approach without complicating it: just remember that under this hypothesis, the least square method is equivalent to maximum likelihood.

Instead, observability is a property of the system that one must always try to explore. The states of non-linear time-varying dynamic systems may be locally unobservable giving a completely unreliable estimate of the state (in those areas the result is noise integral, hence random walk).

4.2 State estimation process

State estimators adopted are based on the filtering technique and only their discrete-time form is considered in this thesis work, in order to be easily implemented in a recursive algorithm.

The term "filtering" assumes a new meaning in state estimation, it is well beyond the idea of separation of the components of a mixture. According to [52] it can be seen as the solution of an inversion problem, in which one knows how to represent the *measurable variables* as functions of the variables of principal interest, called *state variables*. In essence, it inverts this functional relationship and estimates the independent variables as inverted functions of the dependent measurable variables. These variables of interest are also allowed to be dynamic, with dynamics that are only partially predictable. However one needs to define what the term "state" means before presenting the state estimators. The states of a system are those variables of principal interest that provide a complete representation of the status of the system at a given instant of time. If the values of the measurable variables are known at the present time, it is possible to estimate the values of the output of the system using *state-space models*. State-space models can be generally divided into linear models and nonlinear.

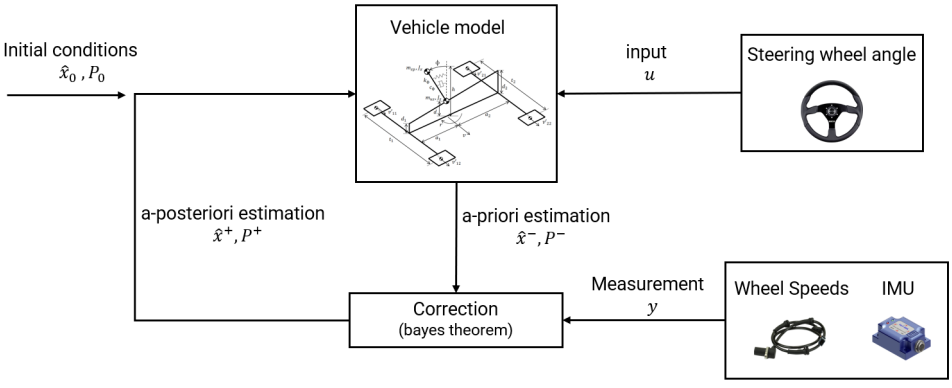

Fig. 4.1 Discrete Kalman filter cycle.

The state estimators presented in this chapter can be summarized using the flow chart in figure 4.1.

In the *Model box* there are two sets of equations, the first one propagates the state with time using the system equations, giving the *a-priori state estimate* as output, the second one computes the *measurement estimate* based on the knowledge of the *a-priori state estimate*. The *measurement estimate* is compared to the *actual measurement* in order to correct the *a-priori state estimate* and then to obtain the *a-posteriori state estimate*, that is the state estimate referring to current time step. This is what happen in the *Correction box*, whose output is the *a-posteriori state estimate*. The acquired (actual) measurements are available at each time step using the filtering technique, unlike smoothing technique. An initial state estimate must be defined at the beginning, the *initial conditions* of the iterative algorithm.

The *system equations* and the *measurement equations* constitute the plant model, represented in figure 4.1 as the model box. Both sets of equations are obtained from a double-track vehicle model that will we presented in chapter 5. The forward Euler method is adopted to write them in a discrete-time form. It is important to highlight that the equations listed below are the same for all the implemented state estimators, they represent the physical core of the state estimator. There is the need for state estimator because only the physical model of the vehicle is not able to replicate the actual vehicle behaviour in different maneuvers. The state estimator is a mathematical tool that is able to correct the state estimate given by the physical model. It is possible to take into account the inaccuracy of the physical model introducing the *process noise*. In the same way one introduces the *measurement noise* in order to take into account the noisy acquired measurements. There are several noise models in probability theory literature, only the *white noise model* is considered in this thesis work. Also the noise is *Gaussian*, *zero-mean*, *uncorrelated* and considered as *additive*.

For what said above a general form of the equations is:

$$\begin{aligned} \hat{x}_k^- &= f(\hat{x}_{k-1}^+, u_{k-1}) + w_{k-1} \\ y_k &= h(\hat{x}_k^-, u_k) + v_k \end{aligned} \tag{4.1}$$

where x_{k-1}^+ is the *a-posteriori state estimate* at the previous time step and x_k^- is the *a-priori state estimate* at the current time step, also $f(\cdot)$ and $h(\cdot)$ are respectively representative of the system equations and of the measurements equations. y_k is the measurement from the sensor. The other measurable variables in $f(\cdot)$ and $h(\cdot)$ are indicated as u_k and u_{k-1}. Finally w_{k-1} and v_k are respectively the *process noise* and the *measurement noise*, considered additive. In addition they are Gaussian, zero-mean and uncorrelated with Q and R as their covariance matrix.

$$\begin{aligned} w &\sim (0, Q) \\ v &\sim (0, R) \end{aligned} \tag{4.2}$$

4.3 Linear Kalman filter

The linear Kalman filter manages how the mean of the state and the covariance of the state propagate with time. From now on it is referred to as KF. It only deals with linear dynamic systems, estimating the state $\hat{x} \in \Re^n$, where n is the number of states.

At the generic time step k an estimation of x_k is computed before processing the measurements acquired at the time step k, this is called *a-priori state estimate* and indicated as $\hat{x}_k^-$, also its covariance is computed and indicated as P_k^-. Then the estimate of x_k is refined processing the measurement, the resulting estimate is the *a-posteriori state estimate* and indicated as $\hat{x}_k^+$, and

its covariance as P_k^+. What said can be summarized in a mathematical form:

$$\begin{aligned} \hat{x}_k^- &= E[x_k|y_1, y_2, .., y_{k-1}] \\ P_k^- &= E[(x_k - \hat{x}_k^-)(x_k - \hat{x}_k^-)]^T \\ \hat{x}_k^+ &= E[x_k|y_1, y_2, .., y_k] \\ P_k^+ &= E[(x_k - \hat{x}_k^+)(x_k - \hat{x}_k^+)]^T \end{aligned} \tag{4.3}$$

Let now introduce a generic linear system written in the matrix formulation and also adopting the discrete-time form, in order to be implemented in the KF recursive algorithm.

$$x_k = F_{k-1}x_{k-1} + G_{k-1}u_{k-1} + w_{k-1} \tag{4.4}$$

The matrix F_{k-1} relates the state at the previous time step to the state at the current one, while the latter is related to the other measurable variables by the matrix G_{k-1}. Both matrices can be constant or time-dependent, in (4.4) time-dependent matrices are considered and each matrix element is referred to the previous time step $k-1$. Moreover in (4.4) an additive noise is considered.

The measurement equation can be defined under the same hypothesis:

$$z_k = H_k x_k + v_k \tag{4.5}$$

This equation uses the current time state computed by (4.4) in order to update the measurements z to the current time. The matrix H_k can be constant or time-dependent as well, also note that in (4.5) its elements refer to the current time step. An additional noise is present in (4.5) as in (4.4), they fulfil the hypothesis stated in (4.2). Both the equations constitute the process model, that is the physical core of the KF.

The KF algorithm can be divided into two step:

- Time update, it projects the last computed state estimate ahead in time. It is also called *prediction step*.
- Measurement update, it adjusts the projected estimate by an actual measurement at that time. It is also called *correction step* [46].

The *KF* equations can be written using the nomenclature adopted in (4.3) and the hypothesis in (4.2). The time update equations are:

$$\begin{aligned} \hat{x}_k^- &= F_{k-1}\hat{x}_{k-1}^+ + G_{k-1}u_{k-1} \\ P_k^- &= F_{k-1}P_{k-1}^+F_{k-1}^T + Q_{k-1} \\ z_k &= H_k\hat{x}_k^- \end{aligned} \tag{4.6}$$

While the measurement update equations are:

$$\begin{aligned} K_k &= \frac{P_k^- H_k^T}{H_k P_k^- H_k^T + R_k} \\ \hat{x}_k^+ &= \hat{x}_k^- + K_k(y_k - z_k) \\ P_k^+ &= (I - K_k H_k)P_k^- \end{aligned} \tag{4.7}$$

Equations (4.6) and (4.7) can be easily implemented in a recursive algorithm, but the first *previous time state estimate* and its covariance must be defined. They are indicated as:

$$\begin{aligned} \hat{x}_0^+ &= E[x_0] \\ P_0^+ &= E[(x_0 - \hat{x}_0^+)(x_0 - \hat{x}_0^+)]^T \end{aligned} \tag{4.8}$$

Where x_0 is an initial value of the state. Note that in (4.7) the amount of the correction is proportional to the *residual error* between the actual measurements, y_k, and the predicted value of the measurements, z_k. Also, the *Kalman gain* takes into account the process noise and the measurement noise through their covariance matrices. This section is necessary in order to point out the basis of the next KFs, in fact the equations (4.6) and (4.7) are

common to every KFs but each one is characterized by the strategy adopted to deal with the nonlinearity of the process.

4.4 Extended Kalman Filter

The EKF is based on the linearization of the nonlinear system around the state estimate.

It is necessary to rewrite the process equations with the aim to translate into a mathematical form what that means. The actual state and measurement vectors can be written using the general form of the process equations with nonadditive noise[1]:

$$\begin{aligned} x_k &= f(x_{k-1}, u_{k-1}, w_k) \\ y_k &= h(x_k, u_k, v_k) \end{aligned} \tag{4.9}$$

Performing now a first-order Taylor expansion of the equations around the previous time state estimate, $\hat{x}_{k-1}^{+}$

$$\begin{aligned} x_k &\approx f(\hat{x}_{k-1}^{+}, u_{k-1}) + \left.\frac{\partial f}{\partial x}\right|_{\hat{x}_{k-1}^{+}} (x_{k-1} - \hat{x}_{k-1}^{+}) + \left.\frac{\partial f}{\partial w}\right|_{\hat{x}_{k-1}^{+}} w_{k-1} \\ y_k &\approx h(\hat{x}_k^{-}, u_k) + \left.\frac{\partial h}{\partial x}\right|_{\hat{x}_k^{-}} (x_k - \hat{x}_k^{-}) + \left.\frac{\partial h}{\partial v}\right|_{\hat{x}_k^{-}} v_k \end{aligned} \tag{4.10}$$

[1] nonadditive noise is only considered in this case and for reasons of generality, as shown in [46].

Where the Jacobian matrices are

$$\begin{aligned}
\left.\frac{\partial f}{\partial x}\right|_{\hat{x}_{k-1}^{+}} &= \frac{\partial f(\hat{x}_{k-1}^{+}, u_{k-1}, 0)}{\partial x} = F_{k-1} \\
\left.\frac{\partial f}{\partial w}\right|_{\hat{x}_{k-1}^{+}} &= \frac{\partial f(\hat{x}_{k-1}^{+}, u_{k-1}, 0)}{\partial w} = W_{k-1} \\
\left.\frac{\partial h}{\partial x}\right|_{\hat{x}_{k}^{-}} &= \frac{\partial h(\hat{x}_{k}^{-}, u_{k}, 0)}{\partial x} = H_{k} \\
\left.\frac{\partial h}{\partial v}\right|_{\hat{x}_{k}^{-}} &= \frac{\partial h(\hat{x}_{k}^{-}, u_{k}, 0)}{\partial v} = V_{k}
\end{aligned} \tag{4.11}$$

Considering now additive noise, the equations (4.10) are:

$$\begin{aligned}
x_k &\approx \hat{x}_k^- + F_{k-1}(x_{k-1} - \hat{x}_{k-1}^+) \\
y_k &\approx z_k + H_k(x_k - \hat{x}_k^-)
\end{aligned} \tag{4.12}$$

Defining the *prediction error* as the difference between the actual vector and the approximated (predicted) vector:

$$\begin{aligned}
\tilde{e}_{x_k} &\equiv x_k - \hat{x}_k^- \\
\tilde{e}_{z_k} &\equiv y_k - z_k
\end{aligned} \tag{4.13}$$

Substituting the (4.13) in (4.10):

$$\begin{aligned}
\tilde{e}_{x_k} &\approx F_{k-1}(x_{k-1} - \hat{x}_{k-1}^+) + \varepsilon_k \\
\tilde{e}_{z_k} &\approx H_k(x_k - \hat{x}_k^-) + \nu_k
\end{aligned} \tag{4.14}$$

Where ε_k and ν_k represent new independent random variable having zero mean and covariance matrices $W_{k-1}QW_{k-1}^T$ and $V_kRV_k^T$ respectively. Those equations are linear and their form is quite similar to the KF's time-update

equations (4.6). Thus applying the KF logic:

$$\hat{x}_k^+ = \hat{x}_k^- + \hat{e}_k \tag{4.15}$$

Where $\hat{e}_k$ is the estimated error using a hypothetical KF, according to [46], where the KF's equation is :

$$\hat{e}_k = K_k \tilde{e}_{z_k} \tag{4.16}$$

Substituting the latter in the (4.15)

$$\hat{x}_k^+ = \hat{x}_k^- + K_k \tilde{e}_{z_k} = \hat{x}_k^- + K_k(y_k - z_k) \tag{4.17}$$

This equation can be used in the measurement-update of the EKF.

This type of filter is referred to as *FO-EKF* from now on, this is because of the first-order Taylor expansion (4.10).

It is now possible to write the time update equations and measurement update equations of the *FO-EKF*. A generic nonlinear process is considered for this purpose, the noise model is now considered additive, Gaussian, zero-mean and uncorrelated, differently than in (4.9):

$$\begin{aligned} x_k &= f(x_{k-1}, u_{k-1}) + w_k \\ y_k &= h(x_k, u_k) + v_k \\ w_k &\sim (0, Q) \\ v_k &\sim (0, R) \end{aligned} \tag{4.18}$$

The following algorithm is based on the hypothesis stated above, so the partial derivative of the process equations with respect to noise terms is null because of that.

Algorithm 1 First-Order Extended Kalman Filter algorithm

1: $\hat{x}_0^+ = E[x_0]$ ▷ *Initial state*
2: $P_0^+ = E[(x_0 - \hat{x}_0^+)(x_0 - \hat{x}_0^+)^T]$ ▷ *Initial state Covariance*
3: **procedure** FO-EKF(T, $\{u\}_{k=1}^T$)
4: **for** $k = 1 \to T$ **do**
5: $\hat{x}_k^- = f(\hat{x}_{k-1}^+, u_{k-1}, 0)$ ▷ *a-priori state estimate*
6: $P_k^- = F_{k-1} P_{k-1}^+ F_{k-1}^T + Q$ ▷ *a-priori state estimate covariance*
7: $z_k = h(\hat{x}_k^-, u_k, 0)$ ▷ *a-priori measurement estimate*
8: $K_k = P_k^- H_k^T (H_k P_k^- H_k^T + R)^{-1}$ ▷ *Kalman gain*
9: $\hat{x}_k^+ = \hat{x}_k^- + K_k(y_k - z_k)$ ▷ *a-posteriori state estimate*
10: $P_k^+ = (I - K_k H_k) P_k^-$ ▷ *a-posteriori state estimate covariance*
11: **end for**
12: **end procedure**

4.5 Kalman filter tuning

The covariance matrices Q and R are design parameters. Choosing these parameters is not always easy. From a physical point of view, the choice can be made as follows: As R approaches zero, the Kalman gain approaches H^{-1}. Considering the second equation of the measurement update equations, this brings the a-posteriori state estimate to be equal to $H^{-1}z_k$, which is the transformed measurement in the state "domain". This means that the measurement is trusted more and more. Setting the R matrix to a little value, easily understandable info is that the measurement noise is very little, and hence, the measurement is "almost true". On the other hand, when Q approach to high values it means the modelled system is considered less reliable, and the estimation can start oscillating depending on measurement properties.

However, process covariance metrics depends on the process, and almost always there is no opportunity to directly observe the system. That is why this matrix is often chosen with a trial-and-error logic.

On the other hand, choosing R equal to the covariance of the measuring instruments provided by the manufacturer could lead to errors and work very poorly if it is the parameter used in the Kalman filter. This is because sensor errors are often correlated over time, while the Kalman filter assumes

that errors are independent. Thus, may be that the noise of some sensors is correlated over time and assume covariance equal to that of the instrument will tend to underestimate the long time-scale variance. [53]

Therefore, Q and R must be assigned by the designer and choosing them is not always easy, not least because the number of parameters can be very large. To overcome this problem and relieve KF developers of the tedious task of tuning noise parameters by hand but, as is showed in [53], is best practice or necessary if the models are complex like that showed in chapter 5, obtaining the Q and R values through the employment of algorithms.

4.5.1 Maximizing The Joint Likelihood

This approach requires access to the full state vector, although it is not always possible. Assuming that this is possible, the function $h(\cdot)$ is the identity function and the noise γ is so small that it can safely be neglected. Let $x_{0:T}$ denote the entire state sequence $(x_0, x_1, \ldots, x_T)$, also let $u_{1:T}$, $y_{0:T}$ and $z_{0:T}$ denote the known input, the first two are high-end measurements and the last is low-end measurement. Assuming the initial probability distribution $p(x_0)$, the joint probability distribution till the time step T is:

$$p(x_{0:T}, y_{0:T}, z_{0:T} | u_{1:T}) = p(x_0) \prod_{t=1}^{T} p(x_t | x_{t-1}, u_t) \prod_{t=0}^{T} p(y_t | x_{t-1}) p(z_t | x_{t-1}) \tag{4.19}$$

Where

$$\begin{aligned} p(x_t | x_{t-1}, u_t) &= \mathcal{N}(x_t; f(x_{t-1}, u_t), Q) \\ p(y_t | x_{t-1}) &= \mathcal{N}(y_t; g(x_t), P) \\ p(z_t | x_{t-1}) &= \mathcal{N}(z_t; h(x_t), R) \end{aligned} \tag{4.20}$$

The method proceeds by maximizing the likelihood of all the data. Since the full state vector is observed ($y_k = x_k$), the covariance matrices R_{joint} and

Q_{joint} are estimated as follows:

$$[R_{joint}, Q_{joint}] = arg\ max_{Q,R}\ [log\big(p(x_{0:T}, z_{0:T}|u_{1:T})\big)] \tag{4.21}$$

It can be shown that subtistuting the (4.19) and the (4.20) in the above equation, it decomposes into the two equations listed below

$$\begin{aligned} Q_{joint} &= arg\ max_{Q}\ [-Tlog(2\pi Q) - \sum_{t=1}^{T}(x_t - f(x_{t-1}, u_t))^T Q^{-1}(x_t - f(x_{t-1}, u_t))] \\ R_{joint} &= arg\ max_{R}\ [-(T+1)log(2\pi R) - \sum_{t=0}^{T}(z_t - g(x_t))^T R^{-1}(z_t - g(x_t))] \end{aligned} \tag{4.22}$$

However the optimal R_{joint} and Q_{joint} can actually be computed in closed form and are given by:

$$\begin{aligned} Q_{joint} &= \frac{1}{T}\sum_{t=1}^{T}(x_t - f(x_{t-1}, u_t))(x_t - f(x_{t-1}, u_t))^T \\ R_{joint} &= \frac{1}{1+T}\sum_{t=0}^{T}(z_t - g(x_t))(z_t - g(x_t))^T \end{aligned} \tag{4.23}$$

As said, this approach never actually run the filter, it trains the elements of the filter. It therefore implicitly assumes that training the elements individually is as good as training the filter as a whole.

4.5.2 Minimizing The Residual Prediction Error

The above technique requires the full state knowledge and doesn't execute the filter. It is here presented a technique that overcome these potential limits. This technique minimizes the prediction error for the values of y_t given by

$$E[y_t|u_{1:t}, z_{0:t}] = g(\hat{x}_t) \tag{4.24}$$

$\hat{x}_t$ is the state estimate provided by the filter algorithm adopted. This is the a-posteriori state estimate, so it takes into account the observations $z_{0:t}$ and the additional input (as known as control input) $u_{1:t}$, considered acquired by high-end sensors. Therefore $\hat{x}_t$ depends implicitly on R and Q. This technique seeks the parameters R and Q that minimize the quadratic deviation of y_t, and so the expectation above, weighted by the inverse covariance Z.

$$\langle Q_{res}, R_{res} \rangle = arg\ min_{Q,R} \sum_{t=0}^{T} (y_t - g(\hat{x}_t))^T Z^{-1} (y_t - g(\hat{x}_t)) \tag{4.25}$$

But if Z is any multiple of the identity matrix, this simplifies to

$$\langle Q_{res}, R_{res} \rangle = arg\ min_{Q,R} \sum_{t=0}^{T} \|y_t - g(\hat{x}_t)\|_2^2 \tag{4.26}$$

In other words this technique choose the parameters R and Q that cause the filter to output the state estimates that minimize the squared differences to the measured values y_t. Unlike the previous technique, this one evaluates the actual performance of the filter.

Finding the covariance matrices through this method, unlike the previous one, involves the usage of optimization algorithm. For every function evaluation of the error function (4.25), the KF must be run on the entire dataset, this can require several minutes and this operation must be repeated many times, depending on the chosen optimization algorithm, that can be local or global.

Local optimization algorithms require a starting point and finds the local minimum closest to it. These methods just described, where applicable, represent the "gold standard" of optimization problems, as they are fast and efficient. Unfortunately, the calculation of derivatives of the error function, which is necessary, is not always possible for various reasons such as a function not described analytically or not continuous or multimodal and so on.

Abbel, in his paper, states that the derivative-based methods can be applied, but also derivative-free methods are viable. Both methods were applied in the context of this work but, for the tuning of the algorithm described in chapter 5, derivative-based methods proved to be ineffective.

For this reason, several global optimization algorithms have been tested. Most of them has been also unsuitable for this problem because they required too many function evaluation and, as stated before, every function evaluation calculation was too slow to reach the global minimum with acceptable computation times. The algorithm that gave the best performances was the Surrogate function, it demonstrated a high efficiency combining both the capability of reaching good results on acceptable computation time.

4.5.3 Surrogate function optimization algorithm

In some optimization problems, such as the one under consideration, the function evaluations can be quite expensive. In the case in examination, the objective function is defined in Simulink simulation environment: for every single evaluation it is necessary to run a simulation, and this requires time.

In these contexts, a common approach is to build a surrogate model, which is a model of the optimization problem that can be efficiently optimized instead of the true objective function. By alternating evaluations of the surrogate model and the real objective function, the optimization problem can be solved more quickly. The surrogate is useful because it takes little time to evaluate. All this makes surrogate optimization the best algorithm for evaluating time-consuming functions.

Fitting such models requires an initial set of points, ideally points that are space-filling, that can cover the design space in the best possible way. The accurate choice of sampling plans is fundamental to cover search spaces with a limited number of points and try to optimize the objective function quickly. Various models of sampling plans are proposed in the literature: [44, 54]

Full factorial sampling: a discrete mesh is created in the workspace and sample points are taken at the vertices of this grid. As the dimension increases, the number of points required increases exponentially.

- Uniform projection plans: The workspace is sampled evenly along each direction.
- Greedy local: It relies on the use of a swapping algorithm to best fill the workspace.
- Quasi-random sequences are deterministic procedures by which space-filling sampling plans can be generated.

Selected sampling plane, surrogate algorithms build a model of the objective function that can be used in place of the real objective function. These surrogate models are designed to be smooth and less expensive than the real optimization function.

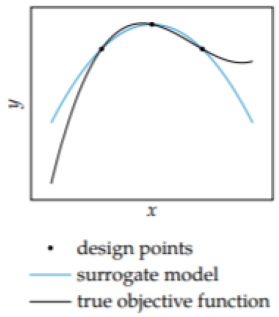

Fig. 4.2 Example of a surrogate function that approximates the true trend by passing only through certain design points.

Given a set of m design points:

$$X = \{x^{(1)}, x^{(2)}, ..., x^{(m)}\} \tag{4.27}$$

and associated function evaluations:

$$y = \{y^{(1)}, y^{(2)}, ..., y^{(m)}\} \tag{4.28}$$

a surrogate model $\hat{f}$ parameterized by θ is designed to mimic the true objective function f [55].

$$\hat{y} = \{\hat{f}_\theta(x^{(1)}), \hat{f}_\theta(x^{(2)}), ..., \hat{f}_\theta(x^{(m)}),\} \tag{4.29}$$

The model is fitted to real values using a regression model based on norm 2:

$$\min_\theta \|y - \hat{y}\|_2 \tag{4.30}$$

In literature, to solve this regression problem exists a large number of works. Several popular surrogate models and algorithms have been proposed for fitting models to data.

- Linear models: It assumes the form:

$$\hat{f} = \theta^T x \tag{4.31}$$

  From this linear model we show that the regression problem has the following analytical solution:

$$\min_\theta \|y - X\theta\|_2^2 \Rightarrow \theta = X^+ y \tag{4.32}$$

  where X^+ is the Moore-Penrose pseudoinverse of the vector X that contains the design points.

- Basis Functions: We define a base B of the design points:

$$B = \begin{bmatrix} b(x^{(1)})^T \\ b(x^{(2)})^T \\ \dots \\ b(x^{(m)})^T \end{bmatrix} \tag{4.33}$$

such that any surrogate model represented as a linear combination of basis functions can be fit using regression:

$$\min_{\theta} \|y - B\theta\|_2^2 \rightarrow \theta = B^+ y \tag{4.34}$$

Linear models, however, cannot capture nonlinear relationships. It is therefore necessary to use basis functions more complex than those based on the linear combination as polynomial, sinusoidal or radial basis function. In particular, the latter is what is used within surrogate optimizers in MATLAB. A radial function ψ depends only on the distance of a point from some centre point c. It is, therefore, possible to write:

$$\psi(x,c) = \psi(\|x-c\|) = \psi(r) \tag{4.35}$$

As reported in [56], the algorithms construct a surrogate as an interpolation of the objective function by using a radial basis function because this has several convenient proprieties:

- Whatever the number of points and the number of "dimensions", the formula for defining the radial basis interpolator remains the same as before.

- Evaluating a radial basis function takes very little time and is easy and little expensive to add a point to an existing interpolation.

- The cubic formulation of the radial basis function minimizes a measure of bumpiness.

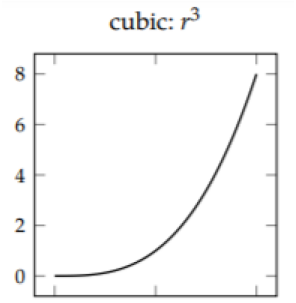

Fig. 4.3 Cubic radial basis function used in MATLAB

Built the surrogate model that allows for short-time function evaluation, the last step is to adopt a technique for choosing which design point to evaluate next. Gaussian processes can be used to guide the optimization process using a variety of strategies that use estimates of quantities such as the lower confidence bound, probability of improvement, and expected improvement. [55].

Given the importance of this algorithm, is provided a brief description of how this is implemented in MATLAB. This algorithm alternates between two phases:

- Construct Surrogate: Use the quasi-random point technique as sampling plans. If a user passes an initial set of points, the algorithm uses those points supplementing them with other quasi-random if they are not equal to the minimum number of points needed to generate the initial surrogate model. From these sample points build to construct a surrogate model of the objective function by interpolating a cubic radial basis function through these points.

- Search for the minimum. Sample the interval with several thousand pseudorandom vectors chosen from the points with the smallest objec-

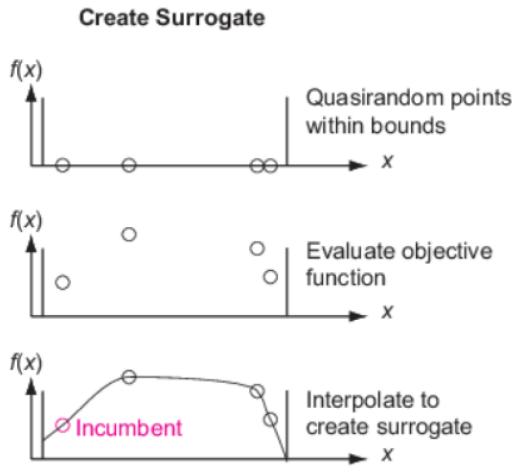

Fig. 4.4 Graphical representation of how to build a surrogate model

tive function value and whose modulus is related to a scale factor that representing the "radius" of the region within which to search for the optimum. These vectors have a normal distribution.

It is obtained thousands of sample points at which the algorithm calculates a merit function:

$$f_{merit}(x) = wS(x) + (1-w)D(x) \tag{4.36}$$

This is an important function, in that its proper use determines the success of the optimization technique. Specifically, it is a convex combination of a scaled surrogate and scaled distance weighted by the parameter w. In particular:

- Scaled surrogate: said S_{min} minimum surrogate value among the sample points, S_{min} the maximum and $s(x)$ the value at the point x, the scaled surrogate is:

$$S(x) = \frac{s(x) - s_{min}}{s_{max} - s_{min}} \tag{4.37}$$

- Scaled distance. Consider the distance of the sample points from the evaluation point x.

$$D(x) = \frac{d_{max} - d(x)}{d_{max} - d_{min}} \tag{4.38}$$

- Weight w: It is an important parameter that takes values between 0 and 1. A small value of w gives importance to points that are far from evaluated points, leading to a search in a new region. Instead, a large value of w, give importance to surrogate values, causing the search to minimize the surrogate. Actually, this value is not kept constant, but as recommended in [57], the value is cyclically alternated between 0.3, 0.5, 0.8, 0.95.

Then the merit function is given by the weighted sum of the surrogate value at these points and their distance from the points where the value of the original expensive objective function is known. The best points are those with the lowest merit function value. The solver then goes to evaluate the value of the real objective function only at these candidates and if it obtains values sufficiently lower than the previous points with which it had gone to generate the surrogate model, the solver deems the search successful and uses these points to update the surrogate model.

If the search is successful three consecutive times, the solver increases the search scale. If, on the other hand, the search is unsuccessful five consecutive times, the search range is halved. Thus, as the solver progresses, it concentrates its search in the surroundings of the points where the function has the minimum value.

Figure 4.5 shows the above schematically:

The advantage to using a surrogate model is, therefore, tied to the possibility of obtaining many evaluations of the function you are trying to optimize in an indirect and very fast way using the surrogate model, and after that, it evaluates the very expensive real function only at a few points where it is believed the function can assume the minimum value.

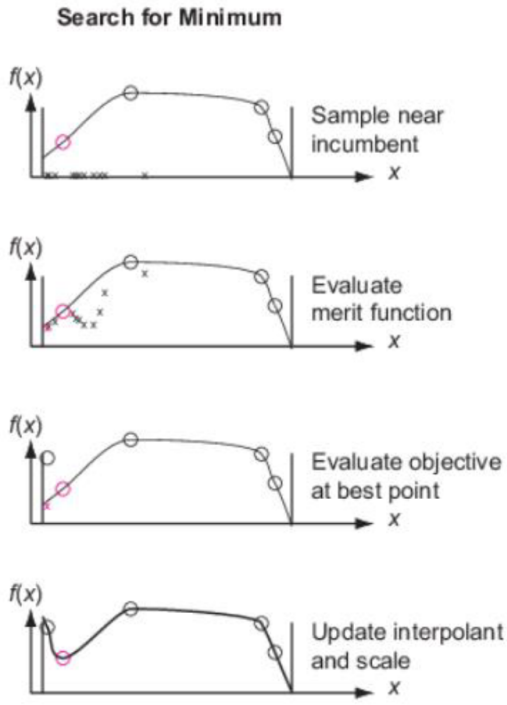

Fig. 4.5 Algorithm minimum search phase.

4.5.4 Tuning Dataset

In machine learning, the algorithm is not the only key affecting the final classification accuracy. Its performance can be significantly affected by the quantity and quality of the training dataset in many cases [46]. Training the algorithm, for example, on a particular track might make it good at estimating states only in that case. Repeatability could also be compromised, as those laps could be influenced by external factors that, when removed, degrade the estimate.

It is therefore necessary that the tuning dataset is formed by objective maneuvers: this makes the tuning operation controllable and repeatable.

It is recalled that their manoeuvers are divided into steady-state (imaginable as a succession of equilibrium states) and transient manoeuvers.

It is difficult to say a priori which maneuvers to select also because related to the type of model wants to optimize. Using all available manoeuvers could be a naive choice: passing an excess of data to the optimizer would increase the time requiring very long optimization times It is therefore necessary to choose the minimum number of sets that are fully representative of all driving situations.

In the case study of this thesis, a good estimation of the vehicle sideslip angle depends on the possibility of the vehicle model to correctly estimate the tires lateral force. The estimation of this force is not simple and depends, in the first instance, on the lateral slip of the tires, from the tire model calibration and from the vertical load acting on them. It is therefore necessary to provide a dataset in which the sideslip angle of the vehicle has been calculated for various lateral slip angles and various vertical loading conditions.

Chapter 5

Adaptive vehicle dynamics state estimator

5.1 Introduction

The vehicle correct state estimation and the ability to mathematically describe such physical system in the widest possible range of operating conditions is crucial for vehicle control. The real-time knowledge of the correct vehicle state is needed not only to properly feed low-level control systems commonly used in commercial cars such as ABS, ESP and traction control, but also to allow the development of more accurate advanced driver assistance (ADAS) systems up to fully autonomous driving scenarios [58, 59].

In the automotive field, the research on state estimation through Kalman Filtering began in the late 90s [60], when the first Extended Kalman Filter (EKF) algorithms, based on single-track models, were proposed. The simplified single-track vehicle models have the advantage of requiring less computational effort and parametrization complexity, whereas Kalman filtering technique compensates for model approximations thanks to sensors' feedback. Usually, a trade-off has to be defined between the increased accuracy obtainable by a more detailed and well parametrized model and the

computational capability of the system where the estimation algorithm has to be employed in real-time. Indeed, over time, the models have become more complex and several authors have begun to propose double-track vehicle models [61–64], which, at the cost of a higher computational effort, allow to obtain a better overall estimation accuracy, exploiting all the data and parameters, often available from OEMs (as tyre models parameters and the suspensions elasto-kinematic characterization obtained from laboratory tests). Another important scenario, where the double-track model outperforms a single-track model, regards the reproduction of vehicle dynamics in case of tyre combined interactions, especially in braking/accelerating phases during turning, where, due to the transfer of lateral load, the inner wheels can reach grip saturation, heavily affecting the cornering stiffness of the front axle [65, 66]. In some of the aforementioned works [61–63], but also in the more recent [67, 68], the modelling of the longitudinal dynamics has been tackled also exploiting the rotational angular velocity sensors as one of the model inputs.

The main issue concerning the tyre-road longitudinal dynamics evaluation based on the measured wheels angular velocities, consists in the fact that even small errors linked to the wheel rolling radius estimation, or to the encoder measurement noise, can create high estimation errors within the forces estimated at the non-driving axle, which have to be compensated by the driving axle in order to ensure that the longitudinal acceleration of the model matches the measured one. Such potentially large misestimation of the longitudinal forces acts reducing lateral ones, affecting the estimation of the global grip at the tyre-road interface, which will result from 10% to 30% higher than the real one. Starting from the works described in [67, 68], the proposed methodology approaches this aspect differently, similarly to [64]. The model input for the longitudinal dynamics is no more the angular speed of each wheel, but the engine and braking moments applied on the wheels, calculated starting from the total longitudinal force evaluated by the accelerometers, installed

on the vehicle, and split among the various corners with a simple logic based on the characteristics of the brakes and the differential. The wheel angular speeds are consequently obtained by solving the wheel dynamics, and the angular speed sensors are used as measurements within the Extended Kalman filter (EKF) algorithm, to correct any drift within the estimation of the vehicle speed. This approach solves the above-mentioned problems, significantly increasing the accuracy of estimation of longitudinal forces, slip ratios and, consequently, of the tyre combined interaction. Compared to the approach proposed in [64], an implicit integrator (Backward Euler) is introduced for the calculation of the wheel angular speed. The reason lays in the fact the explicit integrators, as the forward Euler one, normally employed in Kalman filter algorithms, cannot ensure the convergence of the estimation if the natural frequency of the simulated objects is higher than the integrator frequency. Due to a particularly high frequency concerning the wheel dynamics [69], using an explicit integrator, integration time step of about 0.001 s or smaller becomes necessary, therefore, requiring a high computational load not suitable with real-time operations. On the other hand, employing an implicit integrator, the system remains stable even at frequencies of 100 Hz or lower [70].

Another critical point regards the fact that the tyre-road interaction characteristics could potentially considerably change during use, mainly due to the different road surface characteristics and weather conditions; on the other hand, the thermal and ageing effects occurring during the life cycle of the tyre have to be taken into account [71]. For this reason, almost all the papers cited propose an automatic adaptation of the tyre parameters; some include specific scaling quantities for the tyre physical parameters [60, 62, 64], others use more sophisticated methods [68]. It has to be highlighted that all the methods reported include the wheel model parameters, able to guarantee the maximum congruence between sensors signals and model estimations. However, none of these works have taken into account the road inclination effects within the model dynamics, which, if neglected, can represent an additional source

of misestimation for the tyre parameters. The integration of all the cited aspects, the simultaneous estimation of side-slip angle, of maximum friction and banking angle, has been addressed in more recent times. In 2017, Hadum [72] proposed an estimation algorithm separated in different modules that included an EKF for the vehicle dynamics estimation, a friction estimation algorithm based on the steering rack force sensor and an algorithm for the banking estimation based on a kinematic relation.

The estimation algorithm described in this manuscript aims to take into account as many aspects as possible to make the vehicle estimator able to operate in the widest possible spectrum of operating conditions. The simultaneous estimation of the vehicle side-slip angle, of the tyre parameters including cornering stiffness, and of road inclination, is pursued through the usage of a single and relatively complex vehicle model that includes roll dynamics, detailed parametrization, and combined tyre interaction driven by a robust estimation of the tyre slip ratio. The idea behind this kind of approach is that with a sufficient modeling accuracy, and taking into account all the phenomena that have a significant impact on the lateral dynamics, an EKF can be able to perform the cited simultaneous estimation from the data provided by a six axis IMU with steering wheel and wheel speed sensors.

The roll dynamics part of the model is similar to the one presented in [73], where the banking angle estimation is obtained by means of a model-based Kalman estimator starting from the information regarding the vehicle lateral equilibrium. Furthermore, to increase the estimation accuracy, the proposed model includes a further redundancy concerning the generalized angular velocity provided by gyroscopes available onboard.

The described vehicle parametrization is more detailed compared to the commonly adopted in Kalman filters, since it takes into account not only the usually employed geometric and inertial parameters (i.e. mass, inertia, wheelbase and track dimension), but also roll dynamics parameters, a Pacejka magic formula tyre model with combined interaction [14] and suspension

elasto-kinematics parameters (i.e. toe and camber compliances included by means of lookup tables, containing the non-linear relationships between wheel orientation and vertical movement of the suspension) [74, 75]. This parameters setup is required to provide an accuracy level comparable to that of vehicle simulators used by OEMs, but which is also capable of being employed in a Kalman filter for vehicle monitoring and maintenance purposes [76, 77]. In this way the a-priori estimation performed by the algorithm is extremely accurate, reducing systematic errors' magnitude and making residual errors closer to the normal distribution [78]. For sake of completeness, the developed algorithm can be employed even without the elasto-kinematics of the suspensions: in such case, the slip stiffness of the tyres will adapt to a new value, able to compensate the approximations of the suspension kinematics [66].

In the next paragraph, the double-track vehicle model, used in the EKF algorithm, is described in detail. Paragraph 3 concerns the validation of the model, both with data obtained from simulation and experimental activity from track tests. Simulation data validation is necessary to verify the estimation reliability of data that cannot be measured experimentally, such as the estimated tyre parameters.

5.2 Model-based estimator

5.2.1 Design and hypotheses

The state estimator presented in this chapter is based on an Extended Kalman Filter (EKF) with 14 states. This is a large number compared to what is commonly adopted in literature, but the purpose of this work is to reach the maximum possible accuracy through using a complete and complex model in a single EKF block, rather than interfacing a simpler vehicle model EKF block with additional necessary modules for other subsystems, as the tyre force estimation [68, 79], the parameters' estimation [62], or the correction of the

inaccuracies caused by neglecting the combined tyre interaction in the model [60]. It has to be highlighted that the Unscented Kalman Filter (UKF) is also suitable for the state estimation of nonlinear systems. Compared to the EKF, the UKF performs a better approximation in the covariance propagation over the model nonlinearities [48]. Both UKF and EKF have been implemented and tested on the presented model, offering similar results; this was also higlighted on other works on vehicle state estimation [72, 80]. EKF has been chosen over UKF because UKF can suffer of numerical stability problems if used on models with a large state vector size [81]. This problem gets worse when the algorithm must work in single precision ECUs, common on cars. Furthermore, EKF offers slightly faster computational speed. The possibility of using a Particle Filter (PF) [82], as an alternative to the algorithms mentioned, was discarded for the same reasons that led to prefer EKF over UKF, since the peculiarity of the PF algorithm consists in the fact that it can manage severe nonlinearities at the cost of greater computational effort.

The EKF is based on the state evolution and measurement equations:

$$x_k = f(x_{k-1}, u_k, w_{k-1}) \tag{5.1}$$

$$y_k = h(x_k, v_k) \tag{5.2}$$

where x is the state vector, u is the input vector, w is the process noise, y is the measurement vector, h is the measurement function and v is the measurement noise [46].

5.2.2 Vehicle model: state evolution and measurement functions

The EKF relies on a double-track vehicle model, constituted by two masses: the unsprung mass connected to the wheels, and the sprung mass rolling within the yz plane around the roll axis [83]. The global inclination around the vehicle roll and pitch axis are considered, with the purpose of taking in account

the road inclination (slope and banking). Suspension elasto-kinematics are modeled in detail, including compliances, starting from the K&C (kinematics and compliance, empirical suspension characterization) data provided by Maserati [84]. The tyre is modeled with 5.2 version of the Magic Formula, that includes all steady-state parameters [85, 14]. Figure 5.1 shows how the model is schematized. This model was chosen with the purpose of getting a detailed simulation of the lateral dynamics, using the parametrization process available to a car manufacturer, in order to achieve the simultaneous estimation of side-slip angle, banking angle and tyre parameters. The complexity added to the longitudinal dynamics, such as taking in account the pitch motion and the wheel motion, is necessary to get an accurate simulation of the lateral dynamics.

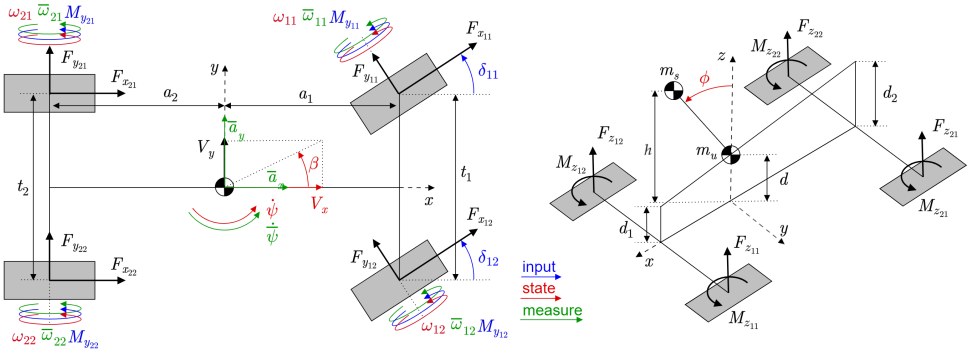

Fig. 5.1 Vehicle dynamics model

The EKF state, measurement and input vectors are defined as follows:

$$x = [V_x, \beta, \dot{\psi}, \phi, \dot{\phi}, \phi_g, \theta_g, \Omega_{11}, \Omega_{12}, \Omega_{21}, \Omega_{22}, \mu, K_1, K_2]^\intercal \tag{5.3}$$

$$y = [a_x, a_y, \psi, \Omega_{11}, \Omega_{12}, \Omega_{21}, \Omega_{22}]^\intercal \tag{5.4}$$

$$u = [\delta_{sw}, p, q, M_{y_{11}}, M_{y_{12}}, M_{y_{21}}, M_{y_{22}}]^\intercal \tag{5.5}$$

where V_x is the longitudinal velocity, β is the vehicle side-slip angle, θ, ϕ and ψ are the pitch, roll and yaw angles respect to the road. The g subscript

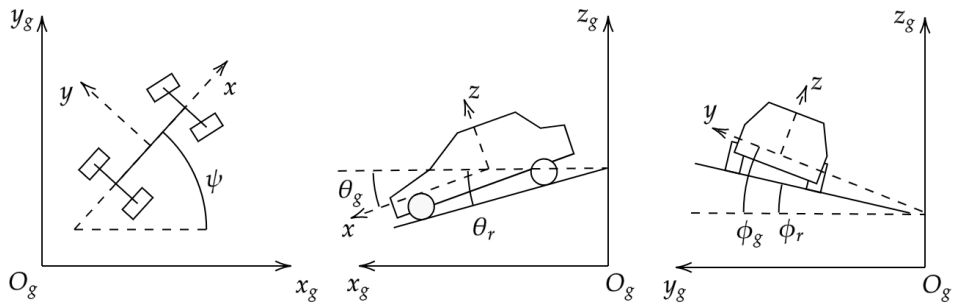

Fig. 5.2 Global and local reference systems

denotes that the angle refers to the global reference system orientation. The subscript r denotes the angle of the road in the global reference system.

$$\theta_g = \theta + \theta_r \tag{5.6}$$

$$\phi_g = \phi + \phi_r \tag{5.7}$$

$$\psi_g = \psi \tag{5.8}$$

a_x and a_y are the longitudinal and lateral accelerations in the vehicle sprung mass reference system, Ω_{11}, Ω_{12}, Ω_{21}, Ω_{22} are the front left, front right, rear left and rear right wheel rotational speed, $M_{y_{11}}$, $M_{y_{12}}$, $M_{y_{21}}$, $M_{y_{21}}$ are the moments provided to the wheel by the engine or brakes, δ_{sw} is the steering wheel angle, p and q are the roll and pitch rates measured by the vehicle sensors, μ is the grip scaling applied to longitudinal and lateral tyre peak force parameter for both front and rear axle, K_1 and K_2 are the front and rear tyre cornering stiffness scaling. Tyre grip and cornering stiffness have been included in the states list to make possible their adaptation to the real road conditions since they will vary with tyre temperature, road and weather.

The state evolution function f, for the first seven of the states listed, is based on the forward Euler integration method:

$$x_{k+1} = x_k + \dot{x}_k \Delta t \tag{5.9}$$

The following equations show how the state derivatives are obtained for the first five states. The following equations were obtained making reference to the Guiggiani's book [66], adding the terms necessary to take in account the road inclination and performing some linearization with the assumption that the side-slip angle and the road inclination does not exceed 15 degrees:

$$\dot{V}_x = \frac{X - \frac{1}{2} d_a C_d A V_x^2}{m} + \beta V_x \dot{\psi} + g\theta_r \tag{5.10}$$

$$\dot{\beta} = \frac{Y + m_s(h-d)\ddot{\phi}}{mV_x} - \dot{\psi} - \frac{g\phi_r}{V_x} \tag{5.11}$$

$$\ddot{\psi} = \frac{N}{J_z} \tag{5.12}$$

$$\ddot{\phi} = \frac{\frac{m_s}{m}(h-d)Y - K_r\phi - C_r\dot{\phi}}{J_x + \frac{m_s}{m}(m-m_s)(h-d)^2} \tag{5.13}$$

$$\dot{\phi} = \dot{\phi} \tag{5.14}$$

where X, Y and N are the total longitudinal force, lateral force and yaw moment exerted from tyres, m, m_s , J_z and J_x are the vehicle total mass, sprung mass, yaw and roll inertia, h and d are the center of gravity and roll center heights, K_r and C_r are the roll stiffness and damping, C_d is the vehicle drag coefficient, A the front section area and d_a is the air density. The roll acceleration equation 5.13 is the most complex of this set: it has been obtained rearranging the vehicle roll equation with non-neglectable unsprung mass shown in [66]. The roll velocity equation 5.14 is trivial and is included to complete the state derivative equations set; it means that the roll state is obtained by the simple integration of the roll velocity obtained from the integration of the equation 5.13. To simplify the equations and reduce the computational cost, linearizations were carried out in the calculation of the side-slip angle and of the inclination angles of the road, losing accuracy in the case of extreme angles. For the same reason, the contribution of lateral aerodynamic drag has been neglected. The dataset used for the work relates to

a sports car on the track, where the angles mentioned have never exceeded 5 degrees, while the approximations made can be considered acceptable within 15 degrees:

X, Y and N are obtained from tyre forces and moments:

$$\begin{aligned} X &= \sum_{ij}(F_{x_{ij}}\cos\delta_{ij} + F_{y_{ij}}\sin\delta_{ij}) \\ Y &= \sum_{ij}(F_{x_{ij}}\sin\delta_{ij} + F_{y_{ij}}\cos\delta_{ij}) \\ N &= \sum_{ij}[(F_{x_{ij}}\sin\delta_{ij} + F_{y_{ij}}\cos\delta_{ij})W_{x_{ij}} - (F_{x_{ij}}\cos\delta_{ij} + F_{y_{ij}}\sin\delta_{ij})W_{y_{ij}} + M_{z_{ij}}] \end{aligned} \tag{5.15}$$

where $F_{x_{ij}}$, $F_{y_{ij}}$ and $M_{z_{ij}}$ are the tyre longitudinal force, lateral force and auto-aligning moment. Subscript ij denotes the i-th axle (1 front, 2 rear) and the j-th side (1 left, 2 right). $W_{x_{ij}}$ and $W_{y_{ij}}$ are the wheel center coordinates to the vehicle center of gravity in the vehicle reference system. They can easily be obtained from vehicle track and wheelbase.

$$\begin{aligned} W_{x_{ij}} &= \begin{bmatrix} a_1 & a_1 \\ -a_2 & -a_2 \end{bmatrix} \\ W_{y_{ij}} &= \begin{bmatrix} t_1 & -t_1 \\ t_2 & -t_2 \end{bmatrix} /2 \end{aligned} \tag{5.16}$$

where a_1, a_2 are the front and rear wheelbase, t_1, t_2 are the front and rear track.

Tyre forces and moments are obtained from Pacejka's Magic Formula, which parameters must be known. The states μ, K_1 and K_2 will constantly be

updated by the Kalman Filter algorithm in order to correct the tyre model.

$$\begin{aligned} F_{x_{ij}} &= F_{x_{ij}}(F_{z_{ij}}, \kappa_{ij}, \alpha_{ij}, \gamma_{ij}, \mu) \\ F_{y_{ij}} &= F_{y_{ij}}(F_{z_{ij}}, \kappa_{ij}, \alpha_{ij}, \gamma_{ij}, \mu, K_i) \\ M_{z_{ij}} &= M_{z_{ij}}(F_{z_{ij}}, \kappa_{ij}, \alpha_{ij}, \gamma_{ij}, \mu, K_i) \end{aligned} \tag{5.17}$$

where $F_{z_{ij}}$ are the tyre vertical loads, κ_{ij}, α_{ij}, γ_{ij} are the tyre slip ratio, slip angle and inclination angle. The vertical forces $F_{z_{ij}}$ are obtained, accordingly to [66], with:

$$\begin{aligned} F_{z_{11}} &= \frac{a_2 gm}{2(a_1+a_2)} + \frac{d_a}{4} C_{l_1} A V_x^2 - \frac{m a_{x_r} h}{a_1+a_2} - \frac{Y_1 d_1}{t_1} - \frac{g m_s (h-d_1)\phi}{t_1} - \frac{K_{r_1}\phi}{t_1} - \frac{C_{r_1}\dot{\phi}}{t_1} \\ F_{z_{12}} &= \frac{a_2 gm}{2(a_1+a_2)} + \frac{d_a}{4} C_{l_1} A V_x^2 - \frac{m a_{x_r} h}{a_1+a_2} + \frac{Y_1 d_1}{t_1} + \frac{g m_s (h-d_1)\phi}{t_1} + \frac{K_{r_1}\phi}{t_1} + \frac{C_{r_1}\dot{\phi}}{t_1} \\ F_{z_{21}} &= \frac{a_1 gm}{2(a_1+a_2)} + \frac{d_a}{4} C_{l_2} A V_x^2 + \frac{m a_{x_r} h}{a_1+a_2} - \frac{Y_2 d_2}{t_2} - \frac{g m_s (h-d_2)\phi}{t_2} - \frac{K_{r_2}\phi}{t_2} - \frac{C_{r_2}\dot{\phi}}{t_2} \\ F_{z_{22}} &= \frac{a_1 gm}{2(a_1+a_2)} + \frac{d_a}{4} C_{l_2} A V_x^2 + \frac{m a_{x_r} h}{a_1+a_2} + \frac{Y_2 d_2}{t_2} + \frac{g m_s (h-d_2)\phi}{t_2} + \frac{K_{r_2}\phi}{t_2} + \frac{C_{r_2}\dot{\phi}}{t_2} \end{aligned} \tag{5.18}$$

where C_{l_1} and C_{l_2} are the front and rear aerodynamic downforce coefficients, d_1 and d_2 are the front and rear roll center height, K_{r_1}, K_{r_2} are the front and rear axle roll stiffness, and C_{r_1}, C_{r_2} are the front and rear axle roll damping. Vehicle roll stiffness K_r and damping C_r that appear in equation 5.13 must be equal to the sum of the contribution of the single axles.

The fourth term of the equation may need a further explanation: it represent the lateral load transfer that is acts rigidly on the chassis. Its value is equal to the lateral force on the axle Y_i times the axle roll center height d_i

divided by the track t_i. The lateral axle force can be obtained as:

$$\begin{aligned} Y_1 &= \frac{a_2 m a_{y_r} + \ddot{\psi} J_z}{a_1 + a_2} \\ Y_2 &= \frac{a_1 m a_{y_r} + \ddot{\psi} J_z}{a_1 + a_2} \end{aligned} \tag{5.19}$$

Vehicle longitudinal acceleration a_{x_r} and lateral acceleration on the unsprung mass on the road reference system a_{y_r} are both oriented like the road an can be obtained with:

$$a_{x_r} = \frac{X - \frac{1}{2} d_a C_d A V_x^2}{m} \tag{5.20}$$

$$a_{y_r} = \frac{Y}{m} \tag{5.21}$$

In order to avoid algebraic loops, a_{x_r} and a_{y_r} must be stored from the last sample $k-1$ [86].

Slip ratios κ_{ij} and slip angles α_{ij} are obtained with the following formulas:

$$\begin{aligned} \begin{bmatrix} V_{tx_{ij}} \\ V_{ty_{ij}} \end{bmatrix} &= \begin{bmatrix} \cos(\delta_{ij}) & \sin(\delta_{ij}) \\ -\sin(\delta_{ij}) & \cos(\delta_{ij}) \end{bmatrix} \begin{bmatrix} \beta V_x + W_{x_{ij}} r \\ V_x - W_{y_{ij}} r \end{bmatrix} \\ \alpha_{ij} &= \arctan\left(\frac{V_{ty_{ij}}}{V_{tx_{ij}}}\right) \\ \kappa_{ij} &= \frac{\Omega_{ij} \rho_{ij} - V_{tx_{ij}}}{V_{tx_{ij}}} \end{aligned} \tag{5.22}$$

where $V_{tx_{ij}}$ and $V_{ty_{ij}}$ are the longitudinal and lateral velocities in tyre reference system. To obtain slip angle and slip ratios, the wheel steering angles δ_{ij} are also required, being determined employing steering wheel angle δ_{sw} and suspensions elasto-kinematics:

$$\delta_{ij} = \delta_{T_{ij}} + \delta_{S_{ij}}(\delta_{sw}) + \delta_{L_{ij}}(F_{z_{ij}}) + \delta_{Cy_{ij}} F_{y_{ij}} + \delta_{Cz_{ij}} M_{z_{ij}} \tag{5.23}$$

The wheel steering angles δ_{ij} are obtained with a complete formulation that includes the static toe angles $\delta_{T_{ij}}$, the steering term $\delta_{S_{ij}}(\delta_{sw})$ and the suspension travel term $\delta_{L_{ij}}(F_{z_{ij}})$, that are implemented with lookup tables, and the compliance terms $\delta_{Cy_{ij}}F_{y_{ij}}$ and $\delta_{Cz_{ij}}M_{z_{ij}}$ to take into account the steering angle variation induced by tyre lateral force and self-aligning moment.

To conclude the section relative to the tyre force calculation, the wheel inclination angles γ_{ij} are obtained with a formulation analogous to that used for δ_{ij}.

$$\gamma_{ij} = \gamma_{T_{ij}} + \gamma_{S_{ij}}(\delta_{sw}) + \gamma_{L_{ij}}(F_{z_{ij}}) + \gamma_{Cy_{ij}}F_{y_{ij}} \tag{5.24}$$

where $\gamma_{T_{ij}}$ is the static inclination angle, $\gamma_{S_{ij}}(\delta_{sw})$ and $\gamma_{L_{ij}}(F_{z_{ij}})$ are the terms for the inclination induced by steering wheel angle and suspension travel that are implemented with lookup tables, and $\gamma_{Cy_{ij}}F_{y_{ij}}$ is the compliance term to take in account the inclination angle variation induced by the lateral force. In order to avoid algebraic loops, $F_{y_{ij}}$ and $M_{z_{ij}}$ used in equations 5.23 and 5.24, are obtained from the last sample $k-1$ as done for the accelerations in the vertical forces calculation. The mentioned quantities are obtained through a specific test-rig or multibody simulations converted in look-up table to reduce the computational cost, as described in [87]. Samples relating to the $F_{z_{ij}}$-δ_{ij}, F_z-γ_{ij}, δ_{sw}-δ_{ij} and δ_{sw}-γij relationships are extracted from these data. These samples are stored by the algorithm described, and a simple linear interpolation between the samples is used to return the continuous functions $\delta_{L_{ij}}(F_{z_{ij}})$, $\delta_{S_{ij}}(\delta_{sw})$, $\gamma_{L_{ij}}(F_{z_{ij}})$ and $\gamma_{S_{ij}}(\delta_{sw})$. From the same experimental data, it emerges that other relations, such as $\delta_{L_{ij}}(F_{y_{ij}})$ and $\gamma_{L_{ij}}(F_{y_{ij}})$, can be effectively approximated to linear. From these, the compliance terms $\delta_{Cy_{ij}}$ and $\gamma_{Cy_{ij}}$ are obtained with a simple linear fitting of the experimental data.

Vehicle roll and pitch angle velocities on the global reference system $\dot{\phi}_g$ and $\dot{\theta}_g$, that are necessary in the equation 5.9, are obtained by the integration of the rotational velocities measured by the gyroscopes. As commonly known, a raw integration of those signals would rapidly drift, leading to a wrong estimation, but this is avoided because the orientation angles are states of

the EKF, so the algorithm would constantly correct the orientation seeking a state configuration that fits all sensors information. Accordingly to [73], and verified in the preliminary phases of this work, the road banking angle can be estimated using an EKF from the steering wheel angle and lateral acceleration sensors, if the tyre model is correctly known, but this estimation procedure seems to give the correct results with a considerable delay because the system needs a certain time to find the banking and side-slip angle configuration that minimizes the error on the available sensors. Adding an additional a-priori information to the EKF, provided by the orientation velocity sensors, increases the response time and the accuracy of a system that is able to estimate the orientation even without this information. Note that the pitch, roll and yaw velocities in the vehicle reference system p, q and r are different from the same quantities measured in the global reference system $\dot{\theta}$, $\dot{\phi}$ and $\dot{\psi}$. Those quantities are related by the following equations from [66], an approximated version of the the roll, pitch, yaw rotation:

$$\begin{aligned} p &\simeq \dot{\phi}_g - \dot{\psi}\theta_g \\ q &\simeq \dot{\theta}_g + \dot{\psi}\phi_g \\ r &\simeq \dot{\psi} \end{aligned} \tag{5.25}$$

Re-arranging those equations, the state derivatives are obtained:

$$\begin{aligned} \dot{\phi}_g &= p + \dot{\psi}\theta_g \\ \dot{\theta}_g &= q - \dot{\psi}\phi_g \end{aligned} \tag{5.26}$$

Those equations express that to get an advantage from having the information from the gyroscopes, global roll and pitch angle must be estimated together. This estimation is needed to obtain the road slope and banking angle values, which are important to get an accurate representation of the vehicle dynamic equilibrium. Without it, in order to preserve the equilibrium, the Kalman

Filter algorithm will alter the vehicle tyre force through the update of the tyre parameters μ, K_1 and K_2.

The equation 5.10, that calculates the longitudinal velocity derivative $\dot{V}_x$ needs a further explanation because the vehicle road slope angle θ_r appears in it, but it has not already defined. In this model, the vehicle pitch motion in the global reference system θ_g is a state, but the vehicle pitch motion relative to the road is treated in a simplified way, as the multiplication between the vehicle longitudinal acceleration and a constant θ_{1g} that represent the vehicle pitch relative to the road under an acceleration of $9.81\frac{m}{s}$. θ_{1g} can be directly measured or calculated from vehicle characteristics. This simplification was done with the purpose of avoiding adding 2 further states (pitch position and velocity with respect to the road) in a system that already has 14 states, in which tuning the process and measuring noise covariance matrices is already a complex task. Roll and pitch motions are treated in a different way: roll motion is modeled in a more detailed way because the lateral dynamics is obviously related to vehicle stability and it deserve the most accuracy possible. This rigid modeling of the longitudinal dynamics will have also a small impact on the vertical force estimation, ignoring the lag between longitudinal acceleration and vertical load transfer. The vehicle pitch motion still cannot be neglected in order to model the road slope and the misalignment between the road and the accelerometer, that due to its inclination will measure a portion of gravitational acceleration. This can induce a variation on the measured longitudinal acceleration up to 10%. So, the vehicle inclination relative to road θ is obtained from the following equation, that is proposed by the author following the assumptions done until now:

$$\theta = \frac{\theta_{1g} a_{x_r}}{g} \tag{5.27}$$

Combining the $\dot{V}_x$ equation (5.10) with the θ equation (5.27) and the θ_g equation (5.6), another formulation of the $\dot{V}_x$ equation is obtained, in which

θ_r does not appear:

$$\dot{V}_x = \frac{X - \frac{1}{2} d_a C_d A V_x^2}{m} + \beta V_x \dot{\psi} + g \left(\theta_g - \frac{\theta_{1g} a_{x_r}}{g} \right) \tag{5.28}$$

Then, a_{x_r} from the equation 5.20 is substituted in 5.28:

$$\dot{V}_x = \frac{X - \frac{1}{2} d_a C_d A V_x^2}{m} (1 - \theta_{1g}) + \beta V_x \dot{\psi} + g \theta_g \tag{5.29}$$

Now the longitudinal dynamics input quantities have to be defined: the "driving moments" applied on the wheel centers $M_{y_{ij}}$, as represented in figure 5.1 and mathematically defined in equation 5.5. Those moments can be obtained with a detailed model of engine and brakes, starting from the vehicle sensors on engine speed, gear, throttle and brake pedals. In the context of this work, such moments were obtained with a simplified formulation exploiting only the longitudinal accelerometer a_x and a simplified modeling of the differential and brakes. This method is simple, but it has disadvantages: the measurement of the a_x quantity is used in the Kalman filter both as a measurement (y) and as input (u); in the latter case, the algorithm is not able to purify the measurement noise, and the calculated $F_{x_{ij}}$ are noisy, as it will be shown later in figure 5.7. To obtain the wheel "driving moments" $M_{y_{ij}}$ from the longitudinal acceleration sensor, it has to be considered again that the sensor and the road reference system are not parallel because of the vehicle pitch motion. Solving the system of equations 5.30, the vehicle longitudinal acceleration in road reference system a_{x_r} can be obtained from the longitudinal acceleration sensor a_x through the constant θ_{1g}:

$$\begin{cases} a_x \simeq a_{x_r} + g\theta \\ \theta = \frac{\theta_{1g} a_{xr}}{g} \end{cases} \tag{5.30}$$

$$a_{x_r} = \frac{a_x}{1 + \theta_{1g}} \tag{5.31}$$

The sum of the tyre longitudinal forces in the vehicle reference system can be obtained from the longitudinal acceleration in the road reference system a_{x_r}. This quantity will be slightly different from the actual total longitudinal force X, as it is obtained from measurement acceleration instead of the model one, and it will be called X_m.

$$X_m = ma_{x_r} + \frac{1}{2} d_a C_d A V_x^2 \tag{5.32}$$

Finally, wheel "driving moments" $M_{y_{ij}}$ are obtained by splitting X_m on the four corners using basic characteristics of the vehicle, then multiplying the forces by the rolling radius ρ_{ij}, where T_i represents the traction moment portion on each axle. For a rear traction vehicle $T_1 = 0$ and $T_2 = 1$. B_i represents the braking moment portion on each axle. For a vehicle with a brake balance of 0.6: $B_1 = 0.6$ and $B_2 = 0.4$. Then, the force is split at the half on sides considering an open differential and symmetrical braking system.

$$M_{y_{ij}} \simeq \rho_{ij} \left[\max\left(\frac{T_i X_m}{2}, 0 \right) + \min\left(\frac{B_i X_m}{2}, 0 \right) \right] \tag{5.33}$$

To obtain wheel speed, the backward Euler integration method is needed because the wheel system is a high frequency system due to the high tyre carcass longitudinal stiffness and the relatively low wheel inertia. This frequency can be easily higher than 100 Hz. Forward Euler integration is stable only if the integration frequency is considerably higher than the natural frequency of the system, $\sim$200 Hz in this case, that combined with the high number of states of this system will lead to a high computational burden incompatible with real-time. Those problems were overcome with the usage of an implicit integrator for the wheel rotational speed state, making the entyre system stable at 100 Hz, which is often the same as the sensors' acquisition frequency available within the onboard state evaluation systems [88].

The backward Euler method is different from the forward Euler (equation 5.9) because the derivative of the state is calculated in the next sample instead

of the current:

$$x_{k+1} = x_k + \dot{x}_{k+1}\Delta t \tag{5.34}$$

In the examined case the generic notation $\dot{x}_{k+1}$ represents the wheel acceleration in the next sampling, $\dot{\omega}_{k+1}$, that can be obtained from the analytical equation of the wheel rotational equilibrium:

$$M_D = \rho F_x(\Omega_{k+1}) + \dot{\omega} J_{w_y} \tag{5.35}$$

where M_D is the wheel "driving moment": the moment provided from the engine or the braking system, J_{w_y} is the wheel rotational inertia, and ρ is the effective rolling radius. All the quantities in this equation are referred to a single corner, so they should include the subscript ij that has been omitted to avoid subscript overloading. In models that use the wheel angular speed as input, an extremely accurate modeling of the tyre rolling radius is necessary, because errors in the estimate of its value have a heavy impact in the estimate of the slip ratios, which ultimately results in a strong impact on the lateral dynamics due to combined interactions. With this modeling, however, the approximation of a ρ constant value can be acceptable because the a-priori estimate of the slip ratio will always be consistent with that of the longitudinal force estimated by the simplified powertrain model; so, for example, in absence of excitations the slip ratio will be zero even if the rolling radius value it's not accurate. The correction of the state performed by the Kalman Filter can make the model fall into the same condition where the angular velocities are used as input. To avoid this, the covariances of measurement of the wheels angular velocities must be large enough to have no significant impact on the slip ratios, but still being able to correct the vehicle velocity drift caused by the longitudinal acceleration integration that excites the model.

$F_x(\Omega_{k+1})$ is the longitudinal tyre force calculated with the Pacejka tyre model with the wheel speed in the next step. All other Pacejka's function arguments are omitted to obtain a more compact synthesized formulation, but

they are all represented in equation 5.36

$$F_x = F_x(\kappa(\Omega, V_x), \alpha, \gamma, F_z) \tag{5.36}$$

where κ is the slip ratio that depends on wheel rotational speed Ω and wheel longitudinal speed V_x, slip angle α, camber angle γ and wheel vertical load F_z. Equation 5.35 includes Ω_{k+1}, that can be obtained at the current instant k via the Taylor expansion cut to the first order.

$$F_x(\Omega_{k+1}) \simeq F_x(\Omega_k) + \frac{\partial F_x}{\partial \Omega}(\Omega_k)\Delta\Omega \tag{5.37}$$

Substituting 5.37 in 5.35, the discrete wheel rotational speed increment $\Delta\Omega$ is obtained:

$$M_D = \rho \left(F_x(\Omega_k) + \frac{\partial F_x}{\partial \Omega}(\Omega_k)\Delta\Omega \right) + \frac{\Delta\Omega}{\Delta t} J_{w_y} \tag{5.38}$$

$$\Delta\Omega = \frac{\frac{M_D}{\rho} - F_x(\Omega_k)}{\frac{\partial F_x}{\partial \Omega}(\Omega_k) + \frac{J_{w_y}}{\rho \Delta t}} \tag{5.39}$$

Note that equation 5.39 includes the partial derivative of F_x, that must be calculated numerically by applying the difference quotient formula on Pacejka's Magic Formula. $\Delta\Omega$ is obtained starting from equation 5.35, that is calculated in the $k+1$ step, so it's true:

$$\Delta\Omega = \dot{\Omega}_{k+1}\Delta t \tag{5.40}$$

That is needed to apply the backward Euler method for the wheel rotational speed integration:

$$\Omega_{k+1} = \Omega_k + \dot{\Omega}_{k+1}\Delta t = \Omega_k + \Delta\Omega \tag{5.41}$$

The last three states are for the tyre parameters correction μ, K_1 and K_2. Those are not updated by the state evolution function f that appears in equation 5.1, but only by the EKF algorithm during the measurement correction phase, with the same approach adopted in [89].

$$\begin{aligned} \dot{\mu} &= 0 \\ \dot{K}_1 &= 0 \\ \dot{K}_2 &= 0 \end{aligned} \tag{5.42}$$

Those scaling factors must act on the macro-parameters of the Pacejka tyre model [14] as it is commonly achieved via λ micro-parameters. μ will scale the μ_x and μ_y macro-parameter for both front and rear tyres, K_1 will scale the $K_{y\alpha}$ macro-parameter for the front tyres, and K_2 will scale the $K_{y\alpha}$ macro-parameter for the rear tyres.

The measurement function h, appearing in equation 5.2, is used to obtain the readings expected from the sensors, listed in 5.4, given the state x as input. The function is defined by the following equations:

$$\begin{aligned} \overline{a}_x &= \dot{V}_x - \beta V_x \dot{\psi} - g\theta_g \\ \overline{a}_y &= V_x \dot{\beta} + V_x \dot{\psi} + g\phi_g \\ \overline{\dot{\psi}} &= \dot{\psi} \\ \overline{\Omega}_{11} &= \Omega_{11} \\ \overline{\Omega}_{12} &= \Omega_{12} \\ \overline{\Omega}_{21} &= \Omega_{21} \\ \overline{\Omega}_{22} &= \Omega_{22} \end{aligned} \tag{5.43}$$

5.2.3 Process and noise covariance matrices

Equations 5.1 and 5.2 show how the process noise w and the measurement noise v are involved in the modelling and measurements. The process noise represents the difference between the true value of the state and the a-priori

estimation made by the model, i.e. the error introduced at each time step by the modeling inaccuracies; the measurement noise represents the error in the sensors readings. w and v are assumed to be independent each other, white, and with normal probability distribution [46]:

$$\begin{aligned} p(w) &\sim N(0,Q) \\ p(v) &\sim N(0,R) \end{aligned} \tag{5.44}$$

Those are strong assumptions, especially for the process noise because model errors tend to be more systematic than measurement errors. To this purpose, the employment of a more complete and complex model will help to reduce the model (systematic) errors magnitude. Q and R are the process and measurement noise covariance matrices, whose proper definition is fundamental to get the best accuracy and robustness of the estimation, but, unfortunately, this is not an trivial task. Traditionally, those matrices are obtained with manual tuning. This can be acceptable for R since the sensors' error will likely be uncorrelated each other, so R will hopefully result in a diagonal matrix (7 values in our case). Furthermore, sensor errors can be evaluated starting from sensors' manufacturer datasheets. Regarding Q matrix, compared to R, the manual tuning can be practically impossible, since usually the matrix will not be diagonal, so it will have a significant number of values (105 in our case) to be calibrated, and those cannot be assigned intuitively. To avoid these problems, the values of the matrices have been determined with two of the algorithms shown in [53] and reported on this thesis in the paragraphs 4.5.1 and 4.5.2, however, the optimization procedure will be also treated here applied for this specific case. The first of the two methods applied is called

"Maximizing the joint likelihood":

$$\begin{aligned} Q_{joint} &= \frac{1}{T}\sum_{k}^{T}(x_k - f(x_{k-1}, u_k))(x_k - f(x_{k-1}, u_k))^{\mathsf{T}} \\ R_{joint} &= \frac{1}{T}\sum_{k}^{T}(y_k - h(x_k))(y_k - h(x_k))^{\mathsf{T}} \end{aligned} \tag{5.45}$$

where x is the vector state, that must be known. This will not always be applicable, but in the context of this work, both high-end simulation data (to which artificial noise was added) and experimental data from advanced additional sensors set (including optical measures of the vehicle velocity and side-slip angle, and global orientation measurement from double GPS antennas and IMU) were available. The states, which cannot be evaluated from experimental data, regard the tyres subsystem, as parameters scaling μ, K_1 and K_2, which indeed were excluded from the model in order to apply this method. In this case, the Q matrix was extended to all states, setting the missing diagonal values manually, and the non-diagonal values to zero. Tyre parameter scaling covariance has been set in such a way that the correction is slow enough to induce only small variations during a single corner. In this way, the KF algorithm will guarantee the vehicle lateral equilibrium by applying the measurement correction term only on the road banking angle and side-slip angle quantities. The tyre parameters scalings will change over a longer time, about 100 seconds, ensuring the correct functioning of the estimator regardless of the correctness of the initial conditions. The "Maximizing the joint likelihood" method does not require any further iterations, once the manual tuning of tyre parameters' scalings has been achieved, making it fast and reliable.

The second method applied, *"Minimizing The Residual Prediction Error"*, is performed running an optimization algorithm with this error function:

$$\langle Q_{res}, R_{res} \rangle = \arg\min_{Q,R} \sum_{k=0}^{T} (z_k - g(x_k))^{\intercal} Z^{-1} (z_k - g(x_k)) \tag{5.46}$$

where z is a set of high-end measurements available in the training phase only, g is the measurement function associated with this set of sensors (analogous to h for y) and Z is the measurement noise covariance associated to z (analogous to R for y). This method is more flexible than the first one, because it does not require the knowledge of all states, but it needs the usage of iterative methods. Furthermore, a solver not employing an explicit gradient computation should be used, as the Surrogate function is, which is describerd in detail in paragraph 4.5.3. Indeed, this scenario will require very high computational effort. Then, Q_{joint} and R_{joint} can be used as initial conditions, and the optimal values for the covariance associated with tyres scalings μ, K_1 and K_2 can be found.

5.3 Results

5.3.1 Validation towards simulation data

The initial phase of the validation activity of the proposed vehicle state estimation approach has been performed with the commercial VI-CarRealTime software solution [90]. The state-of-the-art validation model has been developed by Maserati in the context of real vehicle development, the virtual vehicle was driven by the MaxPerformance algorithm in the circuit of Balocco in dry road conditions, aiming for the lowest lap time possible. Simulation data offer the knowledge of all the time-varying variables and tyre characteristics, contrarily from experimental one, where quantities referring to adhesion condition and tyre cornering stiffness are actually unknown, despite they can be identified with offline procedures [21, 41]. Those results were obtained

by running the estimator at 100 Hz, adding artificial white noise to all the sensors.

The following plots show the estimation of the states that can be measured with test car instrumentation only, not available on commercial vehicles. For industrial confidentiality agreements, all plots except those relative to vehicle orientation will be provided as normalized to the maximum reported value.

Longitudinal velocity is estimated with great precision, as reported in figure 5.3, even during the braking phase where the wheel locking occurs at the rear wheels occurs at $time = 96$ s. It is worth noting that the vehicle speed accuracy is very sensitive to the correctness of the rolling radius parameter.

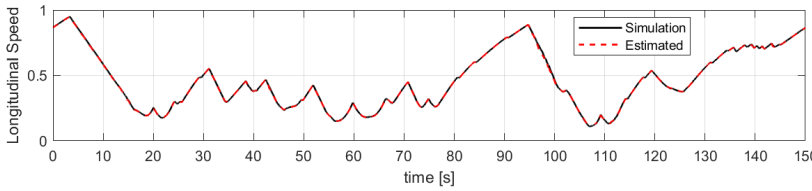

Fig. 5.3 Simulated and estimated longitudinal velocity

Figure 5.4 shows the side-slip angle estimation.

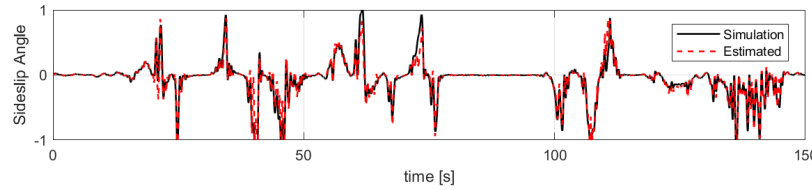

Fig. 5.4 Simulated and estimated side-slip angle

The other most interesting states, in which there is no direct measurement, are the vehicle roll and pitch angles, reported in figure 5.5 and 5.6, respectively. Road slope and banking angle can be easily be evaluated by subtracting vehicle inclination to the road one (equations 5.6 and 5.7), remembering vehicle pitch to road θ is known from equation 5.27 and vehicle roll ϕ is one of the system states.

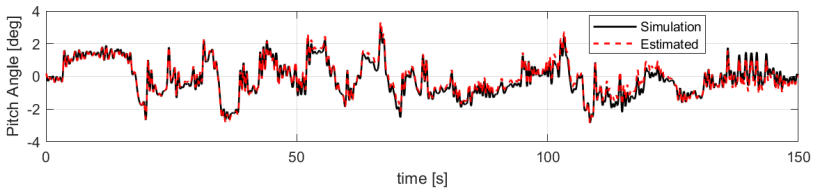

Fig. 5.5 Simulated and estimated vehicle pitch angle in global reference system

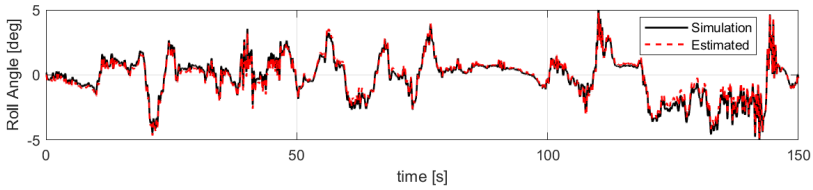

Fig. 5.6 Simulated and estimated vehicle roll angle in global reference system

Tyre forces $F_{x_{ij}}$, $F_{y_{ij}}$ and $F_{z_{ij}}$ are not states, but the comparison of these variables with the same ones obtainable from the reference simulation is interesting because these quantities are difficult to be measured with experimental tests (indeed, further additional sensors would be necessary within the experimental dataset to measure the dynamics of each corner) [91, 92]. The described comparison is shown in figure 5.7, 5.8 and 5.9.

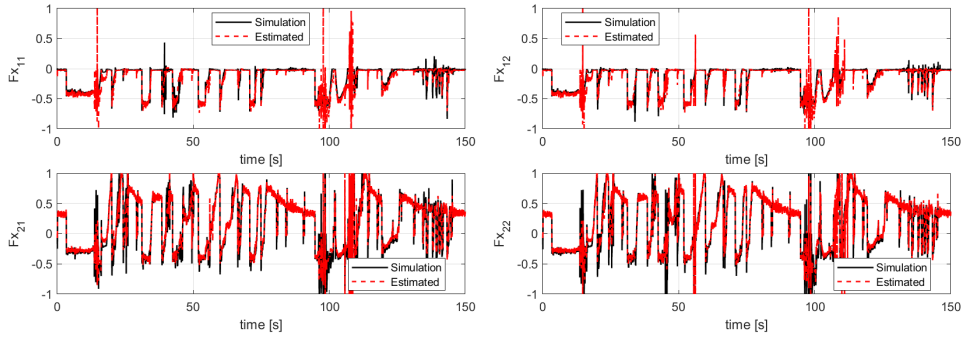

Fig. 5.7 Simulated and estimated tyre longitudinal force

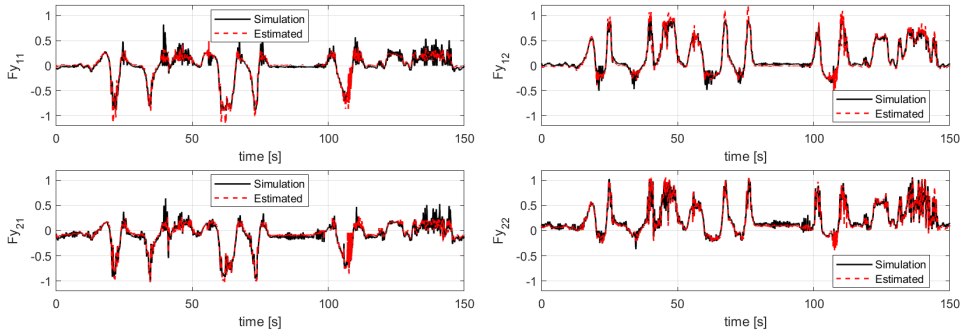

Fig. 5.8 Simulated and estimated tyre lateral force

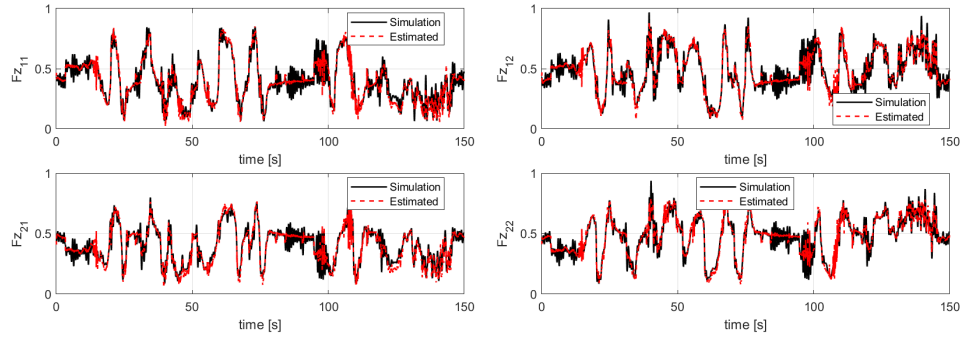

Fig. 5.9 Simulated and estimated tyre vertical force

To replicate experimental operating conditions, where tyre dynamic behavior is usually unknown, tyre parameters initially set in the EKF estimator were not the same ones adopted in the simulation, whose parameters in their turn were identified with the already cited procedure that is available in the experimental context [16, 41]. The above-mentioned methodology is able to guarantee that the differences between the estimation accuracy achieved in simulation and in experimental scenarios are minimum. Longitudinal forces shown in figure 5.7 are noisy, compared to lateral and vertical. This can be explained due to the fact that longitudinal forces $F_{x_{ij}}$ are calculated with equations exploiting the longitudinal accelerometer signal a_x as input (affected by a considerable noise) and simple modelling approaches are adopted for differential and brakes, respectively (5.31, 5.32, 5.33). Then, the wheel rotational speed and consequently the slip ratios κ_{ij} are obtained through the wheel dynamics (equation 5.39). This method is more complex than using wheel speed sensors as input, as it is commonly done in literature, but it ensures a more accurate and stable estimation of slip ratios, that it is absolutely necessary to achieve a correct tyre combined interaction. Slip ratios are shown in figure 5.10 and slip angles in figure 5.11.

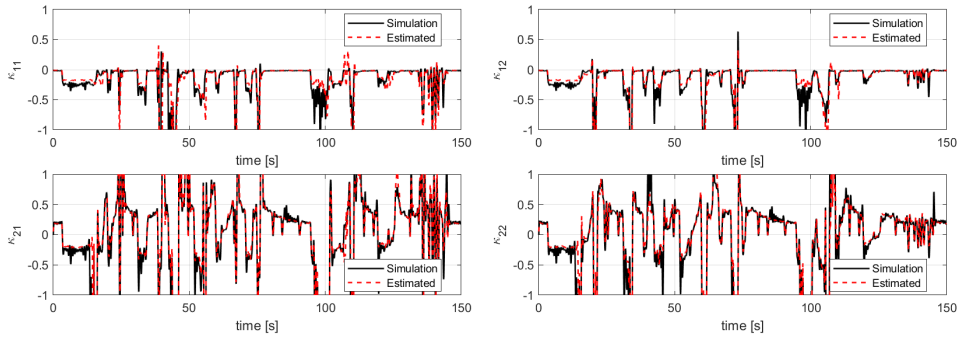

Fig. 5.10 Simulated and estimated tyre slip ratios

In case a correct set of tyre parameters is provided to the estimator, tyre parameters scaling states μ, K_1 and K_2 must be expected to remain stable

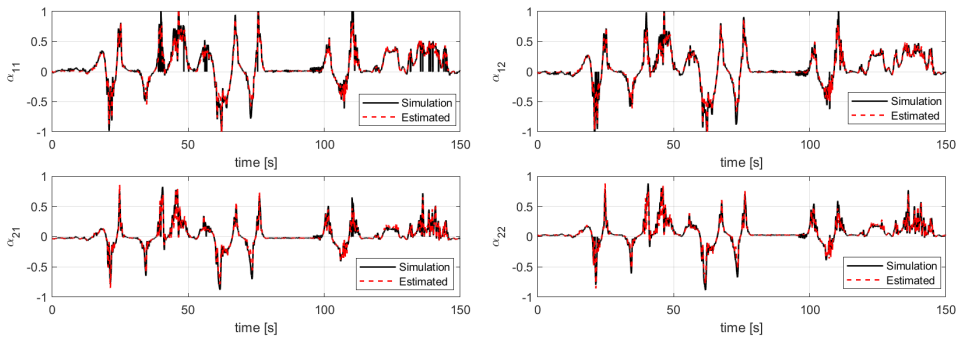

Fig. 5.11 Simulated and estimated tyre slip angles

around the starting value 1, as shown in figure 5.12. If those parameters are not stable, the tyre model parameters are expected to be not correct, or the diagonal values of the Q matrix relative to those states could be too high. Figure 5.13 shows six new cases in which the initial conditions of one of the

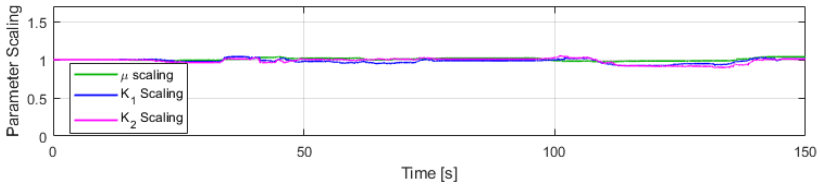

Fig. 5.12 μ, K_1 and K_2 states over time in simulation environment, with correct initial conditions

three scaling factors has been set wrong on purpose, to demonstrate that all the parameters tend to converge to the expected value 1 over time, proving that the proposed algorithm can estimate the correct value of necessary tyre parameter scalings.

5.3.2 Validation towards experimental data

The experimental environment presents many additional complexities, often ignored in the validation case studies of the various state estimators presented

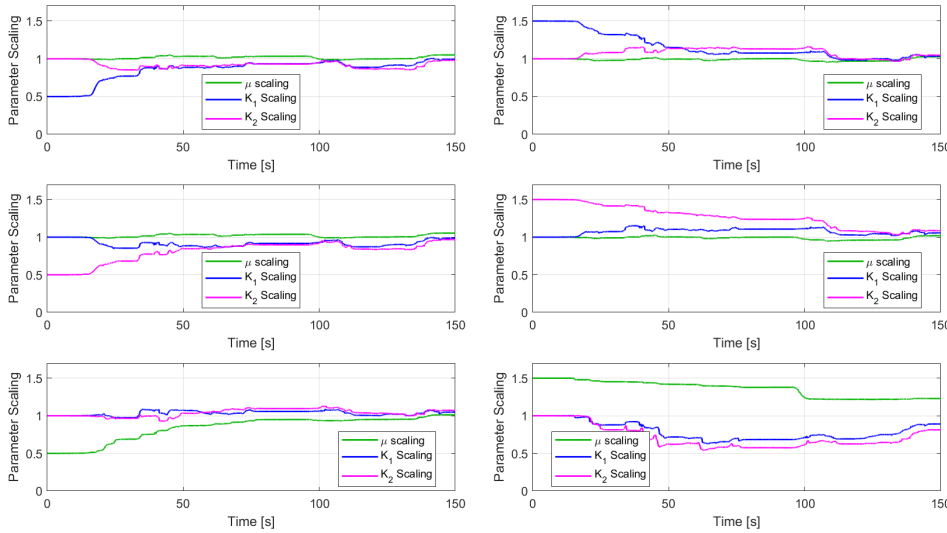

Fig. 5.13 μ, K_1 and K_2 states over time in simulation environment, with wrong initial conditions

in literature. This validation test, performed in racing conditions in the handling circuit at the Nardò Technical Center, presents all the main issues that can cause estimation errors employing the more simple models. These phenomena can be summarized as follows:

- is the estimation algorithm still valid within dynamic scenarios with tyres working over the adherence peak?
- are the grip limit variations due to combined tyre interaction taken into account?
- how is the measurement uncertainty concerning the wheel angular speed measurement faced?
- is the inclination of the road (slope and banking) taken into account?

- can the variation of the tyre conditions (temperature, pressure, wear, etc) or road characteristics (texture, material, wet/ice/dust, etc) be included within the kinematic and dynamic estimation of each vehicle corner?

For the following figures, the validation of the tyre forces will be not addressed, since, as mentioned, the validation data regarding the corners dynamics were not available.

Figures 5.14, 5.15, 5.16, 5.17, show the estimation of longitudinal velocity, side-slip angle, vehicle pitch and roll in global reference system compared to the experimental ones, respectively. Longitudinal velocity and side-slip angle are measured through Correvit S-motion optical sensors [93], and the vehicle inclination angles through OxTS inertial navigation system [94], that includes an IMU and double GPS antennas.

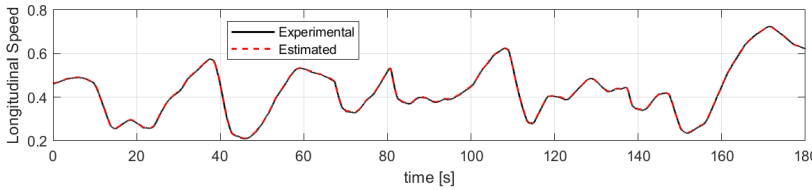

Fig. 5.14 Experimental and estimated longitudinal velocity

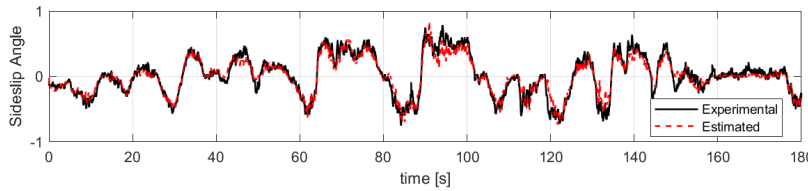

Fig. 5.15 Experimental and estimated side-slip angle

Figure 5.18 shows how, for the lateral acceleration signal, the Kalman filter acts as a real-time low pass filter with zero lag: this is possible thanks to the redundancy between model and sensor information.

Figure 5.19 shows the tyre parameters scaling μ, K_1 and K_2 in the experimental environment. The chosen time range in the previous images is

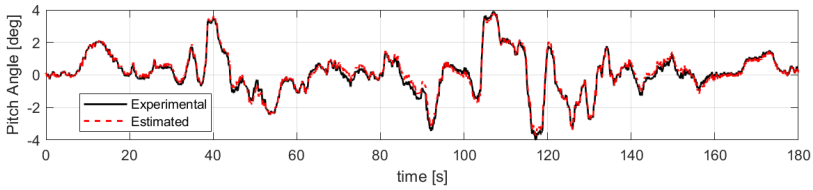

Fig. 5.16 Experimental and estimated vehicle pitch angle in global reference system

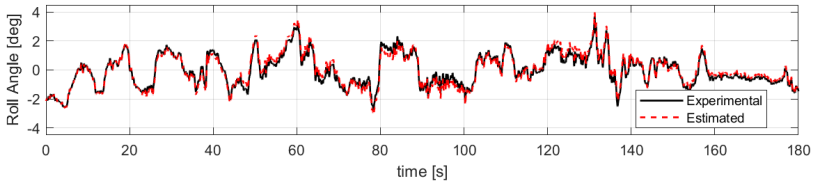

Fig. 5.17 Experimental and estimated vehicle roll angle in global reference system

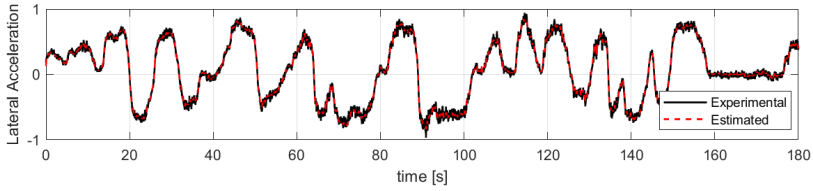

Fig. 5.18 Experimental and estimated lateral acceleration

not sufficient to show the tyre characteristics changes, so in this figure the time range is larger. The estimator shows a grip increase (μ) in the first minutes of tyre usage, caused by reaching of optimal temperature range, then a stabilization followed by a slight decrease of grip in the last minutes, caused by wear. Cornering stiffnesses K_1 and K_2 decrease over time due to tyres heating, particularly relevant for rear stiffness K_2. This behavior is coherent with expectations and with the offline analyses performed with [16, 41].

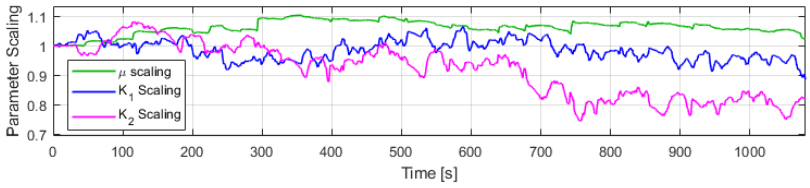

Fig. 5.19 μ, K_1 and K_2 states over time in experimental environment

All the graphs presented have been normalized with respect to hidden quantities for confidentiality reasons with Maserati, which provided the data. In this way it is not possible for the reader to understand whether the limit conditions of the vehicle have been reached in the tests shown. To overcome this problem, figure 5.20 is proposed, where the lateral acceleration with respect to the axle slip angle is shown. This type of graph was chosen because it can be directly obtained from the experimental data and because it allows to use the same normalization constants used in the previous graphs; in particular, the axle slip angles have been normalized with the same constant as the side-slip angle. The green samples in the dataset represent a highlight of the simulation points at the apex of a curve, which occurred between the the second 84 and 86 in the experimental dataset. It can be seen that the vehicle is working at the beginning of the non-linearity zone. Axle characteristic are

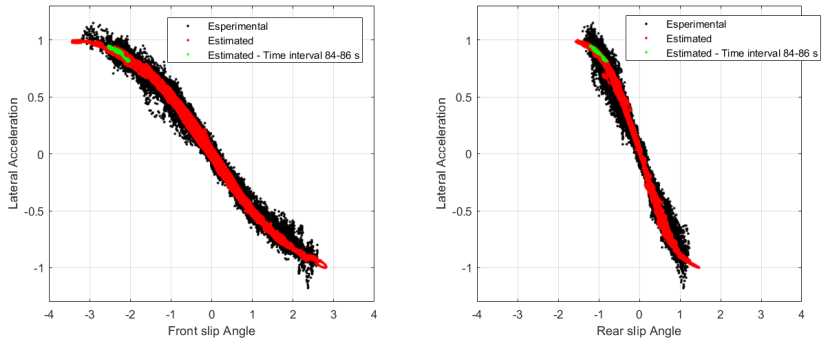

Fig. 5.20 Experimental and Estimated lateral acceleration vs axle slip angle

calculated with the following equation:

$$\begin{aligned} \alpha_1 &= atan\left(\frac{V_y + \dot{\psi} a_1}{V_x}\right) - \delta_{sw}\delta_r \\ \alpha_2 &= atan\left(\frac{V_y - \dot{\psi} a_2}{V_x}\right) \end{aligned} \tag{5.47}$$

Where δ_r is the nominal steering ratio.

Conclusions and Further Developments

In the presented thesis the author's PhD path has been described, aimed to the estimation of vehicle state, with particular detail on tyre operational characteristics, has been described.

The target, fixed in collaboration with Maserati S.p.a, that actively supervised the research activity and provided data both from experimental test carried with the best instruments available and from state-of-the art simulation models, evolved progressively, finally becoming the development of the methodologies described on chapters 2, 3 and 5.

The TRICK methodology has been upgraded to be employed for the estimation of tyre forces in real time, in a robust, accurate way, with low computational burden. Compared to the original formulation, the estimation accuracy is increased for both longitudinal and lateral forces. However, the increase in accuracy relative to lateral forces has been obtained hybridizing the forces calculated from accelerometer with a small component from a pre-identified Pacejka model.

Poor grip can be detected by comparing the forces obtained from this method with those from the Pacejka model, which was identified under normal grip conditions. In this stage, the correction made relative to the opposing lateral forces is useful to increase the overlap of the TRICK - Pacejka signals, which otherwise could be interpreted as a lack of grip.

It must be highlighted that the procedure is dependent from having the chassis velocity measurements, and performed by instruments that cannot be installed in commercial vehicles, due to their high cost. For use cases when this measurement cannot be available, the grip estimation must be performed with tools based on Kalman filter algorithms, that are much more complex and can perform the grip estimation only after a period of time that is needed to the model state to adapt to the real road grip conditions, when the TRICK based algorithm doesn't need any adaptation time and can instantly detect a lack of exerted force compared to the reference model.

The second estimation methodology, described in chapter 3, is able to correctly identify the lateral stiffness of the tyre carcass, the relaxation lengths and all the physical quantities calculated by the model.

The developed model behaviour well match both the data from the reference model and from the experimental tests. The reference model, in the Vi-CarRealTime environment, has allowed the validation of all the physical quantities calculated by the model, mostly hard to be measured in track tests.

To run the procedure, acquisitions from equipment commonly available in the automotive experimentation are needed: accelerometers, gyroscopes and an optical chassis speed sensor.

The required parameterization is extremely reduced compared to that needed by the reference model, but is nevertheless conspicuous as it requires some kinematics and compliance data, and a complete set of parameters for the Magic Formula. Reducing the number of known parameters is a development objective, but already at present it is possible to obtain most of the vehicle parameters from tests carried out with laboratory instruments without the aid of expensive equipment. The identification of the relaxation lengths is carried out at low accelerations, where the tyre is stressed in the area of linear behavior, therefore it will be possible to identify simpler tyre models capable of achieving the same purpose, but also identifiable by road tests.

Before the third methodology is presented, which is based on the employment of the Extended Kalman filter algorithm, this is explained in detail in chapter 4. This section treats also in general the thematic of Kalman filtering and the problematic of tuning this algorithm if applied on complex physical models.

In chapter 5 a state estimator based on an Extended Kalman Filter and an advanced accurate vehicle model have been presented. The mathematical model consists of a double-track model with roll motion, constituted by two masses. The model also includes a detailed suspension elasto-kinematics formulation and a full version of the empirical Magic Formula tyre model. The elasto-kinematics parametrization was provided by the test car manufacturer, but the presented model is usable even if the elasto-kinematics parameters are not available. If a simplified elasto-kinematics formulation has to be employed, the estimator will have a slight loss of accuracy. The Magic Formula parameters have been obtained from the vehicle acquisitions through the methodology shown in [16, 41]. The estimator is designed to work on the widest range of vehicle operating conditions: tyres working over their adhesion peak, with high combined interaction, on sloped and banked road, with tyre characteristics changing over time due to the thermodynamics variations and wear.

The main tyre parameters are updated over time to ensure that the estimation is accurate even in conditions different to the ones in which the vehicle has been parameterized. To ensure the stability of the tyre parameters, their rate of change has been set slow enough to not being able to make significant updates over a single maneuver, which means that the system is eventually unable to detect sudden changes in grip caused by exceptional conditions like an oil spot. The automatic tuning of parameters can also compensate for errors in axle cornering stiffness caused by poor elasto-kinematics parametrization, guaranteeing the correct estimation of the vehicle behavior. It must be noted that the estimation of the parameters works correctly in the case studies pre-

sented because the tyres are almost constantly exerting lateral forces, often working in their nonlinear range, making the tyre states observable by the EKF algorithm, which is not necessarily the case in urban driving. If the tyres are not excited, the states related to them will evolve following a random walk path.

A six-axis IMU, steering angle sensor, and wheel speed sensors are required to feed the discussed state estimator.

The process noise matrix Q and the measurement noise matrix R, needed to run the Kalman filter algorithm, cannot be manually identified because of the complexity of the proposed model, so, specific calibration methodologies described in [53] have been adopted to the purpose.

Future developments will be addressed in the use of GPS to increase the robustness of the estimator, allowing to reduce the accuracy currently required in the parameterization process. At the moment, the estimation of some states is very dependent on the correctness of the parameters, as for example, the longitudinal speed will be properly estimated only if the rolling radius value of the tyres is correct. Furthermore, using GPS measures will increase the amount of information available, making it possible to automatically correct some important parameters such as sensors' offsets, currently evaluated and corrected with manual offline procedures.

References

[1] Alan Neville Gent and Joseph D Walter. *Pneumatic tire*. he University of Akron, 2006.

[2] James E Mark, Burak Erman, and Mike Roland. *The science and technology of rubber*. Academic press, 2013.

[3] Alan N Gent. *Engineering with rubber: how to design rubber components*. Carl Hanser Verlag GmbH Co KG, 2012.

[4] Heinz Heisler. *Advanced vehicle technology*. Elsevier, 2002.

[5] Leslie H Sperling. *Introduction to physical polymer science*. John Wiley & Sons, 2005.

[6] Jo Yung Wong. *Theory of ground vehicles*. John Wiley & Sons, 2008.

[7] Bruce Louden. Non-pneumatic tyre assembly, January 10 2012. US Patent 8,091,596.

[8] European Tyre and Rim Technical Organisation. Standards manual, 2014.

[9] ISO8855:2011. Road vehicles - vehicle dynamics and road-holding ability - vocabulary, 1992.

[10] Massimo Guiggiani. The science of vehicle dynamics. *Pisa, Italy: Springer Netherlands*, page 15, 2014.

[11] William F Milliken, Douglas L Milliken, et al. *Race car vehicle dynamics*, volume 400. Society of Automotive Engineers Warrendale, PA, 1995.

[12] Thomas D Gillespie. Fundamentals of vehicle dynamics. Technical report, SAE Technical Paper, 1992.

[13] Hans Pacejka. *Tire and vehicle dynamics*. Elsevier, 2005.

[14] Hans B Pacejka and Egbert Bakker. The magic formula tyre model. *Vehicle system dynamics*, 21(S1):1–18, 1992.

[15] Egbert Bakker, Lars Nyborg, and Hans B Pacejka. Tyre modelling for use in vehicle dynamics studies. *SAE Transactions*, pages 190–204, 1987.

[16] Flavio Farroni. Trick-tire/road interaction characterization & knowledge-a tool for the evaluation of tire and vehicle performances in outdoor test sessions. *Mechanical Systems and Signal Processing*, 72:808–831, 2016.

[17] G Capone, D Giordano, M Russo, M Terzo, and F Timpone. Ph. an. ty. mha: a physical analytical tyre model for handling analysis–the normal interaction. *Vehicle System Dynamics*, 47(1):15–27, 2009.

[18] F Mancosu, R Sangalli, F Cheli, G Ciarlariello, and F Braghin. A mathematical-physical 3d tire model for handling/comfort optimization on a vehicle: Comparison with experimental results. *Tire Science and Technology*, 28(4):210–232, 2000.

[19] Joško Deur, Vladimir Ivanović, Markos Troulis, Carlo Miano, Davor Hrovat, and Jahan Asgari. Extensions of the lugre tyre friction model related to variable slip speed along the contact patch length. *Vehicle System Dynamics*, 43(sup1):508–524, 2005.

[20] TNO Automotive. Mf-tyre/mf-swift 6.1. 1 help manual. *TNO Automotive, The Netherlands*, 2009.

[21] Flavio Farroni, Lorenzo Mosconi, Aleksandr Sakhnevych, and Francesco Timpone. Trick real time. a tool for the real-time onboard tire performance evaluation. In *Conference of the Italian Association of Theoretical and Applied Mechanics*, pages 1020–1032. Springer, 2019.

[22] Rajesh Rajamani. *Vehicle dynamics and control*. Springer Science & Business Media, 2011.

[23] Olga Galluppi, Simone Formentin, Sergio M Savaresi, and Carlo Novara. Multivariable nonlinear data-driven control with application to autonomous vehicle lateral dynamics. *Journal of Dynamic Systems, Measurement, and Control*, 141(10), 2019.

[24] Moustapha Doumiati, Ali Charara, Alessandro Victorino, and Daniel Lechner. *Vehicle dynamics estimation using Kalman filtering: experimental validation*. John Wiley & Sons, 2012.

[25] Karl Henrik Johansson, Martin Törngren, and Lars Nielsen. Vehicle applications of controller area network. In *Handbook of networked and embedded control systems*, pages 741–765. Springer, 2005.

[26] Joanny Stephant, Ali Charara, and Dominique Meizel. Experimental validation of vehicle sideslip angle observers. In *IEEE Intelligent Vehicles Symposium, 2004*, pages 150–155. IEEE, 2004.

[27] Vicente Milanés, José E Naranjo, Carlos González, Javier Alonso, and Teresa de Pedro. Autonomous vehicle based in cooperative gps and inertial systems. *Robotica*, 26(5):627–633, 2008.

[28] J SvendeniuS. Tire modeling and friction estimation. phdthesis. *Lund University, Department of Automatic Control, Lund University, Box*, 118, 2007.

[29] Rajesh Rajamani, Neng Piyabongkarn, Jae Lew, Kyongsu Yi, and Gridsada Phanomchoeng. Tire-road friction-coefficient estimation. *IEEE Control Systems Magazine*, 30(4):54–69, 2010.

[30] Georgios Mavros. A study on the influences of tyre lags and suspension damping on the instantaneous response of a vehicle. *Proceedings of the Institution of Mechanical Engineers, Part D: Journal of Automobile Engineering*, 222(4):485–498, 2008.

[31] Lorenzo Mosconi, Flavio Farroni, Aleksandr Sakhnevych, Francesco Timpone, Alessandro Capobianco, and Fabio Sebastiano Gerbino. Identification of tire transient parameters from vehicle onboard sensors data. In *The International Conference of IFToMM ITALY*, pages 813–822. Springer, 2020.

[32] Gregory Smith and Mike Blundell. A new efficient free-rolling tyre-testing procedure for the parameterisation of vehicle dynamics tyre models. *Proceedings of the Institution of Mechanical Engineers, Part D: Journal of Automobile Engineering*, 231(10):1435–1448, 2017.

[33] Pavel Sarkisov, Günther Prokop, Jan Kubenz, and Sergey Popov. Physical understanding of transient generation of tire lateral force and aligning torque. *Tire Science and Technology*, 47(4):308–333, 2019.

[34] Justin Sill and Beshah Ayalew. On the frequency domain analysis of tire relaxation effects on transient on-center vehicle handling performance. In *ASME International Mechanical Engineering Congress and Exposition*, volume 43864, pages 755–762, 2009.

[35] Tetsushi Mimuro, Masayoshi Ohsaki, Hiromichi Yasunaga, Kohji Satoh, and Robert G Dubensky. Four parameter evaluation method of lateral transient response. *SAE transactions*, pages 1499–1508, 1990.

[36] Georgios Mavros, Homer Rahnejat, and PD King. A framework for the characterization of the transient handling responses of non-linear vehicles. *Proceedings of the Institution of Mechanical Engineers, Part K: Journal of Multi-body Dynamics*, 221(1):1–11, 2007.

[37] KTR Van Ende, F Küçükay, R Henze, FK Kallmeyer, and J Hoffmann. Vehicle and steering system dynamics in the context of on-centre handling. *International journal of automotive technology*, 16(5):751–763, 2015.

[38] Flavio Farroni, Aleksandr Sakhnevych, and Francesco Timpone. A three-dimensional multibody tire model for research comfort and handling analysis as a structural framework for a multi-physical integrated system. *Proceedings of the Institution of Mechanical Engineers, Part D: Journal of Automobile Engineering*, 233(1):136–146, 2019.

[39] Nobutaka Tsujiuchi, Takayuki Koizumi, Masami Matsubara, Kinya Moriguchi, and Ichiro Shima. Prediction of spindle force using measured road forces on rolling tire. Technical report, SAE Technical Paper, 2009.

[40] Chongfeng Wei and Oluremi Ayotunde Olatunbosun. The effects of tyre material and structure properties on relaxation length using finite element method. *Materials & Design*, 102:14–20, 2016.

[41] Flavio Farroni, Raffaele Lamberti, Nicolò Mancinelli, and Francesco Timpone. Trip-id: A tool for a smart and interactive identification of magic formula tyre model parameters from experimental data acquired on track or test rig. *Mechanical Systems and Signal Processing*, 102:1–22, 2018.

[42] Francesco Braghin, Federico Cheli, and Edoardo Sabbioni. Identification of tire model parameters through full vehicle experimental tests. *Dynamics Systems, Measurement and Control*, 2011.

[43] IJM BESSELINK, HB PACEJKA, AJC SCHMEITZ, and STH JANSEN. Mf-tyre 5.2 user manual mf-tyre 5.2 user manual, 2004.

[44] Daniel Chindamo, Basilio Lenzo, and Marco Gadola. On the vehicle sideslip angle estimation: a literature review of methods, models, and innovations. *applied sciences*, 8(3):355, 2018.

[45] Hongyan Guo, Dongpu Cao, Hong Chen, Chen Lv, Huaji Wang, and Siqi Yang. Vehicle dynamic state estimation: state of the art schemes and perspectives. *IEEE/CAA Journal of Automatica Sinica*, 5(2):418–431, 2018.

[46] Gary Bishop, Greg Welch, et al. An introduction to the kalman filter. *Proc of SIGGRAPH, Course*, 8(27599-23175):41, 2001.

[47] Michael Zeitz. The extended luenberger observer for nonlinear systems. *Systems & Control Letters*, 9(2):149–156, 1987.

[48] Simon J Julier and Jeffrey K Uhlmann. Unscented filtering and nonlinear estimation. *Proceedings of the IEEE*, 92(3):401–422, 2004.

[49] Jacob Westfall, David A Kenny, and Charles M Judd. Statistical power and optimal design in experiments in which samples of participants respond to samples of stimuli. *Journal of Experimental Psychology: General*, 143(5):2020, 2014.

[50] Atsushi Sakai and Yoji Kuroda. Discriminative parameter training of unscented kalman filter. *IFAC Proceedings Volumes*, 43(18):677–682, 2010.

[51] Timothy D Barfoot. State estimation for robotics, 2021.

[52] Angus P. Andrews Mohinder S. Grewal. *Kalman filtering: Theory and practice using MATLAB*. Wiley-IEEE Press, 3 edition, 2008.

[53] Pieter Abbeel, Adam Coates, Michael Montemerlo, Andrew Y Ng, and Sebastian Thrun. Discriminative training of kalman filters. In *Robotics: Science and systems*, volume 2, page 1, 2005.

[54] Howard Dugoff, Paul S Fancher, and Leonard Segel. An analysis of tire traction properties and their influence on vehicle dynamic performance. *SAE transactions*, pages 1219–1243, 1970.

[55] Mykel J Kochenderfer and Tim A Wheeler. *Algorithms for optimization*. Mit Press, 2019.

[56] H-M Gutmann. A radial basis function method for global optimization. *Journal of global optimization*, 19(3):201–227, 2001.

[57] Rommel G Regis and Christine A Shoemaker. A stochastic radial basis function method for the global optimization of expensive functions. *INFORMS Journal on Computing*, 19(4):497–509, 2007.

[58] L Walta, VAWJ Marchau, and K Brookhuis. Stakeholder preferences of advanced driver assistance systems (adas)—a literature review. In *Proceedings of the 13th World Congress and Exhibition on Intelligent Transport Systems and Service*, 2006.

[59] Jesse Levinson, Jake Askeland, Jan Becker, Jennifer Dolson, David Held, Soeren Kammel, J Zico Kolter, Dirk Langer, Oliver Pink, Vaughan Pratt, et al. Towards fully autonomous driving: Systems and algorithms. In *2011 IEEE Intelligent Vehicles Symposium (IV)*, pages 163–168. IEEE, 2011.

[60] M.C. Best, T.J. Gordon, and P.J. Dixon. An extended adaptive kalman filter for real-time state estimation of vehicle handling dynamics. *Vehicle System Dynamics*, 34(1):57–75, 2000.

[61] J. Dakhlallah, S. Glaser, S. Mammar, and Y. Sebsadji. Tire-road forces estimation using extended kalman filter and sideslip angle evaluation. In *2008 American Control Conference*, pages 4597–4602, 2008.

[62] T. A. Wenzel, K. J. Burnham, M. V. Blundell, and R. A. Williams. Dual extended kalman filter for vehicle state and parameter estimation. *Vehicle System Dynamics*, 44(2):153–171, 2006.

[63] M. Doumiati, A. Victorino, A. Charara, and D. Lechner. Unscented kalman filter for real-time vehicle lateral tire forces and sideslip angle estimation. In *2009 IEEE Intelligent Vehicles Symposium*, pages 901–906, 2009.

[64] S Antonov, A Fehn, and A Kugi. Unscented kalman filter for vehicle state estimation. *Vehicle System Dynamics*, 49(9):1497–1520, 2011.

[65] Ehsan Hashemi, Mohammad Pirani, Amir Khajepour, and Alireza Kasaiezadeh. A comprehensive study on the stability analysis of vehicle

dynamics with pure/combined-slip tyre models. *Vehicle system dynamics*, 54(12):1736–1761, 2016.

[66] Massimo Guiggiani. The science of vehicle dynamics. *Pisa, Italy: Springer Netherlands*, page 15, 2014.

[67] Wei Liu, Hongwen He, and Fengchun Sun. Vehicle state estimation based on minimum model error criterion combining with extended kalman filter. *Journal of the Franklin Institute*, 353(4):834–856, 2016.

[68] X. Jin, G. Yin, and A. Hanif. Cubature kalman filter-based state estimation for distributed drive electric vehicles. In *2016 35th Chinese Control Conference (CCC)*, pages 9038–9042, 2016.

[69] Francesca Cura and Graziano Curti. Dynamic and acoustic characterisation of automotive wheels. *Shock and Vibration*, 11(3, 4):493–504, 2004.

[70] Klaus-Jürgen Bathe and Gunwoo Noh. Insight into an implicit time integration scheme for structural dynamics. *Computers & Structures*, 98:1–6, 2012.

[71] F Farroni, A Sakhnevych, and F Timpone. Physical modelling of tire wear for the analysis of the influence of thermal and frictional effects on vehicle performance. *Proceedings of the Institution of Mechanical Engineers, Part L: Journal of Materials: Design and Applications*, 231(1-2):151–161, 2017.

[72] Martin Haudum, Johannes Edelmann, Manfred Plöchl, and Manuel Höll. Vehicle side-slip angle estimation on a banked and low-friction road. *Proceedings of the Institution of Mechanical Engineers, Part D: Journal of automobile engineering*, 232(12):1584–1596, 2018.

[73] Jie Ling, Hui Chen, and Fan Xu. Estimation of vehicle sideslip angle with adaptation to road bank angle and roll angle. In *Proceedings of SAE-China Congress 2014: Selected Papers*, pages 403–410. Springer, 2015.

[74] A Eichberger and W Rulka. Process save reduction by macro joint approach: The key to real time and efficient vehicle simulation. *Vehicle System Dynamics*, 41(5):401–413, 2004.

[75] William Crego Prescott, Gert Heirman, Joris De Cuyper, Ludger Dragon, Andre Lippeck, Horst Brauner, et al. Using high-fidelity multibody vehicle models in real-time simulations. Technical report, SAE Technical Paper, 2012.

[76] RW Ngigi, Crinela Pislaru, Andrew Ball, and Fengshou Gu. Modern techniques for condition monitoring of railway vehicle dynamics. In *Journal of Physics: Conference Series*, volume 364, page 012016. IOP Publishing, 2012.

[77] Mathias Jesussek and Katrin Ellermann. Fault detection and isolation for a nonlinear railway vehicle suspension with a hybrid extended kalman filter. *Vehicle System Dynamics*, 51(10):1489–1501, 2013.

[78] Qianqian Wang, Jiao Wang, Pengju Zhao, Jianqiang Kang, Few Yan, and Changqing Du. Correlation between the model accuracy and model-based soc estimation. *Electrochimica Acta*, 228:146–159, 2017.

[79] Francesco Braghin, Federico Cheli, and Edoardo Sabbioni. Identification of tire model parameters through full vehicle experimental tests. *Journal of Dynamic Systems, Measurement, and Control*, 133(3), 2011.

[80] Chaiwat Nuthong and Steuer-und Regelungstechnik. *Estimation of tire-road friction forces using Kalman filtering for advanced vehicle control*. PhD thesis, Universitätsbibliothek der Universität der Bundeswehr München, 2009.

[81] Junjian Qi, Kai Sun, Jianhui Wang, and Hui Liu. Dynamic state estimation for multi-machine power system by unscented kalman filter with enhanced numerical stability. *IEEE Transactions on Smart Grid*, 9(2):1184–1196, 2016.

[82] Fredrik Gustafsson. Particle filter theory and practice with positioning applications. *IEEE Aerospace and Electronic Systems Magazine*, 25(7):53–82, 2010.

[83] Taehyun Shim and Chinar Ghike. Understanding the limitations of different vehicle models for roll dynamics studies. *Vehicle system dynamics*, 45(3):191–216, 2007.

[84] Chao Liu, Junyu Zhou, Axel Gerhard, Jan Kubenz, and Günther Prokop. Characterization of the vehicle roll movement with the dynamic chassis simulator. In *Vehicle and Automotive Engineering*, pages 129–141. Springer, 2018.

[85] TNO. *MF-Tyre User Manual Version 5.2*, 2001.

[86] Ralf Kübler and Werner Schiehlen. Two methods of simulator coupling. *Mathematical and computer modelling of dynamical systems*, 6(2):93–113, 2000.

[87] Peter Holdmann, Philip Köhn, Bertram Möller, and Ralph Willems. Suspension kinematics and compliance-measuring and simulation. Technical report, SAE Technical Paper, 1998.

[88] Yafei Wang, Binh Minh Nguyen, Hiroshi Fujimoto, and Yoichi Hori. Multirate estimation and control of body slip angle for electric vehicles based on onboard vision system. *IEEE Transactions on Industrial Electronics*, 61(2):1133–1143, 2013.

[89] Michele Russo, Riccardo Russo, and Agsotino Volpe. Car parameters identification by handling manoeuvres. *Vehicle System Dynamics*, 34(6):423–436, 2000.

[90] Marco Fainello and Diego Minen. Active vehicle ride and handling development by using integrated sil/hil techniques in a highperformance driving simulator. In *5th International Munich Chassis Symposium 2014*, pages 183–184. Springer, 2014.

[91] Jesús Blasco, Francisco Valero, Antonio Besa, and Francisco Rubio. Design of a dynamometric wheel rim. In *New Advances in Mechanisms, Transmissions and Applications*, pages 243–250. Springer, 2014.

[92] Federico Cheli et al. Cyber tyre: A novel sensor to improve vehicle's safety. Technical report, SAE Technical Paper, 2011.

[93] Lu Xiong, Xin Xia, Yishi Lu, Wei Liu, Letian Gao, Shunhui Song, Yanqun Han, and Zhuoping Yu. Imu-based automated vehicle slip angle and attitude estimation aided by vehicle dynamics. *Sensors*, 19(8):1930, 2019.

[94] Yuquan Wang, Jan Mangnus, Dragan Kostić, Henk Nijmeijer, and Sven TH Jansen. *Vehicle state estimation using gps/imu integration*. IEEE, 2011.

Appendix A

MF-Tyre model

A.1 Parameters

MF-TYRE model by Pacejka is here reported as it is written in **??**. The Magic Formula model equations contain the non-dimensional model micro-parameters p, q, r and s and, in addition, a set of scaling factors λ. Other parameters and variable quantities used in the equations are:

- g gravity,
- V_c magnitude of the velocity of the wheel contact centre C,
- V_{cxy} components of the velocity of the wheel contact centre C,
- V_{sxy} components of slip velocity V_s (of point S) with $V_{sy} \approx V_{cy}$,
- $V_r (= R_e\Omega = V_{cx} - V_{sx})$ forward speed of rolling,
- R_0 unloaded tyre radius,
- R_e effective rolling radius,
- Ω wheel speed of revolution,

- F_{z0} nominal load,
- df_z the normalised change in vertical load $df_z = \frac{F_z - F_{z0}}{F_{z0}}$,
- κ the longitudinal slip $\kappa = -\frac{V_{sx}}{V_{cx}}$

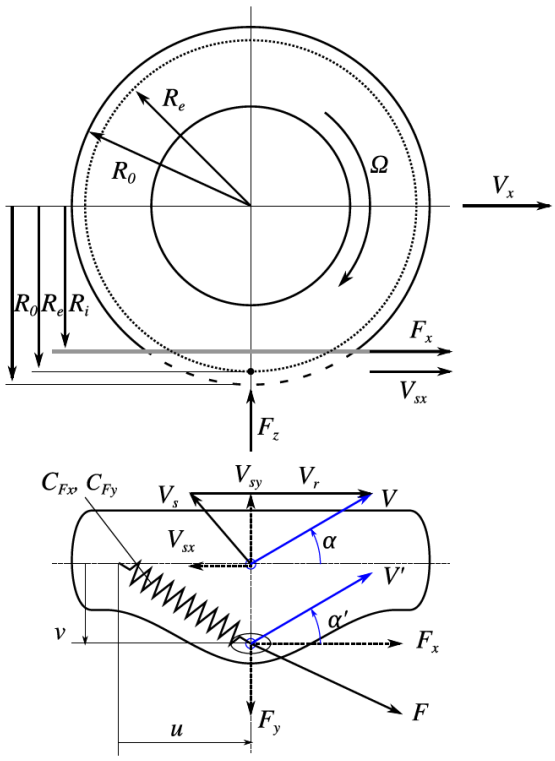

Fig. A.1 Tyre reference quantities

Figure A.1 shows the meaning of the reported kinematic quantities.

A.2 Longitudinal Force (pure longitudinal slip)

$$F_{x0} = D_x \sin[C_x \arctan\{B_x\kappa_x - E_x(B_x\kappa_x - \arctan(B_x\kappa_x))\}] + S_{Vx} \quad \text{(A.1)}$$

$$\kappa_x = \kappa + S_{Hx} \quad \text{(A.2)}$$

$$C_x = p_{Cx1}\lambda_{Cx}(>0) \quad \text{(A.3)}$$

$$D_x = \mu_x F_x \zeta_1 (>0) \quad \text{(A.4)}$$

$$\mu_x = (p_{Dx1} + p_{Dx2} df_z)\lambda_{\mu x}(>0) \quad \text{(A.5)}$$

$$E_x = (p_{Ex1} + p_{Ex2} df_z + p_{Ex3} df_z^2)(1 - p_{Ex4} sign(\kappa_x))\lambda_{Ex}(\leq 1) \quad \text{(A.6)}$$

$$K_{x\kappa} = F_z(p_{Kx1} + p_{Kx2} df_z)\exp(p_{Kx2} df_z)\lambda_{Kx\kappa} \quad \text{(A.7)}$$

$$B_x = K_{x\kappa}/(C_x D_x + \varepsilon_x) \quad \text{(A.8)}$$

$$S_{Hx} = (p_{Hx1} + p_{Hx2} df_z)\lambda_{Hx} \quad \text{(A.9)}$$

$$S_{Vx} = F_z(p_{Vx1} + p_{Vx2} df_z)(|V_{cx}|/(\varepsilon_{Vx} + |V_{cx}|)\lambda_{Vx}\lambda'_{\mu x}\zeta_1 \quad \text{(A.10)}$$

A.3 Lateral Force (pure side slip)

$$F_{y0} = D_y \sin[C_y \arctan\{B_y\alpha_y - E_y(B_y\alpha_y - \arctan(B_y\alpha_y))\}] + S_{Vy} \quad \text{(A.11)}$$

$$\alpha_y = \alpha + S_{Hy} \quad \text{(A.12)}$$

$$C_y = p_{Cy1}\lambda_{Cy}(>0) \quad \text{(A.13)}$$

$$D_y = \mu_y F_y \zeta_2 (>0) \quad \text{(A.14)}$$

$$\mu_y = (p_{Dy1} + p_{Dy2} df_z)(1 - p_{Dy3}\gamma^2)\lambda_{\mu y}(>0) \quad \text{(A.15)}$$

$$E_y = (p_{Ey1} + p_{Ey2} df_z)[1 - (p_{Ey3} + p_{Ey4}\gamma) sign(\alpha_y)]\lambda_{Ey}(\leq 1) \quad \text{(A.16)}$$

$$K_{y\alpha 0} = p_{Ky1} F'_{z0} \sin[2\arctan(p_{Ky2} F'_{z0})]\lambda_{Ky\alpha} \quad \text{(A.17)}$$

$$K_{y\alpha} = K_{y\alpha 0}(1 - p_{Ky3}\gamma^2)\zeta_3 \quad \text{(A.18)}$$

$$B_y = K_{y\alpha}/(C_y D_y + \varepsilon_y) \quad \text{(A.19)}$$

$$S_{Hy} = (p_{Hy1} + p_{Hy2} df_z)\lambda_{Hy} + p_{Hy3}\gamma\lambda_{Ky\gamma}\zeta_0 + \zeta_4 - 1 \quad \text{(A.20)}$$

$$S_{Vy} = F_z[(p_{Vy1} + p_{Vy2} df_z)\lambda_{Vy} + (p_{Vy3} p_{Vy4} df_z)\gamma\lambda_{Ky\gamma}]\lambda'_{\mu y}\zeta_2 \quad \text{(A.21)}$$

$$K_{y\gamma 0} = [p_{Hy3} K_{y\alpha 0} + F_z(p_{Vy3} + p_{Vy4} df_z)]\lambda_{Ky\gamma} \quad \text{(A.22)}$$

A.4 Longitudinal Force (combined slip)

$$F_{xs} = G_{x\alpha} F_{x0} \tag{A.23}$$

$$G_{x\alpha} = \cos[C_{x\alpha} \arctan\{B_{x\alpha}\alpha_s - E_{x\alpha}(B_{x\alpha}\alpha_s - \arctan(B_{x\alpha}\alpha_s))\}]/G_{x\alpha 0} \tag{A.24}$$

$$G_{x\alpha 0} = \cos[C_{x\alpha} \arctan\{B_{x\alpha}S_{Hx\alpha} - E_{x\alpha}(B_{x\alpha}S_{Hx\alpha} - \arctan(B_{x\alpha}S_{Hx\alpha}))\}] \tag{A.25}$$

$$\alpha_s = \alpha^* + S_{Hx\alpha} \tag{A.26}$$

$$B_{x\alpha} = r_{Bx1} \cos[arctan(r_{Bx2}\kappa)]\lambda_{x\alpha} \tag{A.27}$$

$$C_{x\alpha} = r_{Cx1} \tag{A.28}$$

$$E_{x\alpha} = r_{Rx1} + r_{Ex2} df_z \tag{A.29}$$

$$S_{Hx\alpha} = r_{Hx1} \tag{A.30}$$

A.5 Lateral Force (combined slip)

$$F_{ys} = G_{y\kappa}F_{y0} + S_{Vy\kappa} \tag{A.31}$$

$$G_{y\kappa} = \cos[C_{y\kappa}\arctan\{B_{y\kappa}\kappa_s - E_{y\kappa}(B_{y\kappa}\kappa_s - \arctan(B_{y\kappa}\kappa_s))\}]/G_{y\kappa 0} \tag{A.32}$$

$$G_{y\kappa 0} = \cos[C_{y\kappa}\arctan\{B_{y\kappa}S_{Hy\kappa} - E_{y\kappa}(B_{y\kappa}S_{Hy\kappa} - \arctan(B_{y\kappa}S_{Hy\kappa}))\}] \tag{A.33}$$

$$\kappa_s = \kappa^* + S_{Hy\kappa} \tag{A.34}$$

$$B_{y\kappa} = r_{By1}\cos[arctanr_{By2}(\alpha - r_{By3})]\lambda_{y\kappa} \tag{A.35}$$

$$C_{y\kappa} = r_{Cy1} \tag{A.36}$$

$$E_{y\kappa} = r_{Ry1} + r_{Ey2}df_z \tag{A.37}$$

$$S_{Hy\kappa} = r_{Hy1} + r_{Hy2}df_z \tag{A.38}$$

$$S_{Vy\kappa} = D_{Vy\kappa}\sin[r_{Vy5}\arctan(r_{Vy5}\kappa)] \tag{A.39}$$

$$D_{Vy\kappa} = \mu_y F_z(r_{Vy1} + r_{Vy2}df_z + r_{Vy3}\gamma)\cos[arctan(r_{Vy4}\alpha)]zeta_2 \tag{A.40}$$

A.6 Relaxation length

In order to account for force dynamics, the force on i-th wheel is thus calculate according to following differential equations

$$\begin{cases} \frac{L_x}{v_i}\dot{F}_{x,i} + F_{x,i} = F_{xs,i} \\ \frac{L_y}{v_i}\dot{F}_{y,i} + F_{y,i} = F_{ys,i} \end{cases} \tag{A.41}$$

Where v_i is the longitudinal velocity of wheel hub in wheel reference frame while L_x and L_y are the so called relaxation length respectively for longitudinal and lateral forces. L_x is comparable to contact path length while L_y is comparable to tyre circumference length.